Novel therapeutic approaches to treat inflammatory conditions with glucocorticoid and calciferol nanoparticles *in vivo* and *in vitro*

Dissertation

for the award of the degree

"Doctor rerum naturalium"

of the Georg-August-Universität Göttingen

within the doctoral program GGNB (Göttingen Graduate School for Neurosciences, Biophysics, and Molecular Biosciences), Molecular Medicine

of the Georg-August University School of Science (GAUSS)

Submitted by

Agathe Anne Véronique Amouret

born in

Rouen, France

Göttingen, 05.09.2022

THESIS COMMITTEE

Prof. Dr. Holger Reichardt (1st Referee)

Institute for Cellular and Molecular Immunology

University Medical Center, Göttingen

Prof. Dr. Lutz Walter (2nd Referee)

Department of Primate Genetics

German Primate Center, Göttingen

Prof. Dr. Francesca Odoardi

Institute for Neuroimmunology and Multiple sclerosis

University Medical Center, Göttingen

Prof. Dr. Carsten Lüder

Department of Medical Microbiology

University Medical Center, Göttingen

Prof. Dr. Ralf Dressel

Institute for Cellular and Molecular Immunology

University Medical Center, Göttingen

Prof. Dr. Thomas Meyer

Molecular Psychocardiology

University Medical Center, Göttingen

Date of thesis submission: 05.09.2022

Date of the oral examination: 27.10.2022

DECLARATION

I hereby declare that I have written this PhD thesis entitled “Novel therapeutic approaches to treat inflammatory conditions with glucocorticoid and calciferol nanoparticles *in vivo* and *in vitro*” independently and with no other sources and aids than quoted.

This thesis has not been submitted elsewhere for any academic degree.

_____

Agathe Anne Véronique Amouret,

Date : 05.09.2022

Göttingen, Germany

Table of content

Abstract

The body is constantly confronted with environmental threats and sometimes the entry of pathogens leads to severe inflammatory conditions such as sepsis or acute lung injury (ALI). Both diseases are characterized by a dysregulated immune system, which compromises homeostasis and induces multiple organ failure, thus being potentially lethal. While pathophysiological changes in ALI are mostly confined to the lung, sepsis is an example of a systemic inflammation affecting different organs including spleen, liver and lung. GCs are used in both conditions to reduce the so called "cytokine storm", but high doses of GCs may also aggravate lymphocytopenia occurring in both diseases, leading to a severe risk of secondary infections and poorer outcome. Targeting specific cell types in GC treatment could allow to overcome this side effect as nanoparticles were shown to be mainly taken up by macrophages. Our results revealed that free synthetic GCs and GC-containing nanoparticles efficiently reduced the pro-inflammatory profile and tissue damage in a mouse model of sepsis. However, in contrast to free GCs, a tendency was observed that using nanoparticles prevented a further aggravation of lymphocytopenia. Nonetheless, the therapeutic efficacy of both GC formulations was similar in sepsis as well as ALI mouse models. Interestingly, the analysis of human peripheral blood monocytes also unveiled a novel function of GCs in regulating the energy metabolism of myeloid cells in inflammatory conditions. Finally, nanoparticles containing calcitriol, the active form of vitamin D, were characterized as a potential alternative to GCs in sepsis or ALI therapy allowing to avoid side-effects of high doses of calcitriol. Our results show a good anti-inflammatory effect of newly formulated calcitriol nanoparticles, which were efficiently engulfed by macrophages and fibroblasts in a clathrin-dependent manner before being localized to the lysosomal compartment. Collectively, the use of nanoparticles offers interesting new possibilities for the treatment of inflammatory conditions with the potential to reduce adverse effects of GCs and calcitriol.

List of Figures

List of tables

Abbreviations

11β-HSD II/ I	11β-Hydroxysteriod Dehydrogenase type II/ I
ACTH	Adreno-Corticotrophin-Releasing Hormone
ALI	Acute Lung Injury
APC	Antigen Presenting Cells
ARDS	Acute Respiratory Distress Syndrome
AT-I	Alveolar Type I
AT-II	Alveolar Type II
BAL	Brochoalveolar Lavage
BALF	Brochoalveolar Lavage Fluid
BDS	Bright Detail Similarity
BMP-NPs	Betamethasone Phosphate-Nanoparticles
BMZ	Betamethasondihydrogenphosphat-Dinatrium (Celestan)
BSA	Bovines Serumalbumin
CBG	Corticosteroid Binding Globulin
CCL	Chemokine C-C motif Ligand
cDNA	Complementary DNA
CRF	Corticotrophin-Releasing Factor
CXCL	Chemokine C-X-C motif Ligand
CytoD	Cytochalasin D
DAMPs	Damage-associated Molecular Patterns
DCs	Dendritic Cells
ddH2O	Deionized Distilled Water
Dex	Dexamethasone

DMSO	Dimethylsulfoxid
DNA	Deoxyribonucleic Acid
dNTPs	Deoxynucleotide Triphosphates
DR	Deep Red
EDTA	Ethylenediaminetetraacetic Acid
ELISA	Enzyme-Linked ImmunoSorbent Assay
FACS	Fluorescence-Activated Cell Sorting
FITC	Fluoresceinisothiocyanat
FSC	Forward Scatter
FSC-A	Forward Scatter Area
FSC-H	Forward Scatter Height
GCs	Glucocorticoids
GM-CSF	Granulocyte-Macrophage Colony Stimulating Factor
H&E	Hematoxylin and Eosin
H_2O_2	Hydrogen Peroxide
HPA	Hypothalamic-Pituitary-Adrenal
Hrs	Hours
i.p.	Intraperitoneally
i.v.	Intravenously
IFN	Interferon
Ig	Immunoglobulin
IL	Interleukine
IOH-NPs	Inorgainc-Organic Hybrid Nanoparticles
LPS	Lipopolysaccharides

mAbs	Monoclonal Antibodies
MCP-1	Monocyte Chemoattractant Protein-1
MDC	Monodansyl-Cadaverine
MHC	Major Histocompatibility Complex
NF-κB	Nuclear Factor kappa B
NK	Natural Killer
NO	Nitric Oxide
OA	Oleic Acid
PAMPs	Pathogen-associated Molecular Patterns
PBMCs	Peripheral Blood Stem Cells
PBS	Phosphate-Buffered Saline
PCA	Principle Component Analysis
PCR	Polymerase Chaine Reaction
PE	Phycoerythrin
PerCP	Peridinin-Chlorophyll-Protein
PFA	Paraformealdehyde
RNA	Ribonucleic Acid
ROS	Reactive Oxygen Species
RT	Room Temperature
RT-qPCR	Real Time-quantitative PCR
SEM	Standard Error of the Mean
SSC	Side Scatter
Th	T helper
TLR	Toll-Like Receptor

TNF	Tumor Necrosis Factor
Tregs	T regulatory cells
VDi-NPs	Cholecalciferol Nanoparticles
VDa	Calciferol
VDa-NPs	Calciferol Nanoparticles
WT	Wild type

1. Introduction

1.1. Sepsis and septic shock

1.1.1. Epidemiology

First defined as an infection leading to the onset of systematic inflammatory response syndrome (SIRS) and as a sepsis-induced hypotension persisting despite adequate fluid resuscitation, sepsis and septic shock definitions have changed over the last decades due to their initial limitations. After an expansion of the diagnostic criteria list in 2001, national societies such as the Society of Critical Care Medicine and the European Society of Intensive Care Medicine agreed on a new definition of sepsis, now defining it as a life-threatening organ dysfunction caused by a dysregulated host response to infection. [1] Since 2017 sepsis is considered as a global health priority by the WHO and a recent scientific publication estimated the number of cases worldwide approximately 50 million with 11 million sepsis-related deaths, placing its mortality rate around 20%. [2] Moreover, being one of the most common reasons worldwide for the admission in intensive care units, sepsis causes enormous cost with an estimated annual healthcare expenditure in the US of 20 billion dollars. [1] However, important disparities are seen around the world, with higher mortality rates in low and middle-income countries such as in sub-Saharan Africa or in both south and east Asia, representing 85% of sepsis and sepsis-related death worldwide. [3] In case it is not recognised and managed early, sepsis can lead to multiple organ failure and septic shock, for which the mortality rate increases up to 60%. [4] Differences have also been observed between ages group, with patients older than 65 years having a 2.3-fold higher chance of dying. Nearly one third of all sepsis cases and half of the sepsis-related deaths are linked to underlying injury or chronic diseases. Indeed, certain groups of the population are at higher risk to develop sepsis than others such as elderly, neonates, pregnant women, hospitalised individuals and person suffering from chronic liver or kidney diseases, autoimmune disorders and immunodeficiency. [5] Sepsis can also result from healthcare-associated infections, which is considered as one of the most frequent adverse events during care worldwide. The most common causes for sepsis in 2017 were diarrheal diseases as well

a low respiratory infection. In maternal and neonatal sepsis, infections with *group B streptococcus* and *Escherichia coli* are leading causes of sepsis. [6], [7] Noteworthy, the antimicrobial resistance often observed in healthcare-related infections can lead to a rapid deterioration of the clinical conditions [8] and considerable difficulties to find appropriate treatment. Collectively, early diagnosing and appropriate treatment are important to improve disease outcome and reduce sepsis-related mortality.

1.1.2. Diagnostic and treatment of sepsis

Sequential Organ Failure Assessment (SOFA) has become the main scoring tool for the identification of sepsis as well as for predicting its hospital-related mortality. [9] Based on oxygen levels, mean arterial pressure, platelet count, Glasgow coma scale, bilirubin levels and creatinine levels, a SOFA score of >2 along with haematological, biochemical and microbiological analysis results should lead to a sepsis diagnosis [2], [10]. However due to limited access to clinical parameters outside ICUs, [11]–[13] a quick SOFA (qSOFA) based on a respiratory rate of at least 22 breaths/minute, a systolic blood pressure lower than 100mm Hg, an altered mental status (Glasgow coma scale) and suspected or confirmed infection was created, enabling an easy first assessment. [10] To confirm diagnosis, a complementary SOFA scoring and further analyses should be done. [14] It is also very important to identify the cause and location of the infection through corporal fluid and potential wound swab cultures or the use of molecular pathogen detection techniques. [15] X-rays, CT scans or ultrasounds can also enable to localise the infection and evaluate the state of various organs. [13] Most recently, the use of biomarkers has been widely investigated to support sepsis diagnostic as well as to monitor the infectious process. Indeed, some biomarkers such as procalcitonin or presepsin are tightly link to bacterial infections while others will give indication about organ dysfunction, metabolism or even inflammation levels based on cytokine and chemokine levels. [13], [15]–[17]

Prompt treatment has to be initiated within a few hours after diagnosis, achieving an adequate oxygen saturation of around 95%, administrating intravenous saline to avoid hypotension targeting a venous pressure of 8-12mm Hg. Moreover, the start of broad-

spectrum antibiosis is essential for better survival and should be adapted as soon as the source of infection has been identified. It is important to note that an anti-microbial de-escalation should be discussed daily as microbial resistance is associated with long antimicrobial administration. [10], [18], [19] Vasopressors such as noradrenaline might additionally be needed to achieve a mean arterial pressure between 65 and 90mm Hg, [15] and patient who also show lactate levels of >2mmol/L are diagnosed to suffer from septic shock. [11] Adjunction therapies are considered for the management of sepsis when other treatments were insufficient. Patients with an exacerbated inflammatory profile could benefits an application of cytokine antagonist or glucocorticoids (GCs). TNFα is preferred target in cytokine agonist treatment. Phase 2 and 3 clinical trials have established the efficiency of two anti-TNFα therapies using Afelimomab or CytoFab antibodies, both leading to diminished IL-6 and TNFα levels and decreasing mortality. [11] Otherwise, GC treatment is believed to reduce inflammation and compensate sepsis-related adrenal insufficiency. [10] Previously being the only approved drug to treat severe sepsis, recombinant human APC (rhAPC) showed anti-inflammatory, anti-apoptotic and anti-coagulant effects. Yet, post-marketing studies did not confirm the clinical efficacy of rhAPC resulting in its withdrawal. Other therapies focused on sepsis-induced lymphopenia, the most current ones being recombinant human IL-7 and anti-PD-L1/PD-1 antibodies. [20] Phase 2 clinical trials using rhIL7 have shown increased lymphocytes counts, [21] while anti-PD-L1/PD-1 antibodies were found to have the potential to reduce apoptosis and to attenuate T-cell dysfunction through sepsis. [11] Enhancing immune response have also been investigating using for example GM-CSF to improve monocyte function and bacterial clearance. [20] Finally, using biomarkers are not only employed to support sepsis diagnosis but also to better monitor sepsis and to enable personalised treatments. [17] Thus, a better understanding of the impact of sepsis on immune cells is needed.

1.1.3. Pathogenesis of sepsis

The complex immune response to infection in sepsis, which is characterized by vascular endothelial injury, severe inflammation, activation of the coagulation cascade, and

inhibition of fibrinolysis, eventually leading to the development of multiple organ dysfunctions is not fully understood (Figure 1). [4]

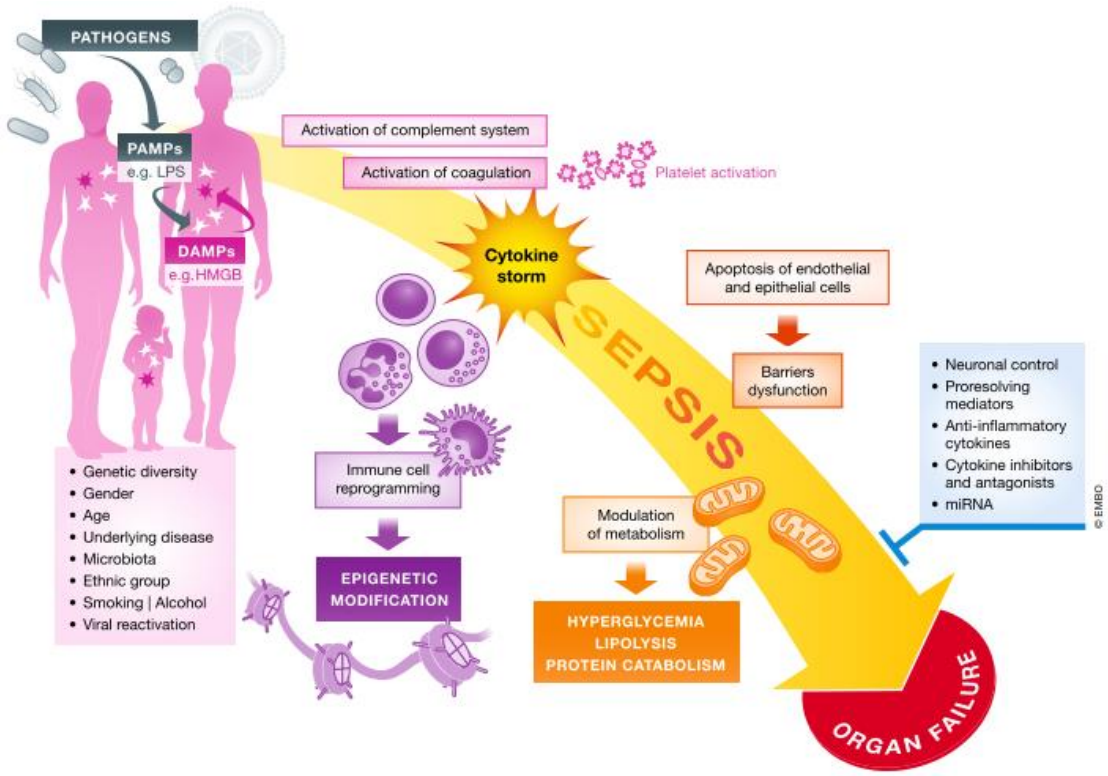

Figure 1: Summary of the players and pathophysiological events occurring during sepsis. *Complex interactions between genetic and chronic health status determine the host response to pathogens. The magnitude and variety of humoral and cellular response may lead to organ dysfunctions, which are a key denominator of sepsis in comparison with other forms of infection. Cavaillon and Singer, 2020*

Upon recognition of pathogen-associated molecular patterns (PAMPs) by pathogen recognition receptors (PRRs), for instance toll-like receptors (TLRs), monocytes and macrophages are activated and secrete pro-inflammatory cytokines such as IL-6, IL-1β or TNFα. [22] Cytokine production increases the expression of adhesion molecule by endothelial cells, causes hepatic secretion of acute phase proteins, attracts neutrophils and fosters the formation of neutrophil extracellular traps (NETs). Overproduction of nitric oxide (NO) is also catalysed by inducible nitric oxide synthase (iNOS) leading to irreversible inhibition of electron transfer chain (ETC) activity. If the inflammatory response exceeds a certain threshold, a systemic injury generalises in the body with production of reactive oxygen species (ROS) and additional cytokines causing protein,

lipid and DNA damage as well as impaired mitochondria function. Complement system activation also plays a role in systemic inflammation since it induces additional ROS production. [5],[11] A generalisation of the inflammation profile is made responsible for an uncontrolled and exacerbated production of pro-inflammatory mediators, a phenomenon called “cytokine storm”, resulting in diffuse endothelial injury with formation of gaps between the cells [1] as well as disruption of the vascular integrity triggering a procoagulant response. [4] While it was believed for a long time to follow pro-inflammatory activities, the anti-inflammatory process happens simultaneously even during the first hours of sepsis and is crucial for the return to a homeostatic state. Anti-inflammatory mediators such as IL-10 supress the production of IL-6 and IFNγ and antagonize TNFα and IL-1 signalling. [5]

The adaptative immune system contributes to the resolution of inflammation and tissue damage through several mechanism. As those mechanism seem to be disrupted during sepsis, an exacerbated anti-inflammatory response occurs and leads to an overall immunosuppression called immune paralysis. Lymphopenia, being considered as an important cause of immunosuppression, is the consequence of B cell, T cell, natural killer (NK) cell but dendritic cell (DC) apoptosis. [23]–[25] Both, $CD4^+$ and $CD8^+$ T cell subpopulations have been found to be reduced through sepsis while regulatory T (Treg) cells seemed to increase. [26] This T-cell exhaustion is linked to high pro- and anti-inflammatory cytokine levels and leads to a reduced production of IFNγ and TNFα and increased expression of programmed cell death-1 (PD-1). Macrophages express PD-1 as well as PD ligand-1 (PD-L1), which is linked to a reduced proliferative capacity of T cells. [23],[27] Moreover, increased numbers of Treg cells cause further immune dysfunction by inhibiting monocyte and neutrophil functions [22]. More specifically, surface expression of HLA-DR by monocytes is diminished [26], [28] and immature neutrophils accumulate. Additionally, B cell apoptosis is linked to a reduced MHC class II and an increased IL-10 expression, [24] and the decrease of other cell types such as NK cells and DCs is also linked to immunosuppression. [22]

In addition to effects on the immune system, sepsis also induces major endocrine and metabolic changes. Activation of endothelial cells and their dysfunction can lead to a disruption of the blood-brain barrier enabling inflammatory and neurotoxic mediators to enter the CNS resulting in a hypothalamic-pituitary-adrenal axis dysfunction with reduced cortisol production called adrenal insufficiency syndrome. [11] However, also other pituitary hormones such as growth hormone as well as thyroid hormones can be affected in sepsis patients. [2] Otherwise, multiple metabolic alterations are seen in septic patient, such as peripheral insulin resistance, increased lipolysis and proteolysis, and mitochondrial dysfunction with a change towards glycolytic metabolism. [2], [5]

Cellular dysfunctions can persist over a long time and impaired T cell responses haven been shown even a month after sepsis including prominent long-lasting $CD4^+$ T cells impairments.[23] Late occurring death of sepsis patients has indeed been associated with persistent immunosuppression, immune dysfunction and chronic catabolism. [22], [23]

1.2. Acute lung injury

1.2.1. Epidemiology of ALI

Acute respiratory distress syndrome (ARDS) was first described in 1967 in 12 patients presenting with acute tachypnoea, hypoxemia, loss of lung compliance and diffuse alveolar infiltration based on X-rays evaluation. [29] More than two decades later, the American-European Consensus Committee tried to bring clarity and uniformity into the definition of both ARDS and Acute Lung Injury (ALI), defining ARDS as a severe form of ALI with an oxygenation level of $PaO_2/FIO_2 \leq 200$ mmHg and $PaO_2/FIO_2 \leq 300$ mmHg, respectively. [30] Indeed, the need of consensus developed with medical progress and the use of supplemented oxygen therapy as well as positive-pressure ventilation. [31] Nonetheless, diagnostic of ALI/ARDS has been questioned and the European Society of Intensive Care Medicine (ESICM) published a new definition of ARDS, the so called Berlin definition, conferring three different levels to it: mild, moderate and severe. [32] ALI and ARDS incidence has been based clinical manifestation, [33] representing 7% of

ICU admitted patients as well as 20% of mechanically ventilated patients according to a European study. [34] In the US, important variations in ALI/ARDS incidence have been reported, ranging from 20 to 80 cases per 100 000 persons annually, an observation. also made in other countries. [33], [35] Several factors such as smoking, population density, respiratory infections, hospital equipment and medical resources are believed to impact this incidence. [36] Age is also a crucial denominator in ALI/ARDS incidence with 16/100 000 person-years cases in the 15-19 years old group and 306/100 000 person-years cases in the 75-84 years old group in the US. [37] Over the last years, the incidence has overall decreased as show by one study from the Mayo Clinic, explained by better treatment protocols, [31] also affecting mortality. [38] Factors such as age, comorbidities, alcohol or drug abuse and smoking promote the development of ALI. However, immunosuppression in cancer or organ transplantation patients, multiple blood transfusions, and high tidal ventilation have also been shown to increase that risk. [33], [35], [39] Recently, more than 40 gene candidate genes have been found to be associated with ARDS, for example angiotensin-converting enzyme 2 protein (ACE2) contributing to the regulation of pulmonary vascular permeability and identified as a cell entry receptor for the new coronavirus being responsible for the severe acute respiratory syndrome (SARS). [40] Notably, the appearance of SARS-CoV2 increased the risk of developing ALI/ARDS by more than 20%. As a matter of fact, pneumonia, which is considered as a direct lung insult, is the leading cause of ALI/ARDS. Others are aspiration lung injury and pulmonary contusion due to trauma. [35], [39], [40]

1.2.2. Diagnosis and treatment of ALI

Based on the Berlin definition, ALI/ARDS is diagnosed if respiratory symptoms worsen within one week after a known clinical insult. Patients present with a ratio of partial pressure of arterial oxygen normalized to the fraction of inspired oxygen PaO_2/FIO_2 lower than 300 mmHg corresponding to mild ARDS and lower than 100 mmHg for the severe form of ARDS. [41] Considered as the gold standard for ARDS diagnosis, chest radiography analyses are characterised by bilateral opacities consistent of pulmonary oedema that can’t be explained by pleural effusions or atelectasis. It is also important

to evaluate cardiac function with echocardiography since oedema formation can be caused by cardiac overload or failure. [32],[41]–[43] Identification of an underlying cause of ALI such as sepsis, pneumonia or pancreatitis are crucial to treat them. This evaluation can require several diagnostic methods such as a CT scan, microbiological cultures, bronchoalveolar lavage (BAL) analysis but also invasive techniques such as biopsies when specific infections are considered or when patients are not responding to previous treatments. [44]–[46]

Most patients diagnosed with ALI/ARDS will require ICU treatment and mechanical ventilation. In mild cases, however, non-invasive ventilation might be sufficient to maintain the patient's oxygenation levels at 88-95% by reducing the breathing work, improving the gas exchange with higher oxygenation and carbon dioxide clearance as well increased end expiratory lung volume. This has the advantage that deep sedation can be avoided. [46] In contrast, patients with more severe ALI/ARDS will be intubated, sedated and ventilated. The ventilation methods have changed over time with the use of only low tidal volumes nowadays to reduced lung injury. Despite its benefit on the patient's outcome, the use of low tidal volume in severe or refractory ARDS can result in acidosis bringing about the need of extracorporeal membrane oxygenation (ECMO). [32],[41]–[43],[46] Prone positioning is widely used to better recruit atelectatic lung regions, therefore relieving external compressive forces and improving the arterial oxygenation. [44] To improve patient-ventilator synchrony, neuromuscular blocking agents can be applied to end spontaneous respiratory movement. [46]

Besides supportive measurements, there are also pharmacological options to treat ALI/ARDS. Even though controversial, the use of low-dose GCs can be recommended to prevent the progression of severe disease if previous treatments were insufficient, based on the GCs ability to inhibit neutrophil activation, fibroblast proliferation and collagen deposition. [44] Several other pharmaceutical therapies have been the object of clinical, preclinical or animal studies, yet most of them showed limitations in treating ALI/ARDS. Surfactant therapy, mainly applied to premature infants to treat neonatal respiratory distress syndrome, has been studied in adults ARDS patients as well to

prevent alveolar collapse and reduce pulmonary oedema yet not showing convincing positive results. [47] Known for its pulmonary vasodilatory effect, inhaled NO has been evaluated in several studies to treat refractory hypoxemia in ARDS patients, [32] and showed a significant 24 hours PaO_2/FIO_2 improvement although it did not have any significant impact on mortality and significantly increased renal failure. [48] Other preclinical studies analysed the capacity of prostaglandin treatment to regulate the inflammatory response by inhibiting platelet aggregation, and to act as pulmonary vasodilator. [49] Nonetheless, no significant oxygenation improvement was observed. [50] Treatment with a β-adrenoceptor agonist in a pre-clinical promoted the clearance of alveolar fluid as well as epithelial and endothelial repair accompanied by a reduction of the alveolar-epithelial permeability. However, small phase 2 trials were stopped despite beneficial effects due to safety and tolerability concerns. Specifically, adverse cardiac effects as well as lactic acidosis were identified. [51] Recently, granulocyte macrophage colony stimulation factor (GM-CSF) was tested as therapeutic option in the treatment of Covid-19 and its associated ALI/ARDS symptoms. Lung injury was reduced in mice but clinical trials showed different results, in particular they failed to reveal a change in mortality. [49], [52] However, encouraging new results using mAbs to GM-CSF or GM-CSFR in the treatment of Covid-19 have stimulated interest in this therapy again. [53]

1.2.3. Pathogenesis of ALI

The lung is constantly exposed to environmental threat such as pathogens. Thus, its cellular complexity, composed of interactions between resident and innate immune cells, is a key to maintain homeostasis status. Being the main barrier against pathogens, the alveoli, also responsible for the gas exchange within the lungs, are composed of alveolar epithelial type I and type II cells, alveolar macrophages (AM), innate lymphoid cells as well as adaptative immune cells. [54], [55] AM represent a unique interface between the pulmonary mucosa and the external environment and therefore play a central role in immune regulation within the alveoli build the first line of defence after pathogen entry. [54] Upon recognition of PAMPs by binding to PRRs on epithelial cells

and alveolar macrophages, an inflammatory signalling cascade which involves the production of pro-inflammatory cytokines like IL-1β, TNFα and IL-8 is initiated. [56], [57] Other innate immune cells such as DCs or NK cells also recognise pathogens through their PRRs, thereby inducing pro-inflammatory cytokines and chemokines as well. (Figure 2) [54]

ALI/ARDS severity is tightly linked to neutrophil migration into the lungs in response to chemokines produced by activated macrophages such as CXCL5 or CXCL2. Attracted neutrophils produce cytotoxic substances including ROS and inflammatory cytokines and form NETs to eliminate pathogens in the extracellular space. [56] After rolling and adhering to the endothelium, neutrophils migrate through the endothelium into the interstitium and alveolar airspace. The endothelial integrity is also disrupted by the destabilisation of vascular endothelial cadherin (VE-cadherin) due to increased levels of thrombin and TNFα, thereby leading to higher NO production by endothelial cells, increased endothelial permeability and neutrophil infiltration. The latter also increases epithelial barrier permeability due the damaged intracellular junctions and apoptosis induction. [58] A protein rich pulmonary oedema fluid accumulates in the lung and promotes an influx of fluid from the capillaries to the lung intersitium finally resulting in impaired gas exchange and hypoxia. [59] Dysfunction of pulmonary surfactant production subsequently results in alveolar collapse and decrease of lung compliance. [60] Sodium transport associated with alveolar oedema resolution and conveyed by epithelial type I and type II cell, seems to be altered by high pro-inflammatory cytokine concentrations present in the oedema fluid. [58] Na/K-ATPase, which is located in the cell surface of alveolar type II epithelial cells, also contributes to lung liquid clearance under normal circumstances. During hypoxia, however, it happens to be degraded by endocytosis resulting in alveolar-epithelial-barrier dysfunction and decreased alveolar fluid clearance. [54]

Macrophages are essential for the resolution of inflammation due to their polarisation from a pro-inflammatory (M1) to an anti-inflammatory phenotype (M2) and the

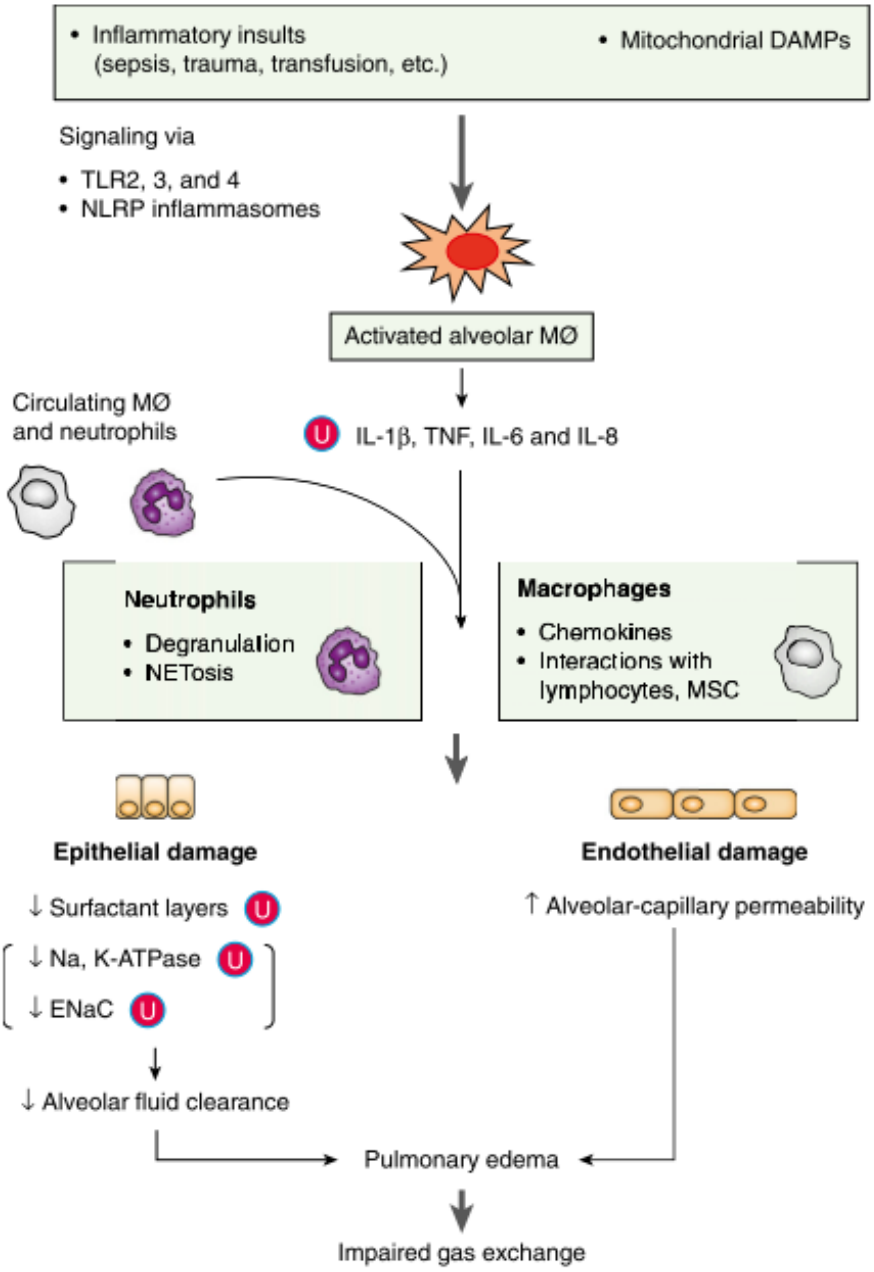

Figure 2: Pathophysiology of ARDS. *Inflammatory insults, including mitochondrial DAMPs, activate alveolar macrophages via TLR and NLR signalling pathways. Activated alveolar macrophages release pro-inflammatory cytokines and recruit circulating monocytes and neutrophils to injured sites. Excessive neutrophils and persistently activated macrophages cause extensive damage to lung epithelia and endothelia, resulting in an impaired alveolar–capillary barrier. Disruption of this barrier allows protein-rich fluid to enter the alveoli, causing fluid accumulation in alveolar spaces (pulmonary oedema) that interferes with gas exchange. Ubiquitination plays an important role in modulating the abundance of key proteins in ARDS, resulting in the secretion of cytokines, lower levels of surfactant proteins, and decreased function of ion channels (Na/K-ATPase and ENaC). ARDS is associated with surfactant depletion, leading to increased NETosis, a process that alters lung cell viability. Mitochondrial DAMPs can directly increase microvascular permeability independently of leukocytes. MF, macrophage. Han and Mallampalli, 2015*

phagocytic capacity of the latter. T helper cells type 2 (Th2) and innate lymphoid cells produce IL-4 and IL-13 thereby increasing IL-10, which contributes to the commitment of macrophages to the M2 phenotype. M2 macrophages activation leads to lung repair process although an overproduction of transforming growth factor beta (TGF-b), can also promote fibroblast proliferation and differentiation in the lung thereby supporting the development of pulmonary fibrosis. [61]

1.3. Glucocorticoids

1.3.1. Generalities

First isolated in 1946 as the "compound E" and being the object a few years later of Hench's and Kendall's Nobel price award, [63],[64] GCs are steroid hormones that are fundamental to the maintenance of stress-related homeostasis. [64] Their release is tightly controlled by the hypothalamic-pituitary-adrenal axis (HPA), and in unstressed conditions GC release is related to the circadian rhythm. However, its production can be increased during physiological or emotional stress. Following stimulation, the hypothalamus produces corticotropin-releasing hormone (CRH) which in turn acts on the anterior pituitary where it induces adrenocorticotropin hormone (ACTH) secretion. Finally, ACTH causes the adrenal glands to produce GCs. [62] Once secreted into the bloodstream, up to 95% of GCs will stay inactive by binding either to the corticosteroid-binding globulin (CBG) or to albumins, leaving only small amounts of free GCs which can diffuse through the cell membrane and exert their functions by interaction either with the GC-receptor (GR) or the mineralocorticoid receptor (MR). [65] The bioactivity of GCs is also regulated by 11β-hydroxysteroid dehydrogenase (11β-HSD) type 1 and 2 within the cells. [66] Under inflammatory conditions, other mechanisms can modulate the availability of GCs such as neutrophils elastase, which cleaves CBG, or inflammatory mediators such as TNFα and IL-1b, which modulate the expression of 11β-HSD. [63]

Due to their broad anti-inflammatory effects [67], GCs were first used in 1946 for the treatment of rheumatoid arthritis (RA). [63] Nowadays, they are widely employed to treat various acute and chronic inflammatory conditions such as RA, inflammatory

bowel disease or multiple sclerosis. [67] However, long-term use of GCs causes major side-effects including osteoporosis, skin and muscle atrophy, hypertension, insulin resistance, impaired wound healing as well as psychological effects such as depression, mood change and insomnia. [68], [69]

1.3.2. GCs and the immune system

With anti-inflammatory effects ranging from the inhibition of signalling pathways and the suppression of pro-inflammatory mediators via interaction with NF-κB or AP-1 transcription factors, to the involvement in the resolution phase by enhancing cellular debris clearance and production of anti-inflammatory mediators, [64],[71] GCs affect the different immune cells through complex mechanisms. (Figure 3)

Dendritic cells (DCs), considered as prototypic antigen presenting cells, differentiate from myeloid precursors. Upon antigen encounter they undergo maturation while migrating towards the lymph nodes. After GCs exposure, activation and maturation of DCs is suppressed, resulting in reduced expression of MHC class II and co-stimulatory molecules as well as cytokines. GCs lead to DC apoptosis and inhibit their migratory capacity to the lymph nodes. Moreover, GCs seem to induce a tolerogenic phenotype of DCs, resulting in increased phagocytic activity and IL-10 expression. [63], [71]

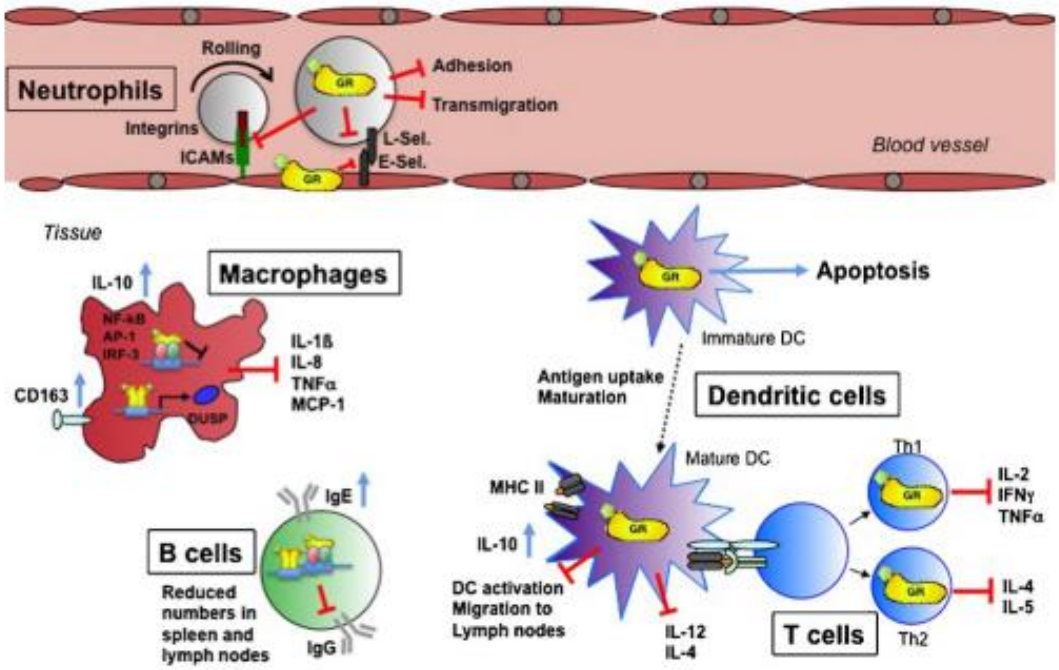

Figure 3: Multiple effects of the GCs on immune cell subtypes. *GCs influence neutrophil functions by suppressing rolling, adhesion and transmigration by reducing expression of adhesion molecules like integrins, selectins (E-Sel., L-Sel.) and intercellular adhesion molecules (ICAMs) in both neutrophils and endothelial cells. GCs efficiently suppress classical macrophage activation by induction of IL-10, an immunomodulatory cytokine and by the inhibition of the release of pro-inflammatory cytokines like TNFα, IFN-γ or IL-1β. Cytokines are suppressed by mechanisms requiring the dimerized GR (by activating GRE dependent genes like DUSP-1) as well as tethering mechanisms, i.e. interfering with NF-κB, AP-1 and IRF-3. GCs influence DCs on all levels of their life cycle. They facilitate antigen uptake of immature DCs but suppress their maturation by reduction of MHC class II and co-stimulatory molecules and cytokine expression. Furthermore, they potently induce apoptosis of DCs and reduce their migratory capacity. Chronic GC treatment leads to a reduction of splenic and lymph node B cells, reduction of IgG production but enhanced IgE generation. T helper cell differentiation and function is affected by GCs through repression of pro-inflammatory cytokines and by regulation of transcription factors. Baschant and Tuckermenn, 2010*

Macrophages are also controlled by GCs since they express PRRs, the signalling of which is reduced by GCs, therefore reducing their production in pro-inflammatory mediators. Additionally, GCs exposure induces a specific anti-inflammatory phenotype in macrophages, referred as M2c. [64],[73] Expression of anti-inflammatory mediators such as CD163, CD206 or Gr-1 are upregulated whereas pro-inflammatory monocyte makers such as CX3CR1 are downregulated in macrophages. [64],[72]

Neutrophils, the main infiltrating cells during the acute inflammation phase especially in sepsis and ALI/ARDS, were first believed to only weakly respond to GCs. However, this turned out be wrong. [73] In fact, their maturation as well as their mobilisation into the circulation is promoted by GCs, but their rolling, adhesion and transmigration are suppressed through reduced expression of integrins and selectin involved in those processes. [72],[74]

GCs affect NK cells become IL-12, which is crucial for the killer activity of those cells, is reduced upon GCs exposure therefore suppressing IFN-γ production from NK cells. [74] Although GC action has not been extensively studied in B cells, GCs seem to reduce their number in both spleen and lymph nodes. Early B cell progenitor proliferation is attenuated, IgE production enhanced and IgG production supressed by GCs. [71] Besides, GCs are also suspected to have an impact on B cells selection [63] and induce increased apoptosis. [75]

GCs effect on T cells has been more extensively studied. Even though the mechanisms are not fully understood, GCs affect T cells maturation as double positive thymocytes are very sensitive to GC-induced apoptosis while TCR triggered apoptosis, determining the single positive stage thymocyte development, seems to be alleviated by GCs. In contrast to thymocytes, peripheral T cells are less sensitive to GC-induced apoptosis with an increased CD28 signalling counteracting rapid apoptosis upon GCs exposure. [71] Noteworthy, $CD4^+$ T cell activation is also indirectly affected by GCs due to the modulation of DC activity. Finally, GCs modify T helper cell polarisation by favouring Th2 and Treg over Th1 and Th17 cell differentiation, due to their inhibition capacity on T cell-derived cytokines. [63]

1.3.3. Sepsis and GC

GCs are widely used to treat the acute inflammatory phase of sepsis and septic shock due to their potent anti-inflammatory properties. In fact, up to 50% of sepsis patients in Europe receive GCs treatment [77],[78] although clinical trials show controversial results concerning ICU free days or mortality improvement upon GCs application. Several factors are believed to be responsible for the low efficiency of GCs starting with a pronounced GC resistance in sepsis patients linked to a dysfunctional GC-GR axis. As a consequence, GC responsiveness is low, which aggravates sepsis pathophysiology due to the reduced lactate clearance and finally results in a poor outcome. [78]–[80] Timing and dosage of GCs treatment also impacting the GCs' efficiency. [81] Indeed, high doses of GCs were used to treat sepsis in the 1980s but later results indicated an increased risk of secondary infections and death. [77] In the meantime, other studies suggested that low doses of GCs (200-300mg) and a longer treatment are superior, with an improved hemodynamic and decreased pro-inflammatory mediators as well as oxidative stress without increasing the risk of secondary infection. [78] Many clinical trials such as the CORTICUS study, in which patients received 50 mg of hydrocortisone every 6 hours for 5 days, did not show clear beneficial effects. However, those studies have been reported to suffer from great limitations in the selection process, as in the last one for example only 5% of eligible patients were enrolled in the study. [76] While

most clinical trials were unable to prove any beneficial effect of GCs on the 90-days survival, the APROCCHSS and ADRENAL clinical trials, both using daily doses of 200 mg hydrocortisone for 7 days, showed a significant reduction of the resolution time as well as shorter mechanical ventilation duration an ICU stay. [82] Several meta-analyse in the last couple of years tried to shed light onto the controversial outcome of GC use and to better understand the variations between individual clinicals trials. Taking together the results of 22 clinical trials in which hydrocortisone or an equivalent corticosteroid were administered for at least 5 days at doses lower than 300 mg per day, it was suggested the mortality outcome upon low-dose GC treatment was lower. [83] A meta-analysis considering 37 clinical trials in which GCs were administered at low doses revealed improved shock reversal and vasopressor free days, decreased ICU stay and a lower SOFA score at day 7. Moreover, mortality after 28 but not 90 days was reduced. [84] Due to the divergent results on GC administration in sepsis and septic shock, the Surviving Sepsis Campaign guidelines recommend the use of GCs for patient who present with a sepsis shock but without significant improvement upon proper fluid resuscitation and vasopressors therapies. [83],[86]

Even though the mechanism of GCs in sepsis is not yet fully understood, evidence in murine models obtained by using GR knock-out mice lacking GR expression in myeloid cells, indicated that the GR in myeloid cell was required to limit endotoxic shock. Similarly, GR^{dim} mice were found to show reduced responsiveness to GCs, enlightening the importance of GR dimerization for GCs' beneficial effects. [71]

1.3.4. Acute lung injury and GC

For more than 50 years, GCs have been used to treat ALI/ARDS but their application remained controversial. In the early phase of acute ARDS, GC treatment has proven to be beneficial for patient and to reduce mortality rates. However, when administered at a later stage, patients did not benefit but rather experienced side-effects. [44],[87] To obtain a better understanding of the therapeutic activity, the pharmacological principle of GCs and their mechanism of action were investigated. In male BALB/c mice injected with LPS as a simple model of ALI, methylprednisolone treatment improved

lung function and ameliorated tissue injury. On a molecular level, methylprednisolone restored the balance of macrophage subsets and inhibited the pro-inflammatory response. [87] In another study, dexamethasone was used to evaluate the mechanism of action of GCs and their cell-type specificity in several strains of GR mutant mice after inducing ALI by combined treatment with LPS and oleic acid. [88] Here, the SphK1-S1P-S1PR1 axis was identified as a crucial regulator of endothelial barrier integrity which contributes to the control of lung inflammation. Treatment with GCs increased S1P serum levels via synergistic activation of SphK1 with pro-inflammatory stimuli, which resulted an amelioration of ALI symptoms. Furthermore, the finding that GCs were unable to suppress ALI in $GR^{LysMCre}$, GR^{dim} as well as $GR^{CD11cCre}$ mice supported the notion that the DNA-binding-dependent function of the GR in monocytes and macrophages plays an essential role for the anti-inflammatory effects of GCs in ALI. [88]

The recent Covid-19 crisis brought about a new urge for the better management of ALI/ARDS, since severe infection with SARS-CoV-2 can also lead to ARDS. New research results and clinical trials were published using GCs as a way to reduce the inflammatory response and the cytokine storm observed in severely affected Covid-19 patients. [89] At the beginning of the pandemic, health organisations were supporting the use of GCs with caution as it had been associated with a higher mortality rate in influenza-induced ALI and a worsened outcome in MERS-CoV patients. Furthermore, more complications were seen in SARS-CoV-1 patients even though methylprednisolone was able to reduce levels of IL-8, MCP-1, and IP-10. [90] Studies and clinical trials of GCs administration in the management of Covid-19 symptoms show divergent results even up to now. When administered to human monocyte THP-1 cells GCs, reduced IL-6 levels which play an important role in the cytokine storm often observed in Covid-19 patients. Dexamethasone was found to be the most potent GC in terms of reducing IL-6 even if hydrocortisone, methylprednisolone, triamcinolone and prednisolone were decreasing its expression as well. [91] When tested on human monocyte-derived macrophages, methylprednisolone appeared to boost RNA replication of SARS-CoV-2 but suppressed the proinflammatory cytokine production as well. The same effect with alleviated body

loss weight and increased viral load and pulmonary inflammation was observed in a hamster model of SARS-CoV-2. [92] A clinical trial with methylprednisolone showed disease improvement in the early pulmonary phase of Covid-19 patients after 3 days of intravenous administration. [93] Several studies also unveiled a beneficial effect of dexamethasone administration on Covid-19 associated ARDS symptoms such as the RECOVERY clinical trial, which is the largest study up to now. Here, dexamethasone resulted in lower 28-day mortality rate amongst patients receiving either invasive mechanical ventilation or oxygen supplementation alone. In contrast, no significant benefit was observed in the GC-treated group compared to the control group in those patient not receiving any respiratory support. [94] Lastly, early administration and the correct dose of GC treatment in Covid-19 appears to be crucial for patients to benefit from it. [96],[97] Currently, the WHO recommends the use of GCs in treatment of Covid-19 associated ARDS to reduce inflammation but limits its recommendation to severe cases of Covid-19. [97]

1.4. Calcitriol

1.4.1. Generalities

Cholecalciferol or vitamin D_3, most commonly referred to as vitamin D, is known to play an important role in calcium homeostasis, bone metabolism and the immune system. [98] Prevailing in the world population, [99] its deficiency is thus associated with osteoporosis but also an increased risk of diseases such as cancer, multiple sclerosis, cardiovascular disorders, diabetes, autoimmunity and infectious diseases. [98], [100], [101] Even though diet is a source of VD, an estimated 80% is produced by our body upon ultraviolet light exposure. [98] Absorption of solar ultraviolet B photons by 7-dehydrocholesterol in the skin leads to the formation of pre-vitamin D_3 and its subsequent conversion into vitamin D_3. Vitamin D_3 is then transported to the liver and converted enzymatically into 25-hydroxy-vitamin D_3 (25-OH-cholecalciferol). Finally, it is metabolised into its biologically active form 1,25-dihydroxy-vitamin D_3 (1,25-$(OH)_2$ cholecalciferol) in the kidneys, also referred to as calcitriol. [100] Once produced, calcitriol enters the circulation and binds to the vitamin D receptor (VDR) to exert its

functions in target tissues, such as enhancing intestinal and renal calcium absorption or osteoclast activity. Moreover, transport of calcitriol is mainly mediated by vitamin D binding protein (DBP) but also to a smaller extent by albumin. [102] Local production of calcitriol can also be enzymatically mediated in many different tissues such as brain, colon, breast, or macrophages. Overall, calcitriol is believed to be responsible for the regulation of up to 200 genes implicated in cell growth and differentiation control. [103] Due to its important function, vitamin D supplementation is widely recommended in individuals at risk for deficiency [101] and its use as a medical treatment is being investigated. Recent clinical trials, such as the Vitamin D Assessment Study (ViDA), showed positive effects in individuals after long term vitamin D supplementation including better lung function among smokers, chronic obstructive pulmonary disease or asthma, as well as better arterial function and bone mineral density. Other diseases such as cancer were not improved upon vitamin D supplementation. However, most of those studies are considered as preliminary therefore needing more investigations. [104] Otherwise, high doses of vitamin D have also been reported to cause side effects such as hypercalcemia. Indeed, this could be observed in the 1950s when the incidence of hypercalcemia in infants increased due to the fortification of milk with 100IU vitamin D. [103] Additionally, animal experiment showed that already a concentration of 2,5μM 25-OH-cholecalciferol leads to vitamin D intoxication. [105]

1.4.2. Calcitriol and the immune system

Since all immune cells express the VDR, calcitriol can widely affect the immune system and control inflammatory processes. [106] However, it is important to note that high levels of calcitriol and a dysregulation of its production is not only linked to side effects such as hypercalcemia but is also suspected to be linked to granulomatous disorders such as sarcoidosis. [107]

In monocytes, calcitriol downregulates TLR-2 and TLR-4 expression, reducing PAMP responsiveness [106] and inhibiting the production of pro-inflammatory mediators such as IL-1, IL-6, IL-8, IL-12 and TNFα. [108] Furthermore, chemotactic and phagocytic

capacity as well as tumour cell cytotoxicity and microbial activity are increased by calcitriol. [109], [110] The maturation, differentiation and activation of DCs are also inhibited by calcitriol. More specifically, differentiated DCs reduce their expression of MHC class II and co-stimulatory molecules such as CD40, CD80 and CD86, which is a characteristic feature of an immature DC phenotype. [106], [108] Consequently, altered DC function leads to a reduced antigen presentation, lower IL-12 secretion and increased tolerogenic IL-10 production. [111] Additionally, IFN-γ production by NK cells is downregulated by calcitriol. [109]

Activated B cell proliferation as well as its immunoglobulins production are supressed by calcitriol [107],[110], the generation of memory and plasma B cells is inhibited, and apoptosis is initiated. [111] In Th cells, 57 genes were found to be downregulated and 45 genes to be upregulated by calcitriol. [106] In fact, calcitriol treatment inhibits Th1 cell development as well as the production of cytokines such as IFN-γ , IL-6, IL-2 and TNFα, leading to a shift to the Th2 phenotype. [108], [112] Interestingly, the dose of calcitriol is crucial in determining this effect: while high doses seem to suppress IFN-γ and enhance IL-5 and IL-13 expression, low doses supress both Th1 and Th2 cytokine expression. Th17 cells, which are associated with many autoimmune disorders, also seems to be inhibited upon vitamin D exposure. [106], [108], [112] In contrast, Treg cells are activated by calcitriol thus leading to immunosuppression [106] with reduced inflammatory cytokine production and increased levels of anti-inflammatory cytokines such as IL-10. [108]

1.4.3. Sepsis and calcitriol

Although vitamin D deficiency occurs in up to 98% of critical care unit patients with sepsis, its effects on the pathogenesis and the outcome of the disease are not yet understood even though both phenomena frequently coexist clinically. [113] This association between vitamin D deficiency and sepsis has also been observed in children and neonates. [114] Importantly, some studies show an increased mortality among severe vitamin D deficiency patients. [115], [116] An induction of local intracellular vitamin D activity by immune cells has been observed in sepsis, resulting in efficient

pathogen clearance and anti-inflammatory and tolerogenic effects. [113] Early clinical data indeed suggested a role of vitamin D in preventing and attenuating infections. [117] In a clinical trial in which septic patients received 2μg of calcitriol, some patients seemed to respond to the treatment. Expression of hCAP-18, an antimicrobial peptide involved in the elimination of pathogens by macrophages, as well as IL-10 mRNA were increased upon calcitriol treatment but no significant differences were observed in pro-inflammatory cytokine plasma levels between the placebo and calcitriol groups. Previous vitamin D deficiency was also analysed in order to see it could be made responsible for the responsiveness or unresponsiveness of patients, but without any successful. [118], [119] In another study, high cholecalciferol doses were administered to ICU individuals leading to a substantial increase in calcitriol serum concentrations after 7 days. [120] Vitamin D supplementation in critically ill patients improved survival and shortened ICU stays, and was associated with reduced levels of C-reactive protein, IL-6 and TNFα indicating possible immunomodulatory effects. [121] A systemic review of several clinical trials which focused on vitamin D supplementation in sepsis revealed conflicting results. Indeed, while some studies showed a significant reduction in IL-1b and IL-6 among septic patient as well as a reduced 30 days ICU re-admission and lower hospital death rate among critically ill patient with severe VD deficiency, other studies did not observe any change in mortality or hospital stay duration upon vitamin D supplementation. [113] This highlights the difficulty to understand which patient could benefit from calcitriol treatment and how vitamin D influences sepsis.

Animal models of sepsis also provided new insights. Vitamin D treatment improved blood coagulation parameters, modulated pro-inflammatory cytokine levels, and enhanced induction of anti-microbial peptides on mucosal and epithelial surfaces. [122] Additionally, pre-treating endothelial cells *in vitro* with vitamin D reduced pro-inflammatory cytokine production induced by LPS and inhibited NF-κB pathway activation. [121] As vitamin D supplementation is cheap and safe, further studies to better understand its role in sepsis appears to be important.

1.4.4. Acute lung injury and calcitriol

Similar to sepsis, vitamin D deficiency is frequently associated with the progression of lung disorders [123], an increased inflammatory incidence [124], and an increased risk of upper respiratory tract infections. [125] Vitamin D plays indeed an important role in th regulation of the upper respiratory tract innate immunity [125] and its deficiency is known to influence the severity and duration of pneumonia. [126] A meta-analysis including 25 randomised double-blind placebo-controlled trials with a total 10 933 patients showed a decreased risk of respiratory tract infections by 12% across lifespan upon vitamin D supplementation. Another meta-analysis of vitamin D supplementation in pulmonary tuberculosis also demonstrated some beneficial effects, suggesting a possible use of vitamin D supplementation as an adjuvant therapy together with antibiotics. More recently, new clinical trials have been conducted in the context of the Covid-19 pandemic. Indeed, vitamin D could reduce the ARDS-caused cytokine storm in Covid-19 patients and modulate neutrophil activity therefore ameliorating ARDS. [126], [127] Randomised controlled clinical trials and meta-analyses showed decreased morbidity upon vitamin D supplementation. [126] Another study showed improved clinical recovery including a shorter hospital stay, lower oxygen requirements and a reduction of inflammatory makers upon supplementation of either cholecalciferol or ergocalciferol during 5 days. [128] Nevertheless, it is important to note that other studies were unable to demonstrate a link between vitamin D deficiency and Covid-19 outcome or a beneficial effect of vitamin D supplementation. [129] Many clinical trials are still ongoing to understand the role of vitamin D in ARDS as well as the impact of vitamin D supplementation in patients. [130] Moreover, differences in the results could be caused by differences in classifying vitamin D deficient and non-deficient cases.

Animal studies revealed that the vitamin D signalling pathway could attenuate acute lung injury caused by LPS injection in rats by targeting Ang-2/Tie-2 and renin-angiotensin signalling pathways, which are tightly linked to an inhibition of inflammation and the maintenance of vascular permeability. [123], [131] In another study, VDR knockout mice showed a compromised barrier defence leading to severe

lung injury, thereby demonstrating an important role of vitamin D in maintaining the integrity of the epithelial barrier. An involvement of vitamin D in alveolar clearance and the formation of edema by alleviating epithelial Na^+ channel activity has also been reported. [123] Another study suggested that vitamin D supplementation reduced lung inflammation in vitamin D-deficient mice. [132] Taken together, the mechanism of vitamin D is yet not fully understood and further studies are needed.

1.5. Use of nanoparticles as novel therapeutic possibilities

1.5.1. Generalities

Over the past years, the use of nanotechnology in medicine has greatly advanced. Pharmaceutically, nanoparticles emerged as a promising drug delivery strategies in order to reduce drug toxicity and side effects with applications ranging from cancer and autoimmunity to cardiovascular, neurodegenerative, and pulmonary diseases. [133] Moreover, their use could also improve drug delivery into the brain due to their small size and possible capacity to cross the blood brain barrier. [134] The composition of nanoparticles is highly variable ranging from the use of biological substances such as albumin, gelatine and phospholipids for liposomes, to chemicals like polymers and solid metal-containing nanoparticles. [135] This wide range of compositions offers modifiable features like size, shape, charge, surface properties or even responsiveness therefore allowing optimised delivery for specific application. [136] Divided into three main categories, lipid-based, polymeric and inorganic nanoparticles, each one has its own advantages and disadvantages. [133] Polymeric nanoparticles allow the precise control of particle characteristics, flexibility in payload for hydrophilic and hydrophobic cargo and easy surface modification. However, there is a possibility for aggregation ad toxicity. Otherwise, inorganic nanoparticles have unique electrical, magnetic and optical properties, are variable in size, structure and geometry, and are well suited for theragnostic applications yet showing limitations in toxicity and solubility. Finally, lipid-based nanoparticles present a simple formulation with a range of physicochemical properties, high bioavailability and payload flexibility, but nonetheless displaying low encapsulation efficiency. [136] Nanoparticles can be engineered to create multivalent

and multifunctional entities finally improving their biological activity. [137] Indeed, formulations such as PEGylation, specific antibody conjugation or specific ligand binding to the nanoparticles open a opportunities of cell targeting thus avoiding effects on healthy cells. [138]

1.5.2. Inorganic-organic glucocorticoid nanoparticles

Long term administration of GCs is also associated with important side effects which could be reduced by using nanoparticles as carriers. In particular, PEGylated liposomes have been widely studied to deliver GCs, but despite their favourable drug release kinetics, [139] they also appeared to be involved in the activation of the complement system. [140] Polymeric micelles which are spherical, colloidal nanoparticles remaining soluble, [141] were also used to deliver GCs and enabled a slow release of the drug due to it protection from degradation. N-(2-hydroxypropyl) methacrylamide copolymers are another vehicle for of delivery of GCs and considered as polymer drug conjugates that retained immunosuppressive action [142] although not being biodegradable. [143] Inorganic carrier such as laponite were also used to deliver GCs however being characterized by a reduced drug load. [144]

To find an alternative to previously used nanoparticles, inorganic-organic hybrid nanoparticles (IOH-NPs) with the composition $[ZrO]^{2+}[R_{funct}(O)PO_3]^{2-}$ were developed. They contain the inorganic cation $[ZrO]^{2+}$ in an equimolar amount as the functional anion $[R_{funct}(O)PO_3]^{2-}$ which can be an active compound like betamethasone phosphate $[BMP]^{2-}$ or a fluorescent dye like flavin mononucleotide $[FMN]^{2-}$. One of the active forms this nanoparticle contains the GC betamethasone and is composed as followed: $[ZrO]^{2+}[(BMP)_{0.9}(FMN)_{0.1}]^{2-}$, referred as BMP-NPs. After formation the nanoparticles achieve a size of 30-40 nm and are characterised by a high content of the active drug reaching up to 90% of its total mass. [145] *In vitro*, the nanoparticles were preferably taken up by fibroblasts and macrophages via macropinocytosis. In macrophages the active form of the nanoparticle, BMP-NPs, induces a shift from a pro-inflammatory (M1) to an anti-inflammatory (M2) phenotype with a reduced expression of MHC class II and CD86 molecules. *In vivo*, IOH-NPs were located in abdominal organs such as liver,

small intestine and stomach after intraperitoneally injection in mice. [146] In a multiple sclerosis model, BMP-NP therapy lost its efficiency in mice lacking the GR in myeloid cells (GR^{lysM}) while a lack of the GR in T cells (GR^{lck}) or brain endothelial cells ($GR^{slco1c1}$) did not affect BMP-NPs treatment. [140] Most recently, BMP-NPs have been found to reduce morbidity, mortality and tissue damage in a totally MHC-mismatched mouse model of acute graft-versus-host disease (aGvHD). BMP-NPs administration could also delay the development of an adoptively transferred B cell lymphoma better compared to free betamethasone treatment, therefore suggesting that IOH-NPs administration could reduce the risk of relapse associated with GC therapy of aGvHD patients but still efficiently improve the disease. [147]

1.5.3. Calcitriol nanoparticles

Evidence that vitamin D could be used as a potent immunoregulator to potentially treat inflammatory disorders has increased over the past years. However, high doses of vitamin D could lead to hypercalcemia. Furthermore, the lipophilic nature of its active form calcitriol [148] make it difficult to administer due to insufficient solubility and limited membrane permeability. Therefore, the use of drug carrier such as metal oxide nanoparticles, polymer nanoparticles, biopolymer micelles as well as nano emulsions and liposomes could allow intravenous, oral or gastrointestinal administration. [149] In an earlier study, PEGylated calcitriol nanoparticles associated with antibodies were used to target macrophages via the specific endocytic receptor CD163. These lipid nanoparticles were able to reduce TNFα as well as HLA-DR expression in LPS induced human macrophages in vitro. In contrast, gene expression of IL-10 expression was upregulated. *In vivo*, those nanoparticles were shown to mainly accumulate in liver, spleen and kidneys. [150] In another study, calcitriol was encapsulated in Poly (lactic-co-glycolic acid) nanoparticles, which were evaluated in human pancreatic and lung cancer cell. This study highlighted the capacity of this drug vehicle to deliver vitamin D and demonstrated similar effects as free calcitriol in terms of decreased cell growth. In contrast, these calcitriol nanoparticle exerted an increased inhibitory effect on lung

cancer cells, inducing cell cycle arrest and majors changes in cell morphological features compared to free calcitriol. [151]

With a similar aim, calcitriol hybrid nanoparticles were developed by Claus Feldmann at the Karlsruhe Institute of Technology consisting of the active drug surrounded by a shell of ZrO_2^+ and phosphonopropionic acid (PPA). They have a diameter of 37±13 nm according to SEM analysis and a hydrodynamic diameter of 92±15 nm as determined by dynamic light scattering. Their synthesis is based on the precipitation of calcitriol nanoparticles via a solvent–antisolvent approach and achieved by adding a solution of consisting of calcitriol and the fluorescent dye lumogen Red (LR) in DMSO to water. The nanoparticles are stabilized by addition of the surfactant tocopherol phosphate. Since the resulting particles are not stable over long periods of time, a protective shell is built by further adding $ZrOCl_2$ and PPA, resulting in a layer of phosphate and carboxyl groups providing stabilization. Due to the presence of the enclosing shell, calcitriol cannot prematurely escape from the nanoparticles and, in addition, the agglomeration of the nanoparticles is prevented by electrostatic repulsion.

1.6. Objectives

The body is constantly confronted with environmental threats and sometimes the entry of pathogens can lead to severe inflammatory conditions such as sepsis or ALI. Both diseases are characterized by a dysregulated immune system which compromises homeostasis and induces multiple organ failure thus being potentially lethal diseases. Whereas pathophysiological changes in ALI are mostly confined to the lung, sepsis is an example of systemic inflammation affecting different organs including spleen, liver and lung. GCs are used in both conditions to reduce the excessive production of cytokines and other mediators and thereby to restore homeostasis within the immune system. Despite the benefits due to their anti-inflammatory activity, their application is also accompanied by major side effects. Besides GC, many studies have also shown a good efficiency of vitamin D in reducing inflammation in various disease models, although high doses could lead to side effects such as hypercalcemia, too. Collectively, new approaches that may allow to decrease the dose of GCs or vitamin D or to improve their efficiency, specificity and tolerability are urgently needed for both drugs. We have therefore hypothesized that the use of nanoparticles for drug delivery could solve these problems at least partially. This thesis is therefore aimed to investigate whether GC therapy using IOH-NP is beneficial in sepsis and ALI mouse models and to preliminary characterize vitamin D nanoparticles for a possible therapeutic use in inflammatory conditions.

To address these issues the thesis is divided into two parts:

- In the first part, the efficiency of the GC betamethasone either in its free form or encapsulated in IOH-NPs is investigated in the treatment of sepsis and ALI in mice.
- In the second part, the cell-type specificity, immunomodulatory activity, cellular uptake mechanism and intracellular fate of vitamin D nanoparticles are tested in cell culture to evaluate their suitability to treat inflammatory conditions.

2. Material and methods

2.1. Material

2.1.1. Instruments

Table 1: Instruments

Equipment	**Supplier**
Akku-jet® pro pipette controller	Brand GmbH, Wertheim
A-Plan 10x0.25 Ph objective	Zeiss, Jena
Axiovert 200M	Zeiss, Jena
BD FACS Canto II	BD Biosciences, Heidelberg
BioTek® Power Wave 340 Plate Reader	BioTek Instruments, Wetzlar
Cell Incubator, HERACell 240	Heraeus, Hanau
Centrifuge 2-5	Sigma Laborzentrifugen, Osterode
Centrifuge 5417R	Eppendorf, Hamburg
Centrifuge 5804R	Eppendorf, Hamburg
CONTOUR™ Next, Ascencia Blood Glucose Monitoring System	Bayer Healthcare AG, Leverkusen
CONTOUR™, Ascencia Blood Glucose Meter	Bayer Healthcare AG, Leverkusen
EasyPet 3	Eppendorf, Hamburg
EasySep™ Magnet	STEMCELL Technologies, SARL, Cologne

Electrophoresis chamber (Type 40-0708, Type 40-1214, Type 40-1410)	Peqlab Biotechnology, Erlangen
Electrophoresis power supply 301	Amersham Bioscience, Freiburg
Fluidigm BioMark™	Life Technologies Corporation, South San Francisco, California, USA
Freezer Hera freeze -80°C	Heraeus, Hanau
Freezer Liebherr Comfort -20°C	Liebherr-International Deutschland GmbH, Biberach an der Riss
Freezer VIP plus -150°C	SANYO Electri Co., Ltd., Moriguchi, Osaka, Japan
IFC Controller MX	Life Technologies Corporation, South San Francisco, California, USA
Infrared Lamp Balance 100W	Philips, Amsterdam, The Netherlands
Laminar airflow cabinet, HERASafe	Haraeus, Hanau
Microscope Telaval 31	Zeiss, Jena
Microtom SM2000R	Leica Biosystem, Wetzlar
Microwave R-212	Sharp, Osaka, Japan
Multichannel pipette S-12, 20-200µL	Brandt, Wertheim
Neubauer improved hemocytometer	Henneberg-Sander GmbH, Giessen-Lützellinden

Nunc™ Immuno Wash 12	Thermo Fischer Scientific, Wilmington, DE, USA
pH-Metre 766 Calimatic	Knick Elektronische, Messgeräte GmbH & Co. KG, Berlin
Photometer Nanodrop 2000	Peqlab Biotechnology, Erlangen
Pipettes Eppendorf Research plus 2.5µL, 20µL, 200µL, 1000µL	Eppendorf, Hamburg
Real-Time PCR System 7500	Applied Biosystems, Foster City, CA, USA
Rectal Probe, BIO-BRET-3	Bioseb, Vitrolles, France
Rodent thermometer BIO-TK8851	Bioseb, Vitrolles, France
Rotilabo®-mini-centrifuge	Carl Roth GmbH & Co. KG, Karlsruhe
Scale Acculab ALC-3100.2	Sartorius, Göttingen
Scale TE313S	Sartorius, Göttingen
Shaker GFL 3006/3005	Gesellschaft für Labortechnik, Burgwedel
Thermocycler Comfort	Eppendorf, Hamburg
Thermocycler Mastercycler EP Gradient	Eppendorf, Hamburg
Tissue Homogenizer Ultra Turrax T18 Basic	IKA, Staufen
Tissue Processor Excelsior ES	Thermo Fischer Scientific, Wilmington, DE, USA

Tissue Tek Prisma Slide Stainer	Sakura Finetek, Staufen
UV System with camera, Gel Imager (Chemostar)	INTAS, Science Imaging Instruments GmbH, Göttingen
VARIOMAG® Power direct magnetic stirrer	Thermo Fischer Scientific, Waltham, USA
Vortex Genie-2	Scientific Industries, Bohemia, New York, USA
Water bath W12	Labortechnik Medingen, Dresden
Water Purification System Arium Pro	Sartorius, Göttingen

2.1.2. Consumables

Table 2: Consumables

Consumable	**Supplier**
6-well, 12-well, 24-well Suspension Culture Plates Cellstar	Greiner bio-one GmbH, Frickenhausen
BD Micro-Fine™+ Demi U-100 Insulin Syringes (0.3mL, 30G)	BD Biosciences, Heidelberg
BD Microlance™ 3 (20G 1.5”)	BD Biosciences, Heidelberg
BD Microstainer® SST™ tubes	BD Biosciences, Heidelberg
Cannula Sterican 24G (0.55 x 25mm) (ALI to remove?)	B. Braun Melsungen AG, Melsungen

CELLSTAR Culture Flasks 75cm^2, 175 cm^2	Greiner bio-one GmbH, Frickenhausen
CELLSTAR PS 100 x 20 mm Cell Culture Dishes	Greiner bio-one GmbH, Frickenhausen
CELLSTAR serological pipettes 5mL, 10mL, 25mL	Greiner bio-one GmbH, Frickenhausen
CryoTube™ Vials	Nunc, Rosklide, Denmark
EASYstrainer^{TM} (40µm, 100µm)	Greiner bio-one GmbH, Frickenhausen
Falcon Tubes (15mL, 50mL)	Greiner bio-one GmbH, Frickenhausen
Fluidigm 48.48 Dynamic Array^{TM} IFC	Life Technologies Corporation, South San Francisco, California, USA
Fluidigm Control line fluid	Life Technologies Corporation, South San Francisco, California, USA
Glas pipettes (10mL, 25mL)	Brand GmbH, Wertheim
Hypodermic needle Sterican® 26G x 0.5, 24G x 1	B. Braun Melsungen AG, Melsungen
Microscope Cover Slips, 24 x 60mm	Menzel-Gläser, Braunschweig
Microscope Slides SuperFrost Plus	Menzel-Gläser, Braunschweig
Multiply® Pro 8-Strip PCR Microtubes	Sarstedt, Nümbrecht
Nitril® Next Gen® single-use gloves	Meditrade®, Kiefersfelden

Nunc-Immuno™ Microwell™ 96 well plates	eBioscience, Sna Diego, USA
Optical adhesive Covers	Applied Biosystems, Foster city, USA
Parafilm	Bemis, Neeth, WI, USA
Pipette tips (2.5µL, 200µL, 1000µL)	Greiner bio-one GmbH, Frickenhausen
PCR reaction tube Multiply® -µStrip Pro 8-Strip	Sarstedt, Nümbrecht
Pipette tips, 2.5µL, 200µL, 1000µL	Greiner bio-one GmbH, Frickenhausen
Reaction tubes (1.5mL, 2mL)	Greiner bio-one GmbH, Frickenhausen
Saphire Microplate, 96 well, natural for PCR	Greiner bio-one GmbH, Frickenhausen
Syringe BD Discardit™ II (2mL, 5mL)	BD Biosciences, Heidelberg
Tissue Cassettes MacrOflow	Th. Geyer GmbH & Co. KG, Renningen

2.1.3. Reagents and chemicals

Table 3: Reagents and chemicals

Chemical/Reagent	**Supplier**
3,3', 5,5'-Tetramethylbenzidin	Sigma-Aldrich Chemie GmbH, Taufkirchen

Assay Loading Reagent 2 ×	Life Technologies Corporation, South San Francisco, California, USA
BD FACS Clean solution	BD Biosciences, Heidelberg
BD FACS Flow Sheath fluid	BD Biosciences, Heidelberg
BD FACS Shutdown solution	BD Biosciences, Heidelberg
Betamethasone phosphate nanoparticles (BMP-NPs)	Prof. Dr. Klaus Feldmann, Institute of Inorganic Chemistry KIT, Karlsruhe [146]
Bovine serum albumin	Carl Roth GmbH & Co.KG, Karlsruhe
Calcitriol	Hycultec GmbH, Beutelsbach
Calcitriol Nanoparticles (VDa-NPs)	Prof. Dr. Klaus Feldmann, Institute of Inorganic Chemistry KIT, Karlsruhe
Celestan soluble 4 mg/ml (betamethasone-dihydrogenphosphat-dinatrium)	MSD Sharp & Dohme GmbH, Haar
Chloroform	Sigma-Aldrich Chemie GmbH, Taufkirchen
Cholecalciferol Nanoparticles (VDi-NPs)	Prof. Dr. Klaus Feldmann, Institute of Inorganic Chemistry KIT, Karlsruhe
Citric acid	Carl Roth GmbH & Co.KG, Karlsruhe
Dimethylsulfoxid 99.8%	Carl Roth GmbH & Co.KG, Karlsruhe
Disodium hydrogen phosphate	Carl Roth GmbH & Co.KG, Karlsruhe
Dithiothreitol	Sigma-Aldrich Chemie GmbH,

	Taufkirchen
DNA Binding Dye 20 ×	Life Technologies Corporation, South San Francisco, California, USA
Empty inorganic-organic hybrid nanoparticles (EP-NPs)	Prof. Dr. Klaus Feldmann, Institute of Inorganic Chemistry KIT, Karlsruhe [146]
Ethanol 99.8%	Carl Roth GmbH & Co.KG, Karlsruhe, Chemsolute® Th. Geyer GmbH & Co. KG, Renningen
Ethidiumbromide solution	Carl Roth GmbH & Co.KG, Karlsruhe
Ethylendiaminetetraacedic acid	Sigma-Aldrich Chemie GmbH, Taufkirchen
F-518 Phusion® HF buffer with 7.5 mM magnesiumchlorid	Thermo Fischer Scientific, Waltham, USA
Fetal calf serum	Abbvie, Ludwigshafen
Gene Ruler 1kb DNA ladder	Thermo Fischer Scientific, Waltham, USA
Gibco® 0.25 % Trypsin - EDTA (1x)	Thermo Fischer Scientific, Waltham, USA
Gibco® 2-Mercaptoethanol	Thermo Fischer Scientific, Waltham, USA
Glycerol	Carl Roth GmbH & Co.KG, Karlsruhe

Hydrogen Peroxide 30%	Carl Roth GmbH & Co.KG, Karlsruhe
Neomycin trisulfate salt hydrate	Sigma-Aldrich Chemie GmbH, Taufkirchen
Nucleoside triphosphate	Genaxxon bioscience, Ulm
OptiLyse® B Lysing solution	Beckman Coulter, Inc., France
Orange G sodium salt	Sigma-Aldrich Chemie GmbH, Taufkirchen
Paraffin wax	Sigma-Aldrich Chemie GmbH, Taufkirchen
pegGOLD Universal Agarose	Peqlab Biotechnology GmbH, Erlangen
Penicillin/ Streptomycin (10.000 U/ml)	Invitrogen, Carlsbad, CA, USA
Potassium chloride	Merck KGaA, Darmstadt
Potassium dihydrogen phosphate	Merck KGaA, Darmstadt
Power SYBR® Green Master Mix	Applied Biosystems, Foster City, USA
QIAzol™ Lysis Buffer	Qiagen, Hilden
Roti Histofix 4 % pH 7 (4 % Paraformaldehyde)	Carl Roth GmbH & Co.KG, Karlsruhe
Sodium carbonate	Merck KGaA, Darmstadt
Sodium chloride, 99.5 % p.a.	Carl Roth GmbH & Co.KG, Karlsruhe
Sodium hydrogen carbonate	Merck KGaA, Darmstadt

SsoFast EvaGreen Supermix with low ROX 2 ×	Bio-Rad Laboratories GmbH, Munich
TaqMan® PerAmp Master mix 2 ×	Applied Biosystems, Foster City, USA
Tween® 20%	Carl Roth GmbH & Co.KG, Karlsruhe

2.1.4. Buffers

Table 4: Buffers

Buffer	**Component**
ELISA Assay Diluent	ELISA Assay Diluent
ELISA Coating buffer (0.1 M Sodium carbonate)	1000 ml ddH_2O 8.4 g $NaHCO_3$ 3.56 g Na_2CO_3 pH 9.5
ELISA Developing solution	ELISA Substrate buffer 1 % TMB in DMSO 0.2 % H_2O_2
ELISA Stop solution	1 M H_2SO_4 in ddH_2O
ELISA Substrate buffer	0.1 M Citric acid 0.2 M Na_2HPO_4 in ddH_2O
ELISA Washing buffer	0.05 % Tween ®

	20 % in PBS
FACS buffer	0.1 % BSA 0.01 % Sodium acid in PBS, pH 7.2
MACS buffer	10 mL FCS 1 mL EDTA In 500 mL PBS
Orange G Loading dye	100 ml ddH_2O 100 mg Orange G sodium salt 30 % Glycerol
PBS/ BSA	0.1 % BSA 0.2 in PBS
Phosphate saline buffer pH 7.2 (PBS)	137 mM NaCl 2.7 mM KCl 10 µM Na_2HPO_4 2 mM KH_2PO_4 in ddH_2O
TAC buffer	20 mM Tris 155 mM NH_4Cl in ddH_2O
TAE buffer	40 mM Tris 20 mM Acetic acid 1 mM EDTA in ddH_2O

2.1.5. Mouse primers

Table 5: Mouse primers

Gene	Sequence 5´- 3´ Foward/Reverse
Aldoa	CAGATGGGTCCAGCTTCAAC
	TGCTTTCCTTTCCTAACTCTGTC
Arg1	AGCCCGAGCACATGCAGCAG
	ACCCCTCCTCGAGGCTGTCCT
Ccl2	AGCTGTAGTTTTTGTCACCAAGC
	GACCTTAGGGCAGATGCAGT
Ccl3	ATATGGAGCTGACACCCCGA
	TCAGGAAAATGACACCTGGCTG
Ccl7	CCCTGGGAAGCTGTTATCTTCAA
	CTCGACCCACTTCTGATGGG
Cd163	TGGTCCAGGAACTGGGCCCA
	GGGTGGGGTGACCTGTGCCA
Cd18	CCCAGGAATGCACCAAGTACA
	AGTGAAGTTCAGCTTCTGGCAC
Cd206	TCCGAAATGTTGAAGGGAAG
	ATTATTCCAAAGGCCCGAAG
Cox2	ATGGGTGTGAAGGGAAATAAGGA
	ATTTGAGCCTTGGGGGTCAG
Cxcl1	ACCGAAGTCATAGCCACACTC
	CTCCGTTACTTGGGGACACC

Cxcl3	CCAGCACAGAAGTCATAGCCAC
	CTTCATCATGGTGAGGGGCTT
Cxcl5	TGCCCTACGGTGGAAGTCAT
	AGCTTTCTTTTTGTCACTGCCC
Cxcl9	GCCATGAAGTCCGCTGTTCT
	TAGGGTTCCTCGAACTCCACA
Cxcl10	CCACGTGTTGAGATCATTCC
	TCACTCCAGTTAAGGAGCCC
Cxcl11	CAGCTGCTCAAGGCTTCCTTA
	CTTTGTCGCAGCCGTTACTC
Dusp1	CTCCAAGGAGGATATGAAGCG
	ACTAGTACTCAGGGGGAGGC
Glut1	AGGTACTTCGAGAAGGCAGG
	ACAACAAACAGCGACACCAC
Glut3	CTCTTCAGGTCACCCAACTACGT
	CCGCGTCCTTGAAGATTCC
Gmcsf	CAGGGTCTACGGGGCAATTT
	ACAGTCCGTTTCCGGAGTTG
Hk2	GCCTCGGTTTCTCTATTTGGC
	ATACTGGTCAACCTTCTGCACT
Hprt	GTCCTGTGGCCATCTGCCTA
	GGGACGCAGCAACTGACATT

Il10	AGGCAGAGAAGCATGGCCCAG
	CGGGAGAAATCGATGACAGCGCC
Il1b	CTCATCTGGGATCCTCTCCA
	AAGCAGCCCTTCATCTTTTG
Il6	AGTTGCCTTCTTGGGACTGA
	CAGAATTGCCATTGCACAAC
Nox2	TCACCTTCGAGGGCAGCCGA
	TCCGTGGCAAAGCGAGCCAG
Sphk1	ACAGTGGGCACCTTCTTTC
	CTTCTGCACCAGTGTAGAGGC
Tlr2	CTGGAGCATCCGAATTGCA
	CATCCTCTGAGATTTGACGCTTT
Tlr4	TGGTTGCAGAAAATGCCAGG
	TAGGAACTACCTCTATGCAGGG
Tnfa	ATGGCCTCCCTCTCATCAGT
	CTTGGTGGTTTGCTACGACG
Ym1	ACTTTGATGGCCTCAACCTG
	AATGATTCCTGCTCCTGTGG

2.1.6. Human primers

Table 6: Human primers

Gene	Sequence 5´- 3´ Foward/Reverse
18SRNA	TCCAGGTCTTCACGGAGCTT
	GGATGTAAAGGATGGAAAATACA
CD163	GCAGTTTCCTCAAGAGGAGAGAA
	ATGGCCTCCTTTTCCATTCCA
CD25	GTGGTGGGGCAGATGGTTTA
	TTGTGACGAGGCAGGAAGTC
GLUT1	TGGCATCAACGCTGTCTTCT
	AGCCAATGGCATACACA
GLUT3	GGACGTGGAGAAAACTTGCTG
	TCAGAGCTGGGGTGACCTTC
HK2	CCTCCCCTCTCGCGTCT
	AGAGATACTGGTCAACCTTCTGC
IL6	TCAATATTAGAGTCTCAACCCCCA
	TTCTCTTTCGTTCCCGGTGG
NOS2	CGCATGACCTTGGTGTTTGG
	CATAGACCTTGGGCTTGCCA
LDHA	ACGTGCATTCCCGATTCCTT
	AACAGCACCAACCCCAACAA
PFKFB3	CAGCTGCCTGGACAAAACAT
	CGTCTGCCTCAGTGTTTCCT

SLC7A5	TGAGCAGCACGCAG TCATCGCAGTACATCGTGGC
TNFA	GCCCATGTAGCAAACCC TATCTCTCAGCTCCACGCCA

2.1.7. Anti-mouse fluorochrome-conjugated monoclonal antibodies

Table 7: Anti-mouse fluorochrome-conjugated monoclonal antibodies

Antigen	**Fluorescent dye**	**Clone name**	**Supplier**
B220	APC-Cy7	RA3-6B2	BD Biosciences
CD3	PerCP	17A2	BD Biosciences
CD4	APC	RM4-5	BioLegend
CD49b	PE	R1-2 to check	BD Biosciences
CD8	PE-Cy7	53-6.7	BioLegend
CD11b	PE-Cy7	M1/70	BD Biosciences
F4/80	FITC	BM8	BioLegend
Gr1	APC-Cy7	RB6-8C5	BioLegend
Ly6C	APC-Cy7	HK1.4	BioLegend
Ly6G	APC	1A8	BioLegend

2.1.8. Anti-human fluorochrome-conjugated antibodies

Table 8: Anti-human fluorochrome-conjugated antibodies

Antibody	Fluorescent dye	Clone name	Supplier
CD14	PE-Cy7	HCD14	BioLegend
CD163	PE	GHI/61	BioLegend
CD25	APC-Cy7	BC96	BioLegend
HLA-DR	Alexa488	L243	BioLegend

2.1.9. Pharmacological inhibitors

Table 9: Pharmacological inhibitors

Inhibitor	Final concentration	Inhibited pathway	Supplier
Cytochalasin D	1 µg/ml	Phago/ Macropinocytosis	Sigma-Aldrich Chemie GmbH, Taufkirchen
Monodansylcadaverine	150 µM	Clathrin-mediated endocytosis	Sigma-Aldrich Chemie GmbH, Taufkirchen

2.1.10. Cell trackers

Table 10: Cell trackers

Dye	Specificity	Fluorescent dye properties	Dilution	Supplier
Lysotracker® deep red	Acidic organelles	Exc.: 647 nm, Em.: 668 nm	1:20.000	Thermo Fischer Scientific, Waltham, USA
Mitotracker® deep red	Mitochondria	Exc.: 644 nm, Em.: 665 nm	1:20.000	Cell Signaling Technologies, Cambridge, UK

2.1.11. Cell lines

Table 11: Cell lines

Cell line	Origin	Mouse strain	Culture medium	Supplier
C2C12	Myoblasts	C3H	DMEM^{++}	ATCC
L929	Fibroblasts from connective tissue	C3H/An	DMEM^{++}	Prof. Dr. Jan Tuckermann, Ulm University
LA-4	Alveolar epithelial cells type II	A/He	NutMix^{++}	Sigma-Aldrich Chemie GmbH, Taufkirchen

MH-S	Alveolar macrophages	BALB/c	RPMI^{+++}	Prof. Dr. Frauke Alves, MPI -EM, Göttingen
RAW 264.7	Derived macrophages	BALB/c	DMEM++	Kindly provided by Prof. Dr. Carsten Lüder, UMG
WEHI 231	Immature B lymphocyte	BALB/c/NZB	DMEM++	Prof. Dr. Marco Herold, WEHI Institute, Melbourne, Australia
WEHI 7.15	T lymphocytes (thymus)	BALB/c	DMEM++	ATCC

2.1.12. Media

Table 12: Media

Medium	**Supplier**
Gibco® DMEM + GlutaMAX™ 1 x/phenol free	ThermoFischer Scientific, Waltham, USA
Gibco® F-12 NutMix	ThermoFischer Scientific, Waltham, USA
Gibco® RPMI1640 + GlutaMAX™ 1 x	ThermoFischer Scientific, Waltham, USA

2.1.13. Supplemented media

Table 13: Supplemented media

Supplemented media	Component
DMEM^{++} and RPMI^{++}	DMEM/ RPMI1640, 10 % FCS, 1 % Penicillin/ Streptomycin
RPMI^{+++}	RPMI1640, 10% FCS, 1 % Penicillin/ Streptomycin, 0.05 mM 2-Mercaptoethanol
F-12 NutMix^{++}	F-12 NutMix, 15 % FCS, 1 % Penicillin/ Streptomycin

2.1.14. Commercial kits and enzymes

Table 14: Commercial kits and enzymes

Commercial kit	Manufacture
CellTiter 96® AQeous One Solution Cell Proliferation Assay Kit	Promega, Madison, WI, USA
EasySep™ negative selection human monocytes isolation Kit	STEMCELL Technologies SARL, Cologne
ELISA MAX™ Standard Set Mouse IL-6	BioLegend, San Diego, USA

ELISA MAX™ Standard Set Mouse IL-1β	BioLegend, San Diego, USA
ELISA MAX™ Standard Set Mouse MCP1	BioLegend, San Diego, USA
ELISA MAX™ Standard Set Mouse TNFα	BioLegend, San Diego, USA
iScript™ cDNA Synthesis Kit	Bio-Rad Laboratories GmbH, Munich
Qiagen RNeasy Plus Universal Mini Kit	Qiagen, Hilden
Quick-RNA™ MiniPrep	Zymo Research Epigenetics, Irvine, USA

2.1.15. Softwares

Table 15: Softwares

Software	**Company**
7500 System SDS Software version 1.4.0.25	Applied Biosystems, Foster City, CA, USA
BD FACS DivaTM Software version 6.1.2	BD Biosciences, Heidelberg
BioMark™ Data collection software	Life Technologies Corporation, South San Francisco, California, USA
BioMark™ Real-Time PCR analysis software	Life Technologies Corporation, South San Francisco, California, USA
BioTek® Gen 5 version 1.09.8	BioTek Instruments, Bad Friedrichshall
FlowJo version 10.6.2	Tree Star, Inc., Ashland, USA

GraphPad Prism 5	GraphPad Software, La Jolla, CA, USA
Nanodrop 2000	Thermo Scientific, Wilmington, WA, USA

2.2. Methods

2.2.1. Mice and housing conditions

C57BL/6J wild type mice used for the experiments were purchased from Janvier Labs located in Le Genest-Saint-Isle, France.

All mice were kept in the central animal facility of the University Medical Center Göttingen, and housed under specific-pathogen-free conditions (SPF) in individually ventilated cages (IVC) in a 12 hours light/dark cycle. Food and water were supplied *ad libitum*. Mice were aged between 12 to 16 weeks.

Female wild type C57BL/6 were used to study the impact of different glucocorticoids treatment on the pathogenic features of septic shock and acute lung injury.

All animal experiments were performed according to national and international guidelines and approved by the responsible authority (*Niedersächsiches Landesamt für Verbraucherschutz und Lebensmittelsicheheit*).

2.2.2. The septic shock mouse model

To induce septic shock, 10 mg/kg bodyweight of LPS were injected intraperitoneally (i.p) and 45 minutes later, 10 mg/kg of either free betamethasone or BMP-NPs were injected i.p. Control mice received an injection with an equal volume of PBS instead of LPS. The mice were then sacrificed 13 to 15 hours after the first injection.

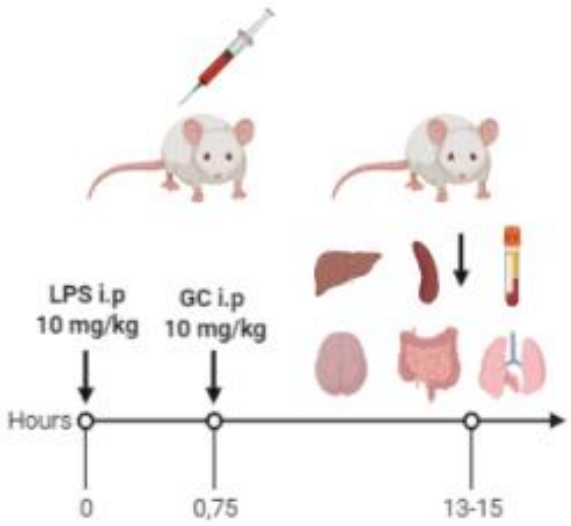

In this model, body temperature and blood glucose levels were measured and blood for FACS analysis was collected before sacrifice. After sacrifice, blood for serum preparation as well as brain, lung, liver, spleen, colon and small intestine for further analyses were sampled.

Figure 4: Sepsis induction protocol (created using Biorender)

2.2.3. The acute lung injury mouse model

To induce septic shock, 10 mg/kg bodyweight of LPS were injected intraperitoneally (i.p). Thirty minutes later, 2.6 µL/g bodyweight of 10% OA diluted in PBS/BSA were injected intravenously (i.v) and 15 minutes later, 10 mg/kg of either free betamethasone or BMP-NPs were injected i.p. Healthy control mice received injections with an equal volume of PBS instead of LPS. The mice were then sacrificed 13 to 15 hours after the first injection.

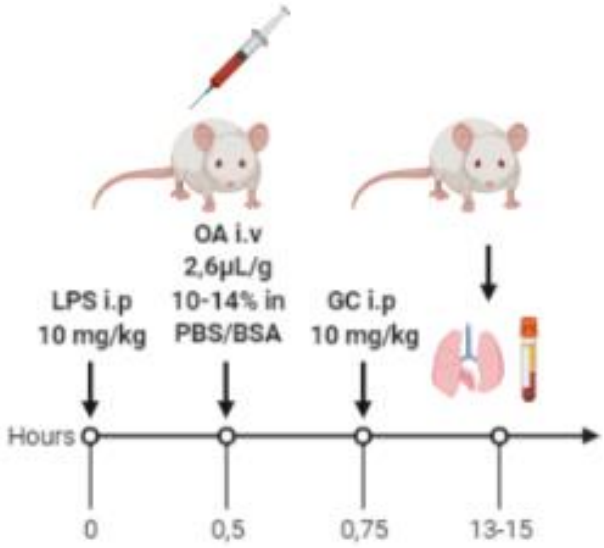

After sacrifice, blood, bronchoalveolar lavage fluid (BALF) and lung samples were collected for further analyses.

Figure 5: Acute Lung Injury induction protocol (created using Biorender)

2.2.4. *In vivo* and *ex vivo* analyses of mice

2.2.4.1. Body temperature

The body temperature of mice was measures with a rodent BIO-TK8851 thermometer, which was equipped with a BIO-BRET-3 rectal probe.

2.2.4.2. Blood Glucose level

The blood glucose level was measured with Ascencia CONTOUR and CONTOUR NEXT test stripes and the corresponding Ascencia CONTOUR blood glucose monitoring system. The tail vein from the mice was puncture and the blood drop obtained was analysed with the automated device.

2.2.4.3. Flow cytometric characterization of the cellular composition of immune cells in the blood

After the 13 to 15 hours of treatment, the tip of the tail from the mice was cut in order to obtain around 8 to 10 drops of blood. Those were collected in ELSEVIER Buffer in FACS tubes and centrifuged at 350 g for 5 min. After discarding the supernatant, the cell pellet was washed twice with FACS buffer and centrifuged before staining. To analyse the lymphocyte population the antibody combination 1 was applied on each sample for 20 minutes and to analyse myeloid cells the combination 2 was applied. Both antibody combinations are presented in the table below.

Table 16: FACS panels 1 and 2 for mouse immune cells analysis

Combination 1 – Blood lymphocytes	**Combination 2 – Blood myeloid cells**
CD49b PE	F4/80 FITC
CD3 PerCP	CD11b PE-Cy7
CD8 PE-Cy7	Ly6G APC
CD4 APC	Ly6C APC-Cy7

B220 APC-Cy7

Following staining, the cells were washed with FACS buffer and centrifuged. Cells were then incubated at RT in the dark after the addition of 100 µL Optilyse solution. After a first phase of incubation, distillated water was added untill a volume of 1 mL, and the incubation continued for 1-2 hours in the dark. After a final step of washing with FACS buffer and centrifugation, the cell suspension was ready to be analyse by FACS using the BD FACS Canto II flow cytometer and the following gating strategy using FlowJo software.

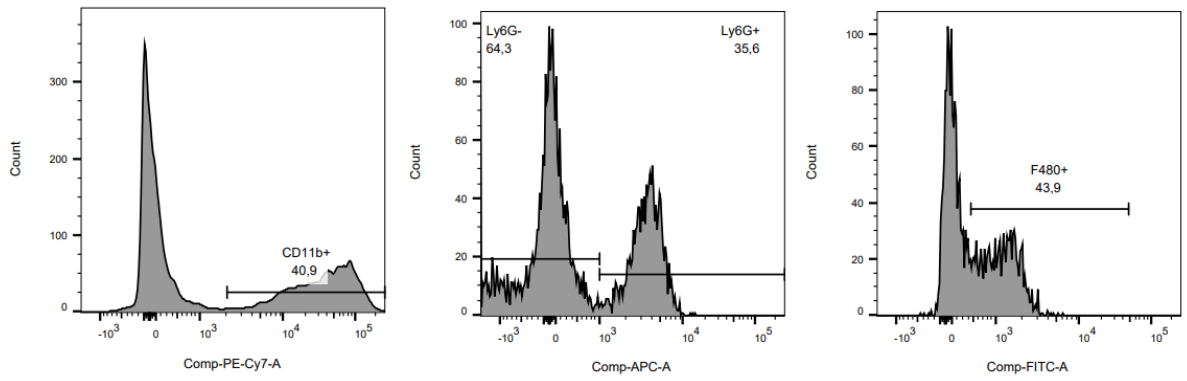

Figure 6: Flow cytometry gating strategy for the analysis of blood myeloid cells

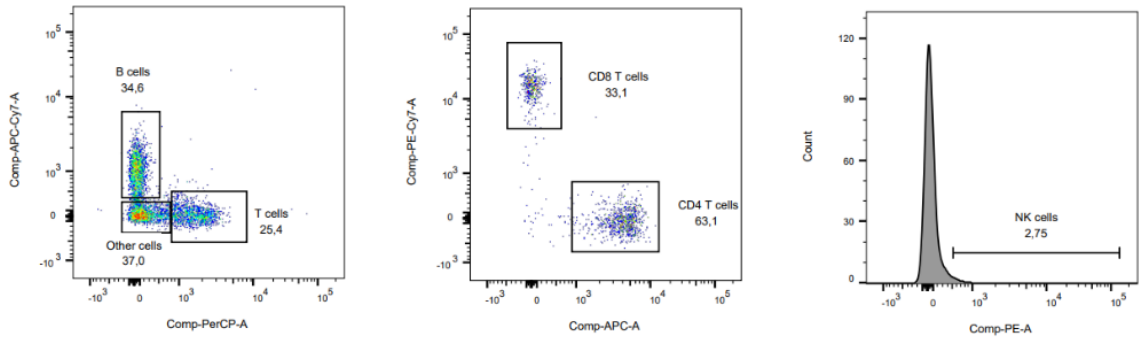

Figure 7: Flow cytometry gating strategy for the analysis of blood lymphocytes

2.2.4.4. Bronchoalveolar lavage and flow cytometry characterization of immune cells in the lung

To prepare infiltrating immune cell in the lung, bronchoalveolar lavage was performed. To insert a venous catheter into the trachea, the thoracic cavity of the mice was opened to expose it. The trachea was then sealed by sutures on the venous catheter to prevent leakage. The lungs were gently flushed 5 times with 1 mL of PBS and the liquid collected after each flush. Between 3 and 4 mL of BALF was obtained in total and centrifuged at 350 g for 7 min to obtain the cell pellet. Afterwards, an erythrolysis step was perfomed. To this end, the cells were resuspended in 2 mL PBS and then 12 mL of TAC buffer were added. After 12 min of incubation, 20 mL of FACS buffer were added and the samples were centrifuged again. To analyse the cellular composition of the BALF, the obtained cells were stained in a total volume of 200 µL by incubation for 20 min with 20 µL of each of the antibodies indicated in the following table before being wash with 4 mL of FACS buffer and centrifuged.

Table 17: FACS panel 3 for mouse immune cells analysis

Combination 3 – BALF cells
CD11b PE-Cy7
F4/80 FITC
GR1 APC-Cy7

After removing the supernatant, the stained cells were ready for analysis using the BD FACS Canto II flow cytometer in combination with FlowJo software following the gating strategy indicated below.

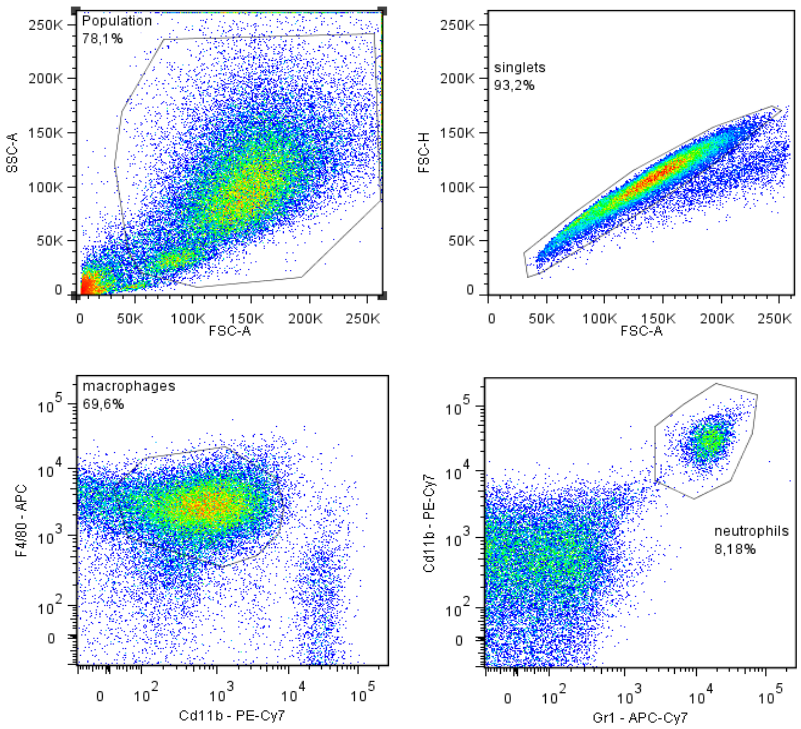

Figure 8: Flow cytometry gating strategy for the analysis of BALF cells

2.2.4.5. Serum collection and analysis

2.2.4.5.1. Serum collection

After sacrifice of the mice, heart puncture was realised with a 24G needle to collect the blood in BD Microstainer SST tubes. After 30 min incubation at RT, the samples were centrifuged at 14.000 x g for 2 min to separate blood cells and serum. The latter was stored at -20°C for further analysis.

2.2.4.5.2. Enzyme-linked Immunosorbent Assay

Cytokine and chemokine concentrations in the serum were analysed by using different Enzyme Linked Immunosorbent Assay (ELISA) kits according to the manufacturer's instruction. The employed ELISA kits and the respective dilution factor of the serum samples are listed in the following table.

Table 18: ELISA kits used for serum analyses

ELISA kit	Dilution factor of the sample
IL-1β	1:5 (20µL sample + 80µL assay diluent)
IL-6	1:100 (1µL sample + 99µL assay diluent)
MCP-1	1:100 (1µL sample + 99µL assay diluent)
TNFα	1:2 (50µL sample + 50µL assay diluent)

Nunc-Immuno™ 96-well plates were coated with 100 µL of the corresponding capture antibody, previously diluted in coating buffer. The plate was incubated in the dark at 4°C overnight. The next morning, the plate was washed and 200 µL of assay diluent were added to prevent unspecific binding and incubation was realised for 1 hour at RT on a shaker. Afterwards, a second washing step was realised and the standards as well as the samples were added according to the previous dilution table corresponding to each kit. Incubation lasted for 2 hrs at RT on a shaker. Washing was repeated, 100 µL of the respective detection antibody diluted in assay diluent was added to each well and incubated for 1 hour on a shaker at RT. After another washing step, 100 µL of Horse Radish Peroxidase (HRP) were added and the plate was incubated for another 30 min. Intensive washing was then realised by leaving the washing solution for 30 s each time before sucking it off. Finally, 100 µL of ELISA avidin solution diluted in assay diluent was added and incubation performed for 15 to 30 min in the dark before the final addition of 50 µL of ELISA Stop solution. Colour change was measured by spectrometry at 450 nm and 570 nm.

2.2.4.5.3. Nitrite assay using Griess reagent

Standards were first prepared from a sodium nitrite stock solution of 2 mM and diluted in RPMI medium. The standards ranged from 125 µM to 0.98 µM with a factor 2 dilution between each. 50 µL of the standards and samples were pipetted in a Nunc-Immuno™ 96-well plates. Samples were added in a 1:5 dilution (10 µL sample + 40 µL of RPMI mdium). Next, 50 µL of 1% sulphanilamide in 2.5% phosphoric acid were added in each well and the plate iwas ncubated for 5 min at RT. Finally, 50 µL of N-Naphtyl-ethylen-diamin-dihydrochlorid were pipetted into the wells following a 5 min incubation at RT. Absorption was then measured at 540 nm by spectrophotometry.

2.2.4.6. Molecular analyses

2.2.4.6.1. RNA Isolation

The Qiagen RNeasy Plus Universal Mini Kit was used according to the manufacturer's instructions to extract total RNA from different mouse tissues. In brief, frozen tissues were mixed with 900 µL QIAzol™ Lysis buffer in 12 mL tubes and homogenized using the tissue homogenizer Ultra Turrax T18 basic. The obtained solution was transferred into a 1.5 mL microtube followed by the addition of 100 µL of gDNA eliminator solution. Tubes were vortexed for 15 s before the addition of 180 µL chloroform and then vortexed a second time for 15 s. Tubes were centrifuged at maximal speed for 15 min at 4°C. The upper phase of around 600 µL was pipetted into new microtubes and mixed with 600 µL of 70% ethanol. After mixing, 600 µL of the sample mixture was transferred onto the RNeasy-Mini column and centrifuged for 20 s at RT at maximal speed. The flowthrough was then discarded. This step was repeated a second time with the rest of the sample mixture. 700 µL of RWT buffer were pipetted onto each column and centrifugation was done for 20 s at RT and 10,000 rpm. The flowthrough was again discarded and 500 µL of RPE buffer was added onto the column. The sample was then centrifuged a first time for 2 min at 10,000 rpm, the flowthrough was discarded and a second step of centrifugation for 1 min was eventually realised in order to dry the column. To eluate the sample, 35 µL of RNase free water were added onto the column and the sample was centrifuged for 1 min at 10,000 rpm. This step was repeated once

again before the RNA concentration was determined by measuring the absorption at 260 nm with the Nanodrop 2000 photometer. The purity of the sample was checked through detection of protein and organic contamination at 280 nm and 230 nm. RNA quality was controlled by controlling the characteristic bands of 18S and 28S rRNA in a ratio 1:2 on an agarose gel. To this end, 0.5µg RNA, 5 µL Orange G and ddH_2O, adjusted to a volume of 20 µL, were loaded on a 1% TAE agarose gel.

2.2.4.6.2. cDNA Synthesis

Starting from total RNA, cDNA was produced using the iScript™ cDNA Synthesis Kit according to the manufacturer's instructions. In brief, 1 µg of the RNA adjusted to a volume of 15.75 µL was mixed with 4 µL of iScript buffer and 0.25 µL of reverse transcriptase. The samples were incubated for 5 min at RT, followed by an incubation step of 30 min at 42°C and finally by a 5 min incubation step at 85°C.

2.2.4.6.3. Polymerase Chain Reaction

The success of the cDNA production was verified by performing a Polymerase Chain Reaction (PCR) using hypoxanthine guanine phosphoribosyl transferase (HPRT) as a housekeeping gene. The PCR reaction mix was prepared as indicated in the following table.

Table 19: Mastermix for test PCR reaction

Volume (in µL)	**Dilution factor of the sample**
12,7	ddH_2O
4	Phusion Reaction Buffer HF
1	HPRT mix 10 µM (primer forward + primer reverse)
1	dNTPs (5 mM)
1	cDNA sample

0,3	PfuS DNA Polymerase

Once the reaction mix was prepared for each sample, the PCR was conducted using a Thermocycler Mastercycler EP Gradient pplying the program shown in the following table.

Table 20: PCR reaction program

Step	Time	Temperature (in °C)	Cycle
Denaturation I	2 min	98.5	1
Denaturation II	20 s	98.5	
Annealing	15 s	64	30
Elongation I	20 s	72	
Elongation II	2 min	72	1

The reaction product obtained in the PCR was then mixed with 7 µL of Orange G before being loaded on a 1% TAE agarose gel.

2.2.4.6.4. Quantitative RT-PCR

To quantify gene expression, quantitative RT-PCR was performed. To this end, 24 µL of a prepared mastermix, as shown in the table below, was added to 1 µL of the respective cDNA sample in Saphire 96-well microplates.

Table 21: Mastermix for qRT-PCR

Volume (in µL)	**Reagent**
12,5	Power SYBR-Green PCR Mastermix
11	ddH_2O
0,5	Primermix 10 µM (primer forward + primer reverse)

Once the plate was loaded, it was put in the Real-Time PCR System 7500 and analyzed using the qRT-PCR program indicated in the table below.

Table 22: qRT-PCR programm

Step	**Time**	**Temperature (in °C)**	**Cycle**
Activation	2 min	50	1
Denaturation	10 min	95	1
Denaturation	15 s	95	40
Annealing and Elongation	1 min	60	
	15 s	95	1
Dissociation stage	1 min	60	
	15 s	95	

The relative expression of each gene was calculated in relation to the housekeeping gene *Hprt* (for mice) by using the ΔΔCT method.

2.2.4.6.5. Fluidigm® gene chip analysis

2.2.4.6.5.1. Preamplification using TaqMan Preamp Master Mix

Preparation of cDNA was done as described in chapter 2.2.4.6.2. above. In a microtube, 1 µL of each 100 µM primer pair were added and supplemented with DNA Susupension Buffer to reach a final volume of 200 µL in order to create the pooled STA (Specific Target Amplification) master mix.

Subsequently, the following premix was prepared as presented in the table below.

Table 23: Preamplification reaction solution using TaqMan PreAmp Master Mix

Component	**Volume per reaction (µL)**	**Volume for 48 reactions w/Overage (µL)**
2x TaqMan PreAmp Master Mix (Life Technologies PN4391128)	2.5	132.0
Pooled STA Master Mix	0.5	26.4
DNase-free water	0.75	39.6
cDNA	1.25	-

To this end, 1.25 µL of each cDNA sample were added in PCR tubes and supplemented with 3.75 of the previously prepared TaqMan PreAmp Master Mix presented in Table 23.

The tubes were then place in the ThermoCycler using the following PCR program:

Table 24: Thermal cycling conditions for preamplification reaction

Step	**Time**	**Temperature (in °C)**	**Cycle**
Hold	10 min	95	1
Denaturation	15 s	95	14

Annealing/Elongation	4 min	60

2.2.4.6.5.2 Clean up reaction with Exonuclease I

Initially, the following reaction mix was prepared:

Table 25: Diluted Exonuclease I mix

Component	**Volume per reaction (µL)**	**Volume for 48 reactions w/Overage (µL)**
DNase free water	1.4	84.0
Exonuclease I Reaction Buffer (New England BioLabs®, PN M0293S or PN M0293L)	0.2	12.0
Exonuclease I, 20 U/µL	0.4	24.0

Two µL of the diluted Exonuclease I mix were added to the 5 µL preamplification reaction from the previous step and the tubes were placed in the ThermoCycler using the following PCR program:

Table 26: Exonuclease I digestion thermal cycler program

Step	**Time**	**Temperature (in °C)**
Digestion	30 min	37
Inactivation	15 min	80

Once the programmed was finished, the samples were diluted by addition of 18 µL of DNA suspension Buffer to each tube. The samples were frozen at -20°C untill the next step.

2.2.4.6.5.2. Preparing sample Pre-Mix and samples

The sample Pre-Mix was prepared as followed:

Table 27: Sample Pre-Mix

Component	Volume per reaction (µL)	Volume for 60 reactions w/Overage (µL)
2x SsoFast EvaGreen Supermix with low ROX (BioRad PN 172-5211)	2.5	180
20x DNA Binding Dye (Fluidigm PN 100-7609)	0.25	18.0

3.3 µl of sample Pre-Mix were added to each well of a 96-well plate. Next, 2.7 µl of preamplified and Exonuclease I-treated samples were added to the individual wells. The plate was vortexed thoroughly and centrifuged.

2.2.4.6.5.3. Preparing the Assay Mix

The individual specific forward (100 µM) and reverse (100 µM) primers were combined and 0.6 µl were added to each well of a 96-well plate. The assay mix was prepared as followed:

Table 28: Assay mix preparation

Component	Volume per reaction (µL)	Volume per reaction w/Overage (µL)
2x Assay Loading Reagent (Fluidigm PN 100-7611)	2.5	3
1x DNA Suspension Buffer (TEKnova PN T0221)	2.25	2.4

Finally, 5.4 µl of the Assay mix were added to each well and the plate was vortexed and centrifuged before pipetting the assays into the Integrated Fluidic Circuit (IFC) inlets.

2.2.4.6.5.4. Priming and loading the Dynamic Array IFC

To prime the 48.48 IFC, control line fluid was injected into each accumulator on the IFC. The film on the bottom of the IFC was removed subsequently. Next, the IFC was placed in an integrated fluidic circuit Controller MX (for 48.48 Dynamic Array), and the program Prime (113×) was initiated. After priming, 5 µl of each assay and 5 µl of each sample were loaded in the respective inlets. The IFC was placed into the IFC Controller MX for loading the chip with the following program: Load Mix (113×) was run. Once the load step finished, any dust particles or debris were removed from the IFC surface using a Scotch Tape. The chip was run with the Biomark Gene expression Data Collection software. Parameters required by the set-up of the Biomark were selected and double-checked, and the "thermal protocol: GE 48 × 48 PCR + Melt v2.pcl" was used. The Table Results and Heat Map were imported; the data were analysed using the ΔΔCt method, and normalized to the house-keeping gene (*Hprt*).

2.2.4.7. *Histology and Immunohistochemistry*

To characterise the morphology of the lung, liver and spleen, the mouse organs were placed in tissue cassettes and fixed in 4% PFA for at least 24 hrs. Thereafter, samples were dehydrated and embedded in paraffin using the automatic Tissue Processor Excelsior ES from the Institute of Pathology of the University Medical Center Göttingen. The samples were then placed upside down in metal forms, which were filled with warm paraffin and left for cooling. Afterward, 2 µm sections of the paraffin-embedded tissue samples were cut using a microtome. All stainings of the tissues were performed at the Institute of Pathology by Jennifer Appelhans from the group of Dr. med. Hanibal Bohnenberger using the automatic system Tissue Tek Prisma Slide Stainer.

2.2.5. Ex-vivo analyses of human monocytes

2.2.5.1. *PBMC isolation*

PBMCs were isolated from Buffy Coat obtained from the Department of Transfusion Medicine of the UMG. To this end, 15 mL of Buffy Coat were mixed with 15 mL of

MACS-Buffer before carefully overlaying it on 15 mL of Lymphprep solution previously placed into a 50 mL tube. The tube was then centrifuged at 800 g for 30 min at 20°C with an acceleration of 5 and no break. A gradient was obtained after centrifugation with the upper phase being serum and right below the serum being the layer of PBMCs. The serum was partially removed and PBMCs were collected into a new tube. Around 10 mL of PBMC cell suspension could be collected and were then washed with 40 mL of MACS-Buffer and centrifuged at 350 g at RT for 7 min. Finally, the cells were counted before isolating monocytes.

2.2.5.2. *Monocyte purification and treatment*

Monocytes isolation was performed using the STEMCELL EasySep™ Human Monocyte Enrichment Kit. To this end, 1 mL of a $5x10^7$ cells/mL cell suspension was mixed with 50 µL of the enrichment cocktail contained in the kit in a FACS tube, vortexed and incubated on ice for 10 min. Beads were vortexed before adding 50 µL of them to the sample and toped with 1.4 mL of MACS Buffer. The mixture was incubated in a magnet for 150 s. The cells were then carefully transferred into a FACS tube. The cells were centrifuged at 350 g at RT for 7 min and resuspended in 200 µL of MACS buffer before counting.

For their treatment the cells were platted at a concentration of $3x10^6$ cells/mL in a 48-well plate with a volume of 250 µL in each well. The cells were then treated for 20 hrs as outlined in the table below.

Table 29: Treatment protocol for human monocytes

Experimental group	**Treatment**
non-activated	no treatment
activated	LPS at 10 ng/mL
activated + dexamethasone	LPS at 10 ng/mL dexamethasone ranging from 10^{-5} M to 10^{-7} M

2.2.5.3. *Flow cytometric characterization of monocyte activation*

After 20 hrs of treatment, 10 % of the cells were collected for flow cytometry analysis and the rest was used for molecular analyses. The cells were stained for 20 min with 3 µL of each antibody indicated in the following table before being wash with 4 mL of FACS buffer and centrifuged.

Table 30: FACS panel 4 for human monocyte analysis

Combination 4 – Human monocytes
CD14 PE-Cy7
CD163 PE
CD25 APC-Cy7
HLA/DR Alexa488

After removal of the supernatant, the cells were ready for analysis using the BD FACS Canto II flow cytometer in combination with FlowJo software and the gating strategy shown below in Figure 9. The cell surface marker expressions were then quantified by the associated Mean Fluorescence Intensity (MFI) of the respective channels.

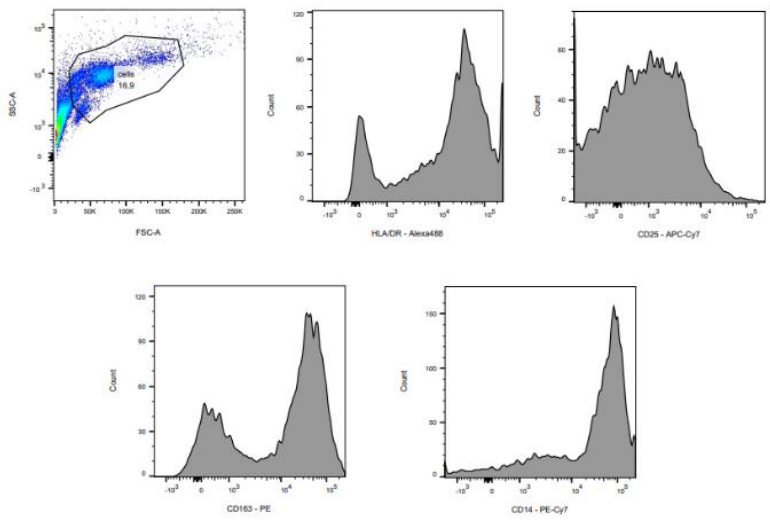

Figure 9: Flow cytometry gating strategy for the characterisation of human monocytes

2.2.5.4. *Molecular analysis*

Total RNA was extracted from human monocytes incubated for 20 hrs as outlined above using the Quick-RNA™ MicroPrep kit from ZYMO. After centrifugation of the suspension, a cell pellet was obtained and 300 µL of Lysis Buffer were added on the top of the cells. The lysate was first centrifuged at 10.000 rpm for 1 min at RT and the supernatant was then transferred onto a yellow column which was placed on a collection tube. After centrifugation, the flow-through was kept and mixed in a 1:1 proportion, corresponding here to 300 µL, with 99.8% ethanol. Once well mixed, the liquid was transferred onto a green column and centrifuged at 10.000 rpm for 30 seconds at RT. The flow-through was discarded and 400 µL of RNA Preparation Buffer were added before being centrifuged. This step was repeated first with 700 µL of Wash Buffer and a second time with 400 µL of Wash Buffer followed this time by a 2 min centrifugation step. Finally, the column was transferred in new microtubes and 30 µL of RNase free water were added onto the column and the samples were centrifuged at 10.000 rpm for 30 s at RT. RNA concentration and the purity of the sample were determined using the Nanodrop 2000 photometer as outlined before. In addition, the RNA preparation was analysed on an agarose gel. Analysis by quantitative RT-PCR was achieved as described before.

2.2.6. *In vitro* analysis of vitamin D nanoparticles

2.2.6.1. Cellular uptake of EP-VDs into different cell lines

VDi-NP uptake was analysed in 7 different cell lines (see Table 11). Cells were cultured in 24-well plates at a concentration of $0.5x10^6$ cells/mL in 1 mL of respective culture medium (see Table 13) at 37°C and 5% CO_2 atmosphere. Two different set ups were used for the evaluation of the uptake. The first one consisted in treating the cells with 25 µg/mL VDi-NP for 30 min to 6 hrs. In a second set up, the cells were treated with VDi-NP at concentrations of 2.5 µg/mL, 8.5 µg/mL or 25 µg/mL and incubated for 24 hrs at 37°C and 5% CO_2 atmosphere. Cells cultured without VDi-NP were used as a control. Subsequently, the cells were prepared for flow cytometric analyses. To this end, MH-S, L929, C2C12 and LA-4 cells were detached from the bottom of the wells by

sucking off the medium and adding 0,25% trypsin-EDTA for 5 min before deactivating the trypsin with medium. For WEHI 7.15, WEHI 231 and RAW264.7 cells trypsin was not needed to detach them from the bottom of the wells. Once the suspension of the cells was obtained, they were centrifuged at 350 g for 5 min. The supernatant was then removed and the cells analysed using the BD FACS Canto II flow cytometer together with FlowJo software following the gating strategy shown in Figure 10 below.

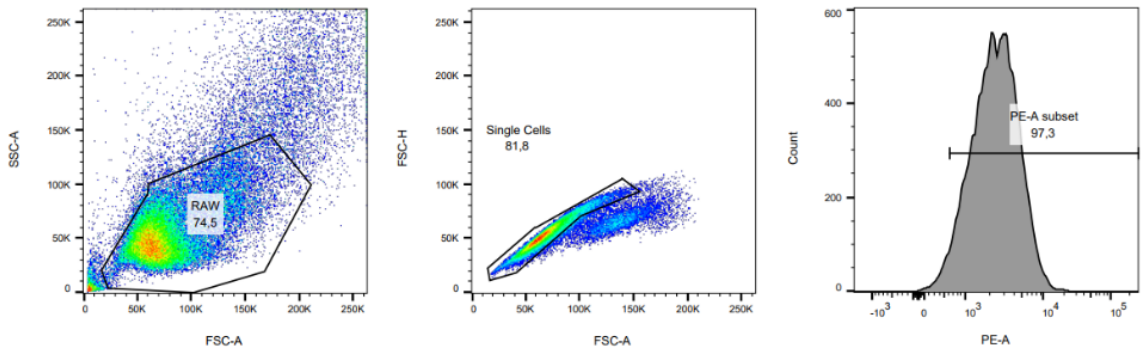

Figure 10: Flow cytometry gating strategy for the analysis of VDi-NP uptake into RAW264.7

2.2.6.2. Viability test of cell lines

The viability of the cells was analysed either after uptake of VD-NPs and/or pharmacological inhibitor treatment. To this end, the cells were cultured in 96-well plates at a concentration of $1x10^6$ cells/mL in 100 µL of respective culture medium. As a negative control, 10% DMSO was added to the cells. The cells were treated either with 2.5 µg/mL, 8.5 µg/mL or 25 µg/mL of VDi-NPs and/or 150 µM of MDC or 1µg/mL of CytoD for 24 hrs at 37°C and 5% CO_2 atmosphere. Untreated cells were used as positive control. After the 24 hrs of treatment, the viability of the cells was assayed by adding 20 µL of the MTS tetrazolium compound (CellTiter 96® AQ_{eous} One Solution Cell Proliferation Assay Kit) and the cells were incubated again for one hour. Bioreduced by metabolically active cells into a coloured formazan product that is soluble in the culture medium, its absorbance was measured at 490 nm by spectrophotometry.

2.2.6.3. Characterization of VDi-NP uptake into RAW 264.7 cells

To characterise the endocytic pathway via which the VD-NPs are taken up into cells, RAW264.7 cells were seeded in 24-well plates at a concentration of 0.5x 10^6 cells/mL in 1 mL of culture medium. Cells were then pre-treated for one hour either with 150 μM MDC or 1 μg/mL CytoD. In a first set up the cells were treated for 24 hrs either with 2.5 μg/mL, 8.5 μg/mL or 25 μg/mL of the VDi-NPs and in a second set up the cells were treated with 25 μg/mL of VDi-NPs for 30 min to 6 hrs. Cells cultured in the absence of inhibitors and VDi-NPs were used as a control. Subsequently, the cells were prepared for flow cytometric analysis by harvested and centrifuged them at 350 g for 5 min. Then the supernatant was removed and the cells analyzed using the BD FACS Canto II flow cytometer together with FlowJo software following the gating strategy shown in figure 10.

2.2.6.4. *Molecular analyses*

To analyse the molecular profile of RAW264.7 cells in the presence of calcitriol either in the free form or contained in nanoparticles (VDa-NPs), the cells were cultured in 24-well plates at a concentration of 0.5x10^6 cells/mL in 1 mL of culture medium at 37°C and 5% CO_2 atmosphere. The cells were pre-treated for 8 hrs either with 10^{-7} M free calcitriol, 10^{-7} M betamethasone or VDa-NPs containing 10^{-7} M or 3x10^{-8} M calcitriol and finally treated for 2 hrs with 100 ng/mL LPS. After a total of 10 hours of treatment, the medium was sucked off and 300 μL of Lysis Buffer were added. RNA was extracted and the molecular analyses were realised as outlined above.

2.2.6.5. Imaging flow cytometry

Imaging Flow Cytometry was used to visualize the localization of VD-NPs in different cellular compartments in RAW 264.7 cells. In brief, 3x10^6 cells were cultured in 15 ml in T75 flasks in the presence of 8.55 μg/ml VDi-NPs for 24 hrs. Medium was removed, cells were washed with medium and fresh medium was added together with either 50 nM Lysotracker® Deep Red (DR) or 50 nM Mitotracker® DR FM for 30 min. Afterwards, the samples were harvested, centrifuged at 350xg for 5 min at 4 °C and the supernatant discarded. The pellet was resuspended in 200 μl FACS Buffer and passed through a

nylon mesh place in a FACS tube. The obtained cell suspension was used for Imaging Flow Cytometry analysis and the cells were recorded using the ImageStream®X Mark II Imaging Flow Cytometry device. Finally, data were processed with the software IDEAS and the colocalization of the cell trackers and NPs determined.

2.2.7. Statistical analysis

Statistical analysis of multiple experimental groups was performed by 1-way ANOVA followed by a Newman-Keuls multiple comparison test using GraphPad Prism 5.03 software (San Diego, CA). Otherwise, a two-tailed Student's t-test was used. Results are depicted as mean values ± SEM with the following levels of significance: *: $p < 0.05$; **: $p < 0.01$; ***: $p < 0.001$; ****: $p < 0.0001$; non-significant (n.s.): $p > 0.05$

3. Results

3.1. Application of GC nanoparticles as a targeted therapy to suppress inflammatory conditions in mouse models of sepsis and ALI

Previous results obtained by Kaiser and colleagues [146] suggested that the use of IOH-NPs is a promising strategy to achieve targeted GC delivery in inflammatory conditions. In diseases such ALI and sepsis, GCs are clinically used to treat the so called “cytokine storm”, although this may also cause lymphocytopenia leading to a severe risk of secondary infections and poor outcome. Targeting specific cell types in GC treatment could allow to overcome this side effect as IOH-NPs were shown to be mainly taken up by macrophages. Thus, in this study we focused on comparing the synthetic GC betamethasone (referred to as BMZ in the following) in its free form with the same drug encapsulated in IOH-NPs (referred to as BMP in following). To determine their therapeutic efficacies, we used two mouse models of fulminant inflammatory conditions, namely sepsis induced by LPS injection and ALI caused by cotreatment with LPS and OA.

3.1.1. GC therapy prevents hypothermia in the mouse model of sepsis

To compare BMZ and BMP effects in the sepsis mouse model, variations in weight, temperature and glucose levels before and after sepsis induction were evaluated. To this end, weight, temperature and glucose levels were daily measured for three days (including the day of induction) in wildtype C57BL/6 mice before sepsis induction. Mice were then injected with LPS and subsequently treated with either BMZ or BMP. After 15 hours, all three parameters were measured again and the difference to the mean of each parameter preceding induction was determined. Induction of sepsis caused a strong reduction of all three parameters compared to control mice (Figure 11). Both types of GC treatment could prevent the decrease in body temperature caused by sepsis (Figure 11B). In contrast, they failed to prevent the loss in body weight and the reduction of blood glucose levels during sepsis (Figure 11A and 11C). Interestingly, no significant differences were observed between the BMZ and BMP treatments.

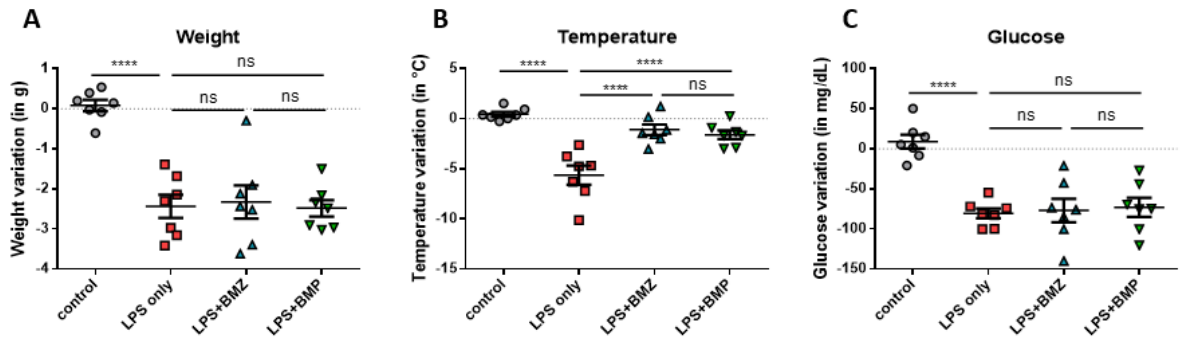

Figure 11: Effects of BMZ and BMP on clinical parameters of mice suffering from LPS-induced sepsis. *WT mice were injected with LPS to induce sepsis or additionally treated with BMZ or BMP. Control mice didn't receive any LPS. Three days before sepsis induction, weight, temperature and glucose levels were daily measured and their means were compared to the parameters measures 15 hours after sepsis induction. The panels in this figure show the variations in weight (A), temperature (B) and glucose (C). n=7; mean +/- SEM. Statistical analysis by 1-way ANOVA with Newman-Keuls multiple comparison test. ****: p<0.0001; n.s.: p>0.05*

3.1.2. BMP treatment slightly improves the cell type specificity of GC administration in the mouse sepsis model

Next, we aimed to determine whether BMP treatment improved targeting of GCs to specific cell types by analysing different blood cell populations. To this end, wildtype C57BL/6 mice were injected with LPS to induce sepsis and subsequently treated with either BMZ or BMP. After 15 hours, blood was collected, stained with two panels of monoclonal antibodies and analysed by flow cytometry. First focusing on lymphocyte populations (Figure 12), sepsis caused a significant reduction in B cells (Figure 12A), T cell (Figure 12B), and NK cells (Figure 12D) compared to control mice. A slight but non-significant change was also be observed for the $CD4^+/CD8^+$ T cell ratio (Figure 12C) revealing a slightly higher proportion of $CD8^+$ T cells in septic mice compared to control mice. BMZ treatment potentiated all tendencies observed in septic mice but without reaching significance. In contrast, septic mice treated with BMP showed similar percentages of B cells and T cells as mice treated only with LPS (Figure 12A/B). Additionally, the $CD4^+/CD8^+$ T cell ratio was not further reduced upon BMP treatment as in was the case for BMZ treatment (Figure 12C). Interestingly, BMZ and BMP provoked a similar further reduction in the percentage of NK cells compared to septic

mice not receiving GC treatment (Figure 12D). It is important to note that none of the data showed significant differences between the groups of septic mice regardless of additional GC treatment and thus only represent strong tendencies. Those, however, indicate a possible difference between BMZ and BMP treatment as to their cell type specificity, which would coincide with the *in vitro* observations made by Kaiser and colleagues in which B and T cells were barely taking up IOH-NPS. [146]

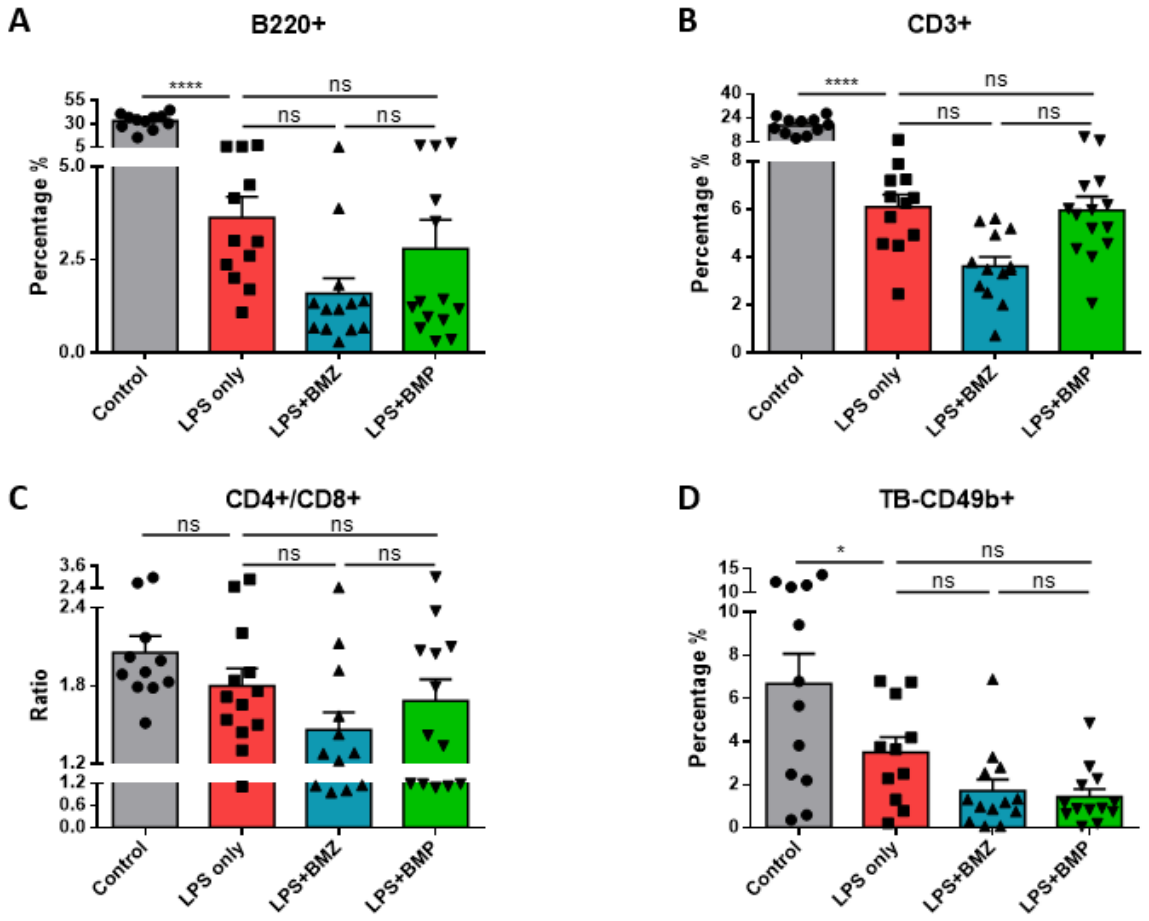

Figure 12: Effects of BMZ and BMP on blood lymphocyte populations of mice suffering from LPS-induced sepsis. *WT mice were injected with LPS to induce sepsis or additionally treated with BMZ or BMP. Control mice didn't receive any LPS. After 15 hours of treatment, blood samples were collected. Cells were stained with monoclonal antibodies conjugated to a fluorophore and analysed by FACS. The panels in this figure show the percentages of $B220^+$ B-cells (A), $CD3^+$ T-cells (B), $B220^-CD3^-CD49b^+$ NK-cells (D), as well as the ratio between CD4+ and $CD8^+$ T cells (C). n=12-14; mean +/- SEM. Statistical analysis by 1-way ANOVA with Newman-Keuls multiple comparison test. *: p<0.05; ****: p<0.0001; n.s.: p>0.05*

Next focusing on myeloid cell populations (Figure 13), sepsis induction significantly increased the percentages of all $CD11b^+$ cells as well as of $CD11b^+Ly6G^+$ neutrophils (Figure 13A/B). In contrast, the percentage of $CD11b^+Ly6G^-F4/80^+$ monocytes (Figure 13C) remained unchanged compared to control mice. Furthermore, BMZ and BMP treatment additionally increased the percentages of all $CD11b^+$ cells and neutrophils (Figure 13A-13B) while they both significantly reduced the percentage of monocytes (Figure 13C) compared to septic mice not receiving GCs. Moreover, no significant differences concerning the effects on myeloid cell populations could be observed between both GCs treatments. Those results thus suggest that BMP affects myeloid cells in a similar way as BMZ, both increasing the percentage of neutrophils and reducing the percentage of monocytes.

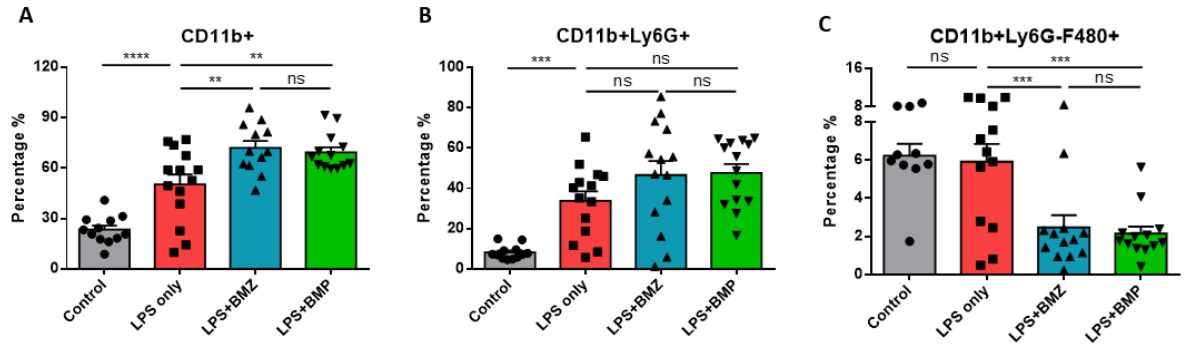

Figure 13: Effects of BMZ and BMP on blood myeloid cell population of mice suffering from LPS-induced sepsis. *WT mice were injected with LPS to induce sepsis or additionally treated with BMZ or BMP. Control mice didn't receive any LPS. After 15 hours of treatment, blood samples were collected, cells were stained with monoclonal antibodies conjugated to a fluorophore and analysed by FACS. The panels in this figure show the percentages of $CD11b^+$ cells (A), $CD11b^+Ly6G^+$ neutrophils (B), and $CD11b^+Ly6G^-F4/80^+$ monocytes (C). n=12-14; mean +/- SEM. Statistical analysis by 1-way ANOVA with Newman-Keuls multiple comparison test. **: p<0.01; ***: p<0.001; ****: p<0.0001; n.s.: p>0.05*

3.1.3. BMZ and BMP treatment counteract histological changes in liver and lung but not in the spleen of mice in the sepsis model

To complement our finding made concerning the cellular composition of the blood, histological analyses of spleen, liver and lung were performed. To this end, wildtype C57BL/6 mice were injected with LPS to induce sepsis and subsequently treated with either BMZ or BMP. After 15 hours, the three tissues were collected, fixed with PFA,

embedded in paraffin and 2 μm sections were prepared. Tissue sections were then stained with H&E.

The spleen plays a significant immunological role as a secondary lymphoid organ but it is also responsible for senescent erythrocyte clearance and serves as a blood reserve. Histological analysis of the spleen revealed that LPS-induced sepsis altered the white pulp showing extended splenic follicles but also the red pulp as characterized by an increased number of erythrocytes compared to the spleen of control mice (Figure 14A/B). However, those changes could neither be rescued by BMZ nor BMP treatment (Figure 14C/D).

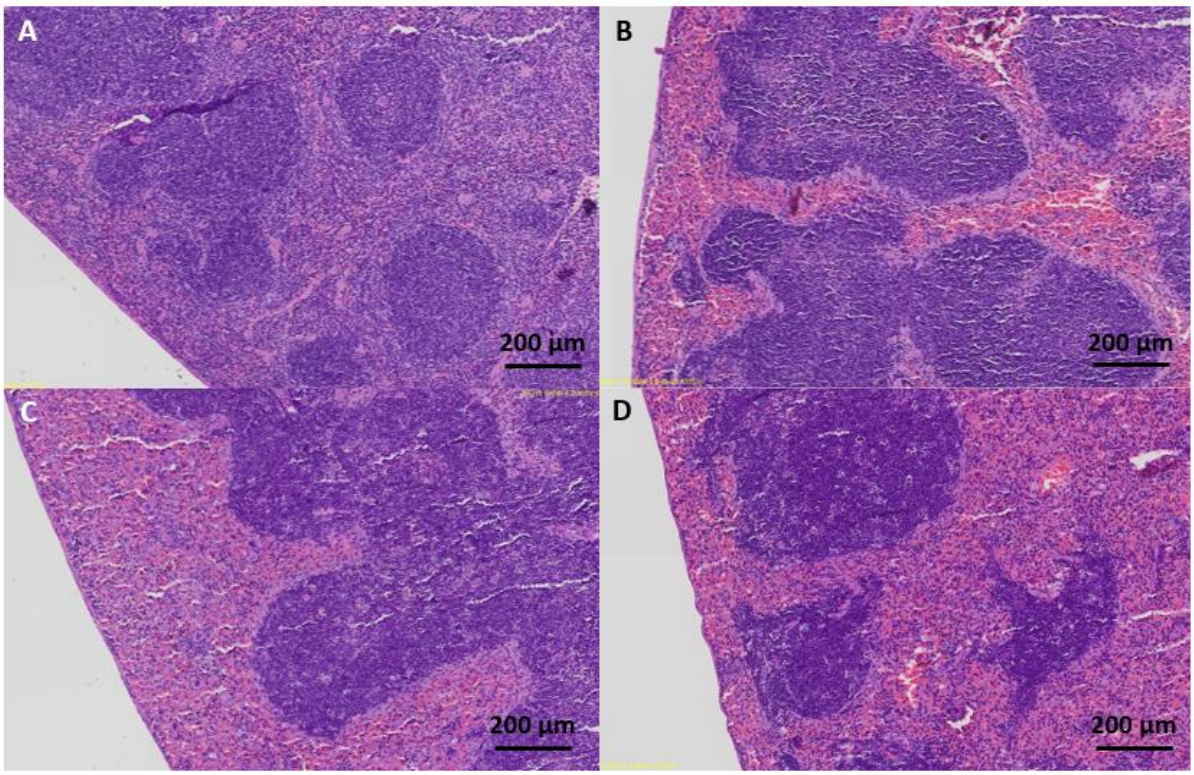

Figure 14: Microscopic images of H&E-stained spleens of C57/BL6 mice suffering from LPS-induced sepsis treated with BMZ or BMP. *WT mice were injected with LPS to induce sepsis or additionally treated with BMZ or BMP. Control mice didn't receive any LPS. After 15 hours, spleens were collected and prepared for histological analyses. The different panels show representative images of the spleen from control mice (A), only with LPS treated mice (B), mice cotreated with LPS and BMZ (C) and mice cotreated with LPS and BMP (D). Scale bar: 200 μm.*

Thereafter, liver sections of from mice subjected to the sepsis model were analysed. H&E staining unveiled important liver injury caused by LPS treatment (Figure 15B) including apoptosis induction (indicated by black arrows), cell infiltration (indicated by red arrows), as well as vascular congestion compared to control mice (Figure 15A). BMZ and BMP treatments both reduced the histopathological features caused by LPS, although not completely (Figure 15C/D).

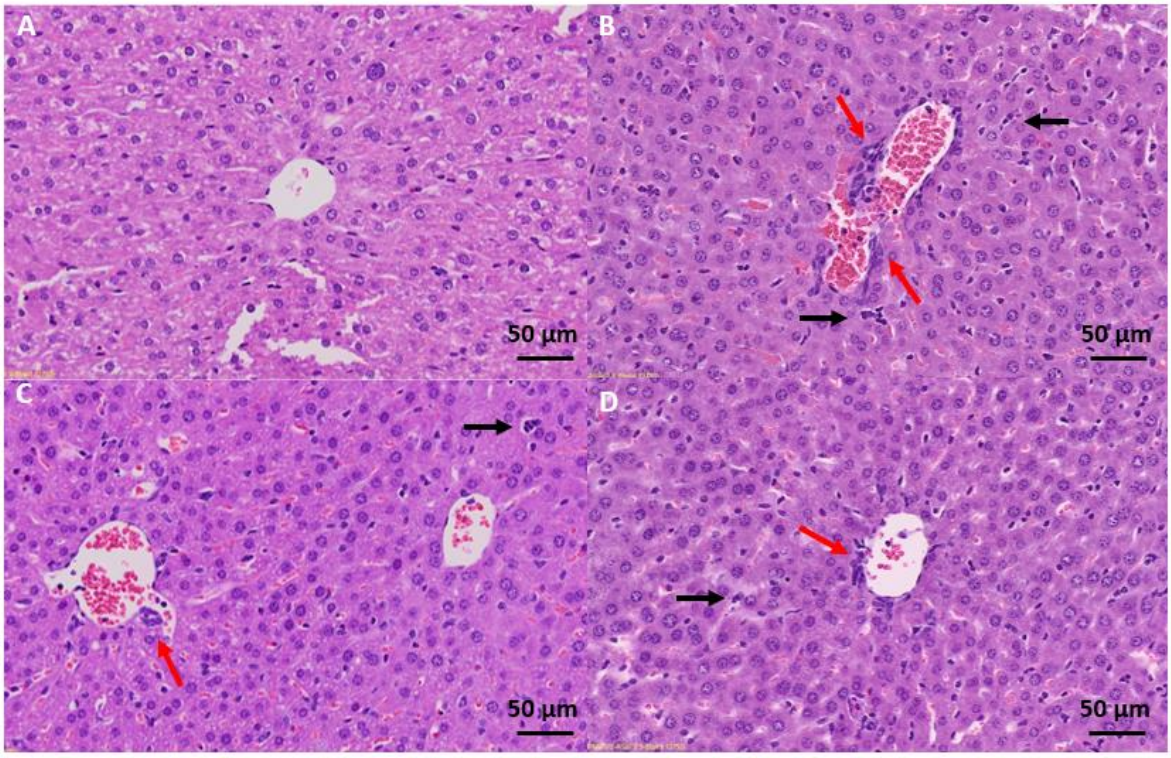

Figure 15: Microscopic images of H&E-stained livers of C57/BL6 mice suffering from LPS-induced sepsis treated with BMZ or BMP. *WT mice were injected with LPS to induce sepsis or additionally treated with BMZ or BMP. Control mice didn't receive any LPS. After 15 hours, livers were collected and prepared for histological analyses. The different panels show representative images of the liver from control mice (A), only with LPS treated mice (B), mice cotreated with LPS and BMZ (C) and mice cotreated with LPS and BMP (D). Scale bar: 50 µm.*

Finally, lung sections of septic mice were analysed. H&E staining showed important lung injury caused by LPS-induced sepsis (Figure 16B), including pulmonary interstitial thickening, cell infiltration and vascular congestion (indicated by the black arrows) compared to control mice (Figure 16A). BMZ and BMP treatments were able to ameliorate these features albeit not fully preventing them (Figure 16C/D).

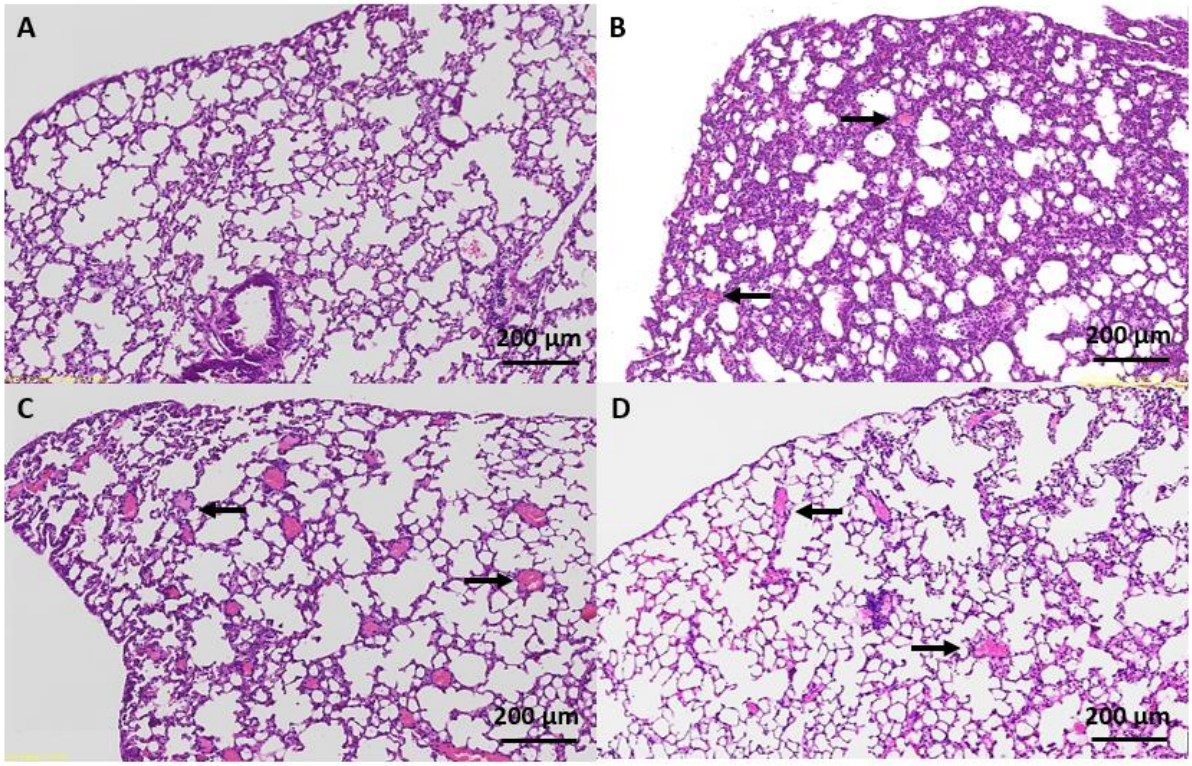

Figure 16: Microscopic images of H&E-stained lungs of C57/BL6 mice suffering from LPS-induced sepsis treated with BMZ or BMP. *WT mice were injected with LPS to induce sepsis or additionally treated with BMZ or BMP. Control mice didn't receive any LPS. After 15 hours, lungs were collected and prepared for histological analyses. The different panels show representative images of the lung from control mice (A), only with LPS treated mice (B), mice cotreated with LPS and BMZ (C) and mice cotreated with LPS and BMP (D). Scale bar: 200 µm.*

3.1.4. Gene regulation by BMZ and BMP treatment in spleen, liver and lung in the mouse sepsis model

Quantitative RT-PCR and high-throughput Fluidigm gene chip assays were performed to determine gene expression profiles in spleen, liver and lung of septic mice after GC treatment. Wildtype C57BL/6 mice were injected with LPS to induce sepsis and subsequently treated with either BMZ or BMP. After 15 hours, organs were collected and RNA was extracted for analysis. Amongst the 28 genes studied in total, 8 genes were analysed by quantitative RT-PCR (*Il6, Il1b, Tnfa, Ccl2, Il10, Arg1, Cd163, Cd206*) whereas all other genes were analysed by Fluidigm gene chip assay.

The first group of analysed genes encode pro-inflammatory cytokines: *Il6, Il1β, Tnfa* and *Gmcsf*. In both spleen and liver (Figure 17 and 18), a reduction of all four genes could be observed for both BMZ and BMP treatment compared to septic mice not

receiving any GC treatment. Results in the lung were somewhat different (Figure 19). While *Il6* and *Tnfa* expressions are also reduced upon GC treatments, the other two genes *Il1b* and *Gmcsf* were increased by both BMZ and BMP.

The second group of analysed genes encode chemokines from both the CCL- and the CXCL-families. All genes belonging to this group were decreased by BMZ as well as BMP treatment in all organs compared to septic mice not receiving any GC treatment (Figures 17-19).

The third group of analysed genes concern molecules primarily expressed by myeloid cells. Differences between individual genes in this group can already be observed in the control group of the three different organs, especially between spleen or liver and lung while both spleen and liver controls show largely similar gene expression levels. Some differences in *Tlr* gene expression were observed, with a decreased level of *Tlr2* in both liver and lung (Figure 18 and 19), while it remained unaltered in the spleen (Figure 17), and an increased expression of *Tlr4* in all three organs of BMZ and BMP treated mice compared to septic mice not receiving GC treatment. Expression of *Cd18*, which plays a role in neutrophil extravation, was increased in the lung (Figure 19), while only slight variations were seen in spleen and liver (Figure 17 and 18) upon BMZ and BMP treatment compared to mice only treated with LPS. The other genes of this group are associated to M2 macrophages polarisation: *Ym1, Il10, Arg1, Cd163* and *Cd206*. While *Ym1, Arg1* and *Cd163* were slightly or even strongly increased in all three organs upon BMZ and BMP treatment, expression of the other genes depended on the respective organ. Indeed, *Il10* expression was increased in both spleen and lung (Figure 17 and 19), whereas it was reduced in the liver (Figure 18) by BMZ and BMP treatment compared to septic mice without GC treatment. *Cd206* expression was reduced by BMZ and BMP in both spleen and liver (Figure 17 and 18), but it was increased in the lung (Figure 19) compared to LPS-treated mice not receiving any GCs.

The fourth group of analysed gene are all enzymes: *Nox2, Cox2, Dusp1,* and *Sphk1*. While a strong decrease in expression was found for all four genes in both spleen and

liver (Figure 17 and 18), only a slight decrease, except for *Dusp1* which was increased, could be observed in the lung upon BMZ and BMP treatment compared to septic mice not receiving any GC treatment.

The fifth group concerns genes involved in energy metabolism: *Aldoa, Hk2, Glut1* and *Glut3*. In spleen and liver, a similar evolution could be observed upon BMZ and BMP treatment compared to septic mice not receiving any GCs treatment, with either no change or a slight increase in *Aldoa* expression and slight reduction in expression for the three other metabolic genes (Figure 17 and 18). In the lung the situation was different. Upon BMZ and BMP treatment, a clear increase of *Aldoa* expression could be observed as well as an important decrease in *Hk2* expression compared to septic mice not receiving any GCs treatment. Interestingly, *Glut1* and *Glut3* expressions in the lung show differences in between the BMZ and BMP treated groups with a slight increase of gene expression upon BMZ and a slight reduction of upon BMP compared to septic mice not receiving any GCs treatment (Figure 19).

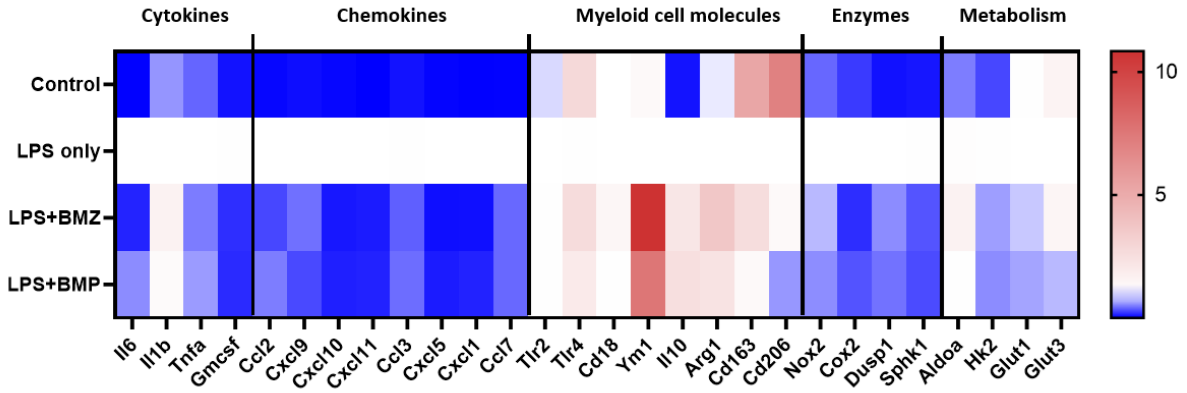

Figure 17: Gene expression analysis of cytokines, chemokines, myeloid cell associated molecules, enzymes and metabolic proteins in the spleen of C57/BL6 mice suffering from LPS-induced sepsis treated with BMZ or BMP. WT mice were injected with LPS to induce sepsis or additionally treated with BMZ or BMP. Control mice didn't receive any LPS. After 15 hours, spleens were collected, RNA was isolated and transcribed into cDNA. Subsequently RT-qPCR analysis was performed for the following genes: Il6, Il1b, Tnfα, Ccl2, Il10, Arg1, Cd163, Cd206, and Fluidigm® gene chip analysis was performed for the rest of the genes. n=4-6

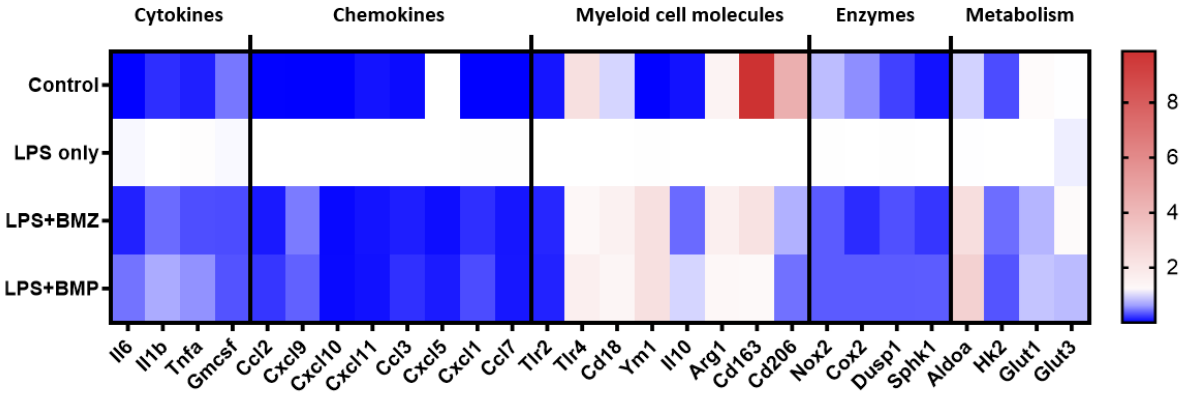

Figure 18: Gene expression analysis of cytokines, chemokines, myeloid cell associated molecules, enzymes and metabolic proteins in the liver of C57/BL6 mice suffering from LPS-induced sepsis treated with BMZ or BMP. *WT mice were injected with LPS to induce sepsis or additionally treated with BMZ or BMP. Control mice didn't receive any LPS. After 15 hours, livers were collcted, RNA was isolated and transcribed into cDNA. Subsequently RT-qPCR analysis was performed for the following genes: Il6, Il1b, Tnfα, Ccl2, Il10, Arg1, Cd163, Cd206, and Fluidigm® gene chip analysis was performed for the rest of the genes. n=4-6*

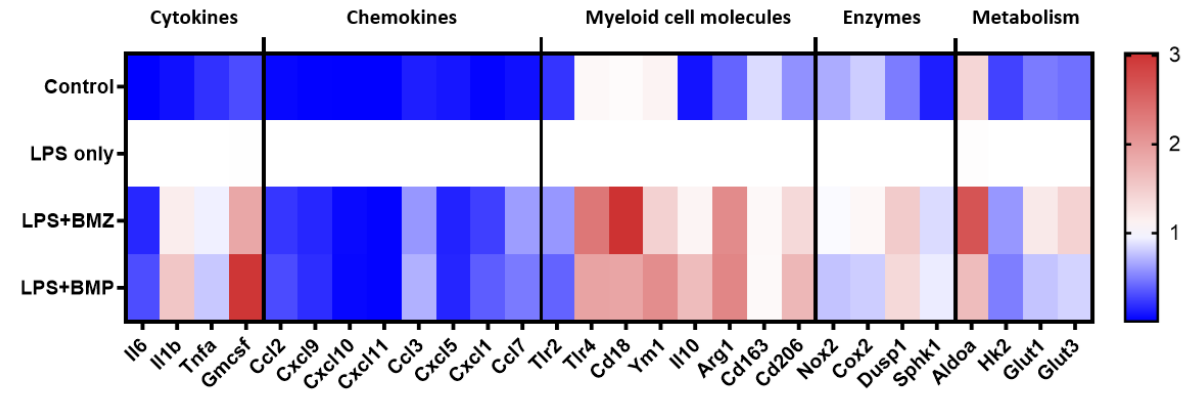

Figure 19: Gene expression analysis of cytokines, chemokines, myeloid cell associated molecules, enzymes and metabolic proteins in the lung of C57/BL6 mice suffering from LPS-induced sepsis treated with BMZ or BMP. *WT mice were injected with LPS to induce sepsis or additionally treated with BMZ or BMP. Control mice didn't receive any LPS. After 15 hours, lungs were collcted, RNA was isolated and transcribed into cDNA. Subsequently RT-qPCR analysis was performed for the following genes: Il6, Il1b, Tnfα, Ccl2, Il10, Arg1, Cd163, Cd206, and Fluidigm® gene chip analysis was performed for the rest of the genes. n=4-6*

3.1.5. BMZ and BMP reduce cytokines and nitric oxide secretion after sepsis induction similarly

Released briefly after activation, pro-inflammatory cytokines and nitric oxide (NO) are mainly secreted by myeloid cells including monocytes, activated macrophages and neutrophils. Therefore, to complement the previous data, BMZ and BMP effects in the sepsis mouse model on four pro-inflammatory cytokines and NO secretion were analysed. To this end, wildtype C57BL/6 mice were injected with LPS to induce sepsis and subsequently treated with BMZ or BMP. After 15 hours, blood was collected, serum prepared and analysed by ELISA or spectrophotometry, respectively. Mice only injected with LPS showed strongly increased levels of all cytokines as well as NO compared to control mice. Additionally, BMZ and BMP treatment in the sepsis mouse model resulted in a significant decrease of IL6, IL1β, TNFα and MCP1 (corresponding to CCL2) secretion compared to LPS-treated mice not receiving GCs (Figure 20A-D). The same observation was made for NO secretion (Figure 20E). Finally, no significant differences were observed between both GCs treatments for any pro-inflammatory mediator.

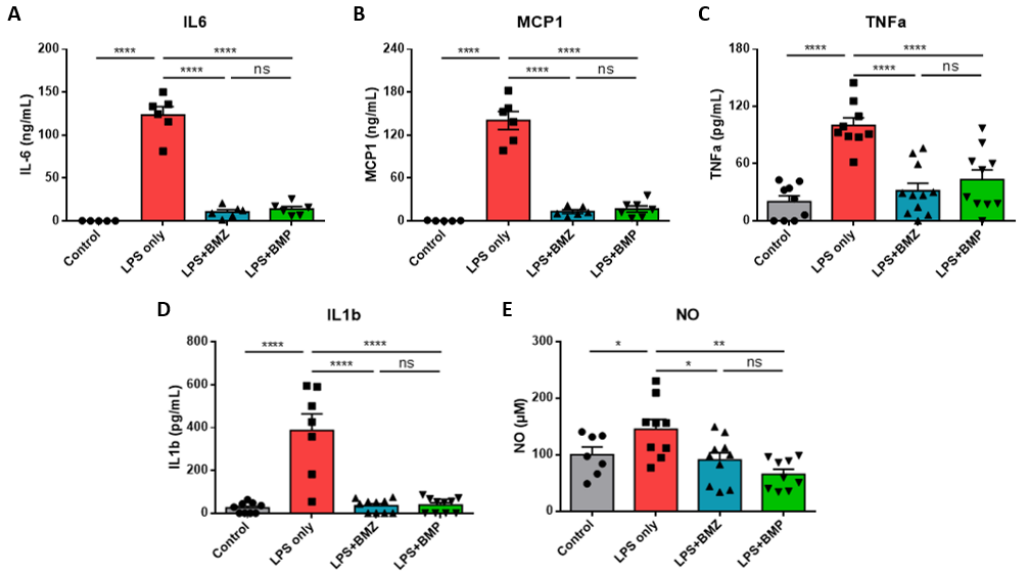

Figure 20: Effects of BMZ and BMP on blood cytokines and nitric oxide levels of mice suffering from LPS-induced sepsis. *WT mice were injected with LPS to induce sepsis or additionally treated with BMZ or BMP. Control mice didn't receive any LPS. After 15 hours, blood was collected and serum prepared for ELISA and spectrophotometry analyses. The panels show IL-6 (A), MCP1 (B), TNFα (C), IL-1β (D) and nitric oxide (E) serum levels. n=5-12; mean +/- SEM. Statistical analysis by 1-way ANOVA with Newman-Keuls multiple comparison test. *: p<0.05; **: p<0.01; ****: p<0.0001; n.s.: p>0.05*

3.1.6. BMZ and BMP reduce pulmonary infiltrates in ALI mouse model

ALI is a severe complication of sepsis characterised by bilateral pulmonary infiltration. Hence, we established an ALI mice model to specifically address this pathological feature and analysed the cellular composition of the BALF in GC-treated mice. To this end, wildtype C57BL/6J mice were first injected with LPS and subsequently treated with oleic acid (OA) to damage the blood-lung barrier resulting in the induction of ALI. Some mice were treated received either BMZ or BMP or left completely untreated as a control. After 15 hours, the BALF was collected and the cells contained therein were stained and analysed by FACS allowing to quantify the neutrophil population (Figure 21). Mice only treated with LPS and OA showed a fulminant neutrophil infiltration in the lung compared to control mice. Furthermore, mice in which ALI was induced but which were additionally treated with either BMZ or BMP were characterized by significantly lower percentages of neutrophils in the BALF compared to the mice only treated with LPS and OA. This observation shows the capacity of both GCs treatments to reduce pulmonary infiltrates in the mouse ALI model.

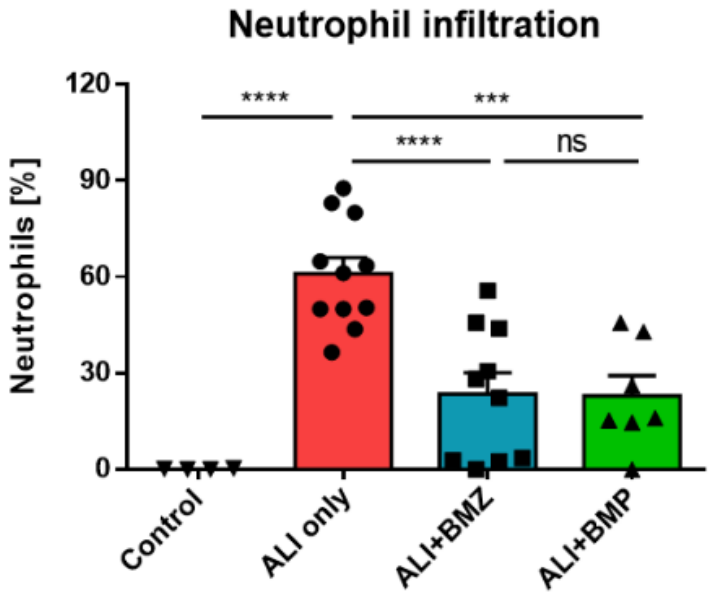

Figure 21: Effects of BMZ and BMP on pulmonary infiltrates of mice suffering from ALI. *WT mice were injected with LPS and OA to induce ALI or additionally treated with BMZ or BMP. Control mice neither received LPS nor OA. After 15 hours, BALF cells were collected, stained with monoclonal antibodies conjugated to a fluorophore and analysed by flow cytometry. n=4-11; mean +/- SEM. Statistical analysis by 1-way ANOVA with Newman-Keuls multiple comparison test. ***: p<0.001; ****: p<0.0001; n.s.: p>0.05*

3.1.7. Gene regulation by BMZ and BMP in the lung of mice subjected to the ALI model

To further investigate effects of both GCs treatment in ALI mice, expressions of some genes were quantified in lung tissue. To this end, wildtype C57BL/6 mice were injected with both LPS and OA to induce ALI and subsequently treated with either BMZ or BMP. After 15 hours, RNA was extracted from the collected lungs for further analyses by quantitative RT-PCR (Figure 22). While BMZ treatment in mice suffering from ALI showed a tendency for reduced *Il1b* expression compared to mice only treated with LPS and OA (Figure 22B), important variations were observed for *Il*6, *Tnf*a and *Cox2* expression without any clear trend (Figure 22A, C and D) compared to ALI mice not receiving GC treatment. In contrast, BMP treatment showed a clear tendency for a reduced expression of all four analysed gene although not reaching significance (Figure 22). Finally, even though some differences in gene expression could be seen between BMZ and BMP treatment for all four genes, those differences were statistically non-significant and require further repetitions of the experiment.

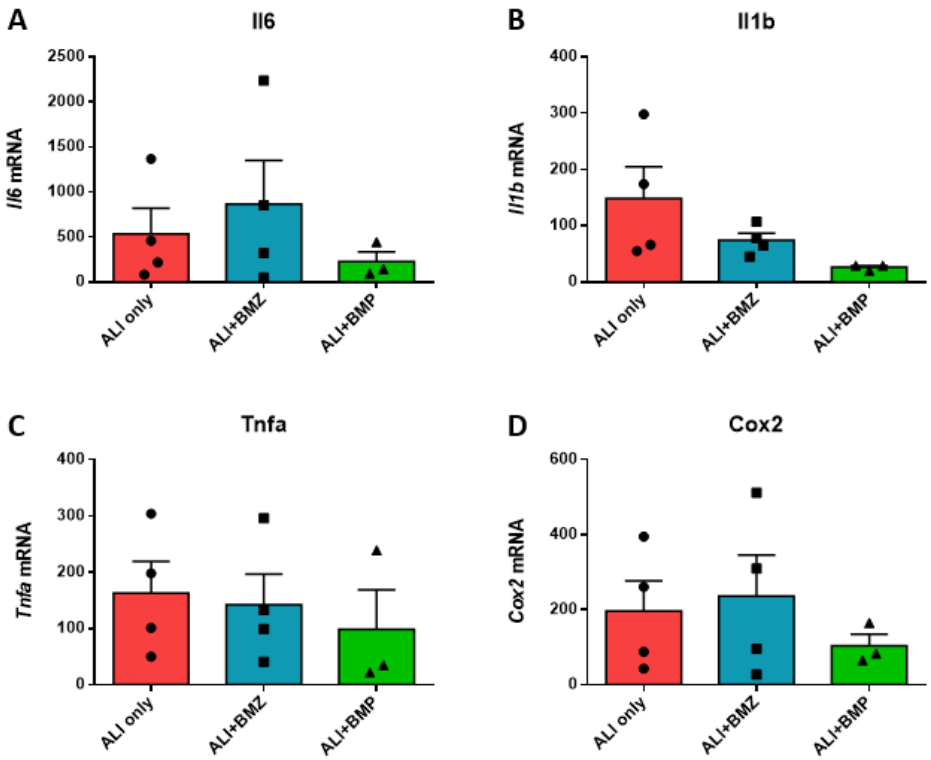

Figure 22: Effects of BMZ and BMP on lung gene expression of mice suffering from ALI. *WT mice were injected with LPS and OA to induce ALI or additionally treated with BMZ or BMP. Control mice neither received LPS nor OA. After 15 hours, lungs were collected. RNA was isolated from the samples, transcribed into cDNA, and subsequently RT-qPCR was performed. The panels show Il6 (A), Il1b (B), Tnfa (C), and Cox2 gene expression. n=3-8; mean +/- SEM. Statistical analysis by 1-way ANOVA with Newman-Keuls multiple comparison test didn't reveal and significant differences.*

3.1.8. BMZ and BMP reduce cytokines and nitric oxide secretion after ALI induction

Since the previous gene expression analyses in the ALI mouse model failed to show clear and significant differences between LPS/OA-injected mice not receiving any GC treatment and those ones receiving either BMZ or BMP, further analyses were conducted to quantify pro-inflammatory cytokines and NO in the serum. To this end, wildtype C57BL/6J mice received LPS and OA to induce ALI and were subsequently treated with either BMZ or BMP. After 15 hours, serum was prepared and analysed by ELISA and spectrophotometry. BMZ and BMP treatment resulted in a significant decrease in IL-6, IL-1β, TNFα and MCP1 secretion compared to ALI mice not receiving any GC treatment (Figure 23A-D). A similar observation was made for NO secretion (Figure 23E). No significant differences were found between both GC treatments.

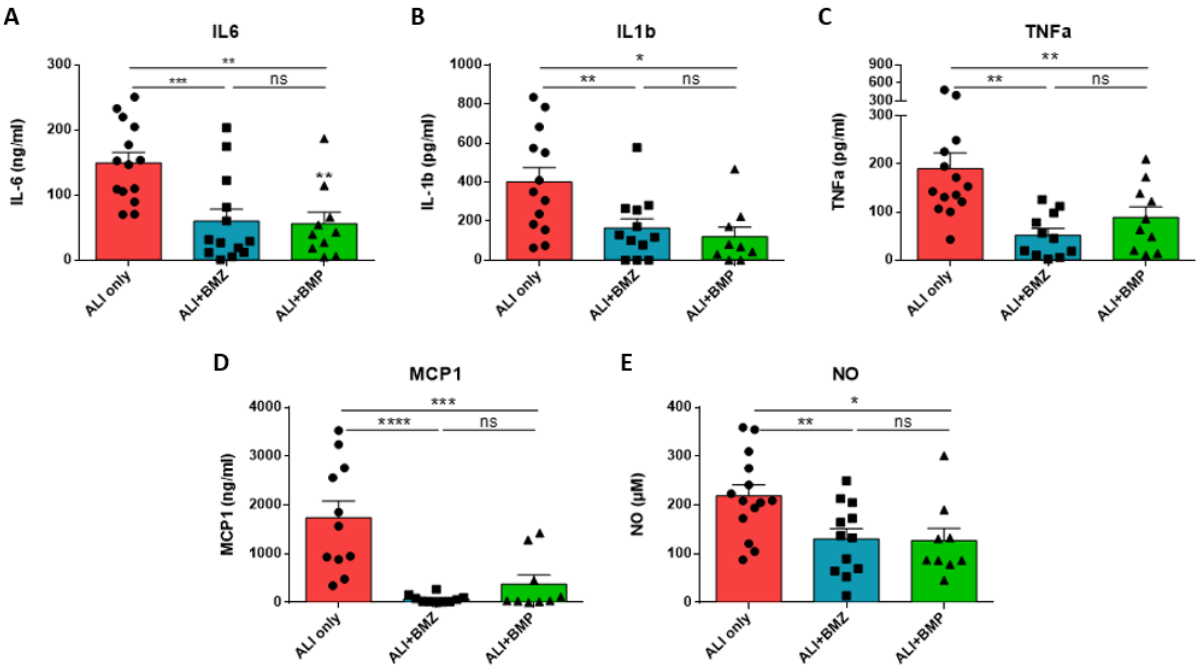

Figure 23: Effects of BMZ and BMP on serum cytokine and nitric oxide levels of mice suffering from ALI. *WT mice were injected with LPS and OA to induce ALI or additionally treated with BMZ or BMP. Control mice neither received LPS nor OA. After 15 hours, blood was collected and serum prepared for*

*ELISA and spectrophotometry analyses. The panels show IL-6 (A), IL-1β (B), TNFα (C), MCP1 (D) and NO (E) serum levels. n=10-15; mean +/- SEM. Statistical analysis by 1-way ANOVA with Newman-Keuls multiple comparison test. *: p<0.05; **: p<0.01; ***: p<0.001; ****: p<0.0001; n.s.: p>0.05*

3.1.9. GCs alter the inflammatory profile of human monocytes *in vitro*

The importance of glucose metabolism for immune cell function has gained much interest in recent years. [152] Since we had observed changes in metabolic gene expression in several organs both after sepsis induction in mice as well as after GC treatment (Figures 17-19), we aimed to further analyse this phenomenon *in vitro*. More specifically, we reached out to determine whether GCs may exert some of their immunomodulatory effects in the context of sepsis by influencing glucose transport and glycolysis in myeloid cells. To obtain sufficiently high numbers of monocytes for analysis, we switched to human PBMCs. Following isolation from buffy coats, human monocytes were seeded in 48-well plates, activated by treatment with LPS and additionally incubated with different concentrations of dexamethasone (Dex) for 20 hrs (Figure 24A). The cells were then harvested and either used for FACS or gene expression analysis. Initially, we confirmed their activation by LPS and repression by Dex treatment, and the suitability as an *in vitro* model for inflammatory conditions. CD25 and CD163 surface expression on human monocytes are two markers of pro-inflammatory activation and monocytes polarisation toward an anti-inflammatory phenotype, respectively (Figure 24B). After LPS exposure, human monocytes showed a significantly increased surface expression of CD25 while CD163 levels remained unaltered compared to non-activated monocytes (Figure 24B). Dex treatment caused a dose-dependent reduction of CD25 surface expression, which is consistent with a lower activation. In contrast, CD163 expression increased with rising concentrations of Dex compared to activated monocytes (Figure 24B). Subsequently, the monocytes were also analysed by quantitative RT-PCR (Figure 24C). Similar changes as observed in the FACS analyses of CD25 and CD163 could also be demonstrated on the mRNA level. Moreover, *IL6* and *NOS2* gene expression in activated monocytes were increased and Dex treatment reduced them in a dose-dependent manner. Those data therefore

suggest that human monocyte activation by LPS is a suitable *in vitro* model for the inflammatory conditions encountered in septic mice.

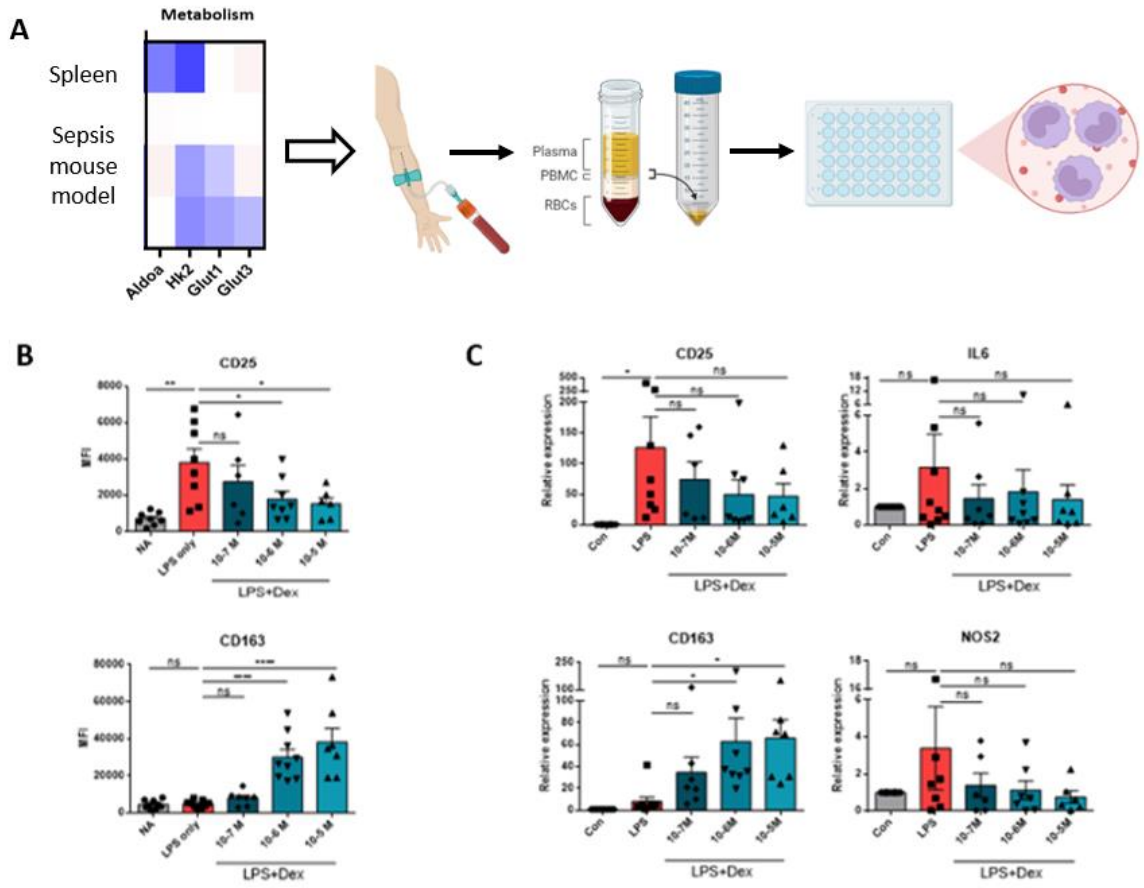

Figure 24: GC effects on human monocytes after LPS stimulation. *Human monocytes were isolated from buffy coats and seeded in 48-well plates. The cells were treated with LPS and/or dexamethasone (Dex) at different concentrations or left untreated (con). The panels show the experimental working flow (A), the analysis of CD25 and CD163 surface expression by FACS (B) and the analysis of CD25, CD163, IL6 and NOS2 gene expression by RT-qPCR (C). n=6-9; mean +/- SEM. Statistical analysis by 1-way ANOVA with Newman-Keuls multiple comparison test. *: p<0.05; **: p<0.01; ****: p<0.0001; n.s.: p>0.05*

3.1.10. GCs reduce metabolic gene expression after LPS stimulation in human monocytes *in vitro*

As we could show that LPS activation of human monocytes is an adequate model to study the inflammatory conditions of sepsis *in vitro*, further analyses were conducted to better understand the GCs' role in metabolic changes. To this end, we studied 6 genes involved at different levels in the glycolytic process. Monocytes were isolated from human PBMCs, activated trough LPS treatment, and in some cases additionally

incubated with different concentrations of Dex for a total of 20 hrs. The cells were then harvested, RNA extracted and analysed by quantitative RT-PCR (Figure 25). The expression of all metabolic genes was increased in activated monocytes compared to unstimulated cells although not always reaching statistical significance. When treated with the different concentrations of Dex, monocytes showed reduced expression of *GLUT1, GLUT3, HK2, SLC7A5* and *PFKFB3* compared to activated monocytes which were not treated with Dex (Figure 25A-C and E/F). However, due to relatively large variations in gene expression, those reductions were not statistically significant. *LDHA* did not show a clear tendency after Dex treatment and cells treated with the highest concentration of Dex even had a similar expression as activated control monocyte (Figure 25D).

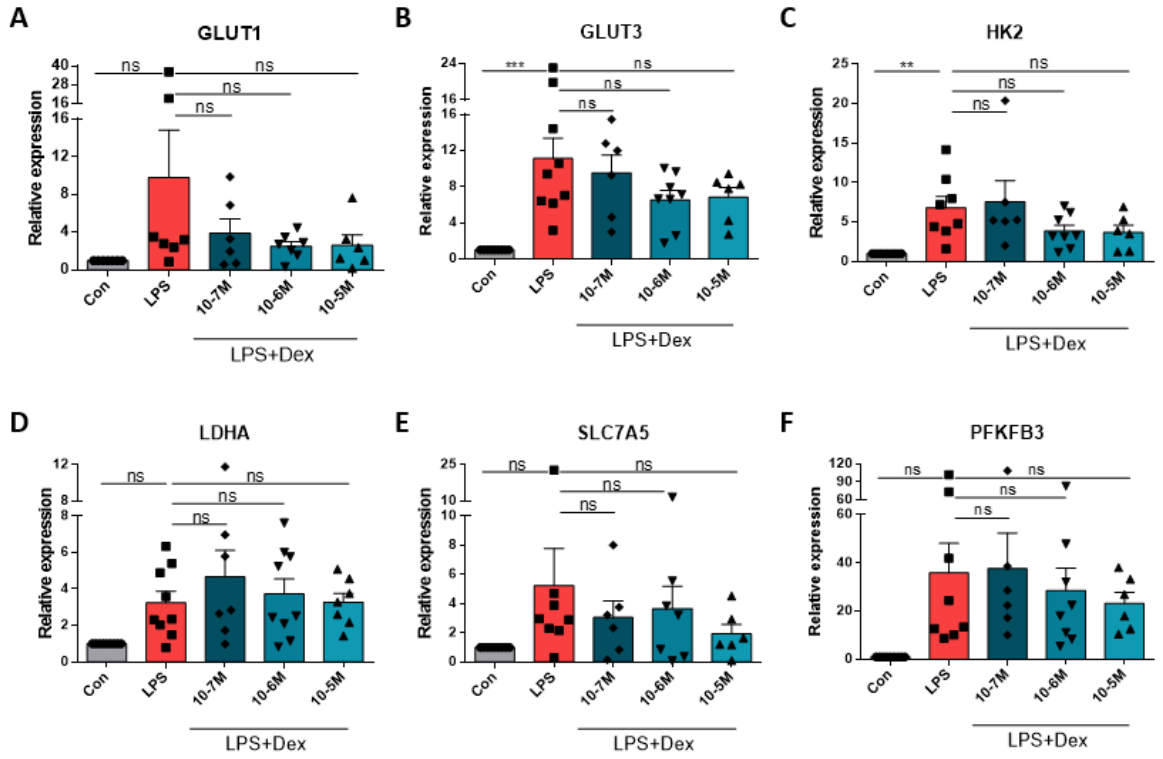

Figure 25: Effects of GCs on metabolic gene expression in LPS-activated human monocytes*. Human monocytes were isolated from buffy coat and seeded in 48-well plates. The cells were treated with LPS and/or dexamethasone (Dex) at different concentrations or left untreated (con). RNA was isolated from the samples, transcribed into cDNA, and subsequently analysed by RT-qPCR. The panels show GLUT1 (A), GLUT3 (B), HK2 (C), LDHA (D), SLC7A5 (E), and PFKFB3 (F) gene expressions. n=6-9; mean +/- SEM. Statistical analysis by 1-way ANOVA with Newman-Keuls multiple comparison test. **: p<0.01; ****: p<0.0001; n.s.: p>0.05*

3.2. Characterization of novel calcitriol-containing nanoparticles

Since calcitriol, the active form of vitamin D, has been shown to exert potent anti-inflammatory effects, it appears to be an interesting drug candidate and alternative to GCs to treat inflammatory conditions such as sepsis or ALI. [121] However, due to possible side-effect of high doses of calcitriol, [103], [105] the use of nanoparticles as a delivery vehicle should be tested as a possible strategy to overcome or minimize those adverse effects. Indeed, in the past years, the use of nanoparticles as novel drug carriers has attracted wide attention to improve targeting of specific cell types. In this work, we investigated IOH-NPs loaded with calcitriol. Previous studies using IOH-NP loaded with GCs indicated that *in vitro* they were preferentially taken up by macrophages while T and B cells didn't engulf them. [146] Since calcitriol is a lipid which cannot be easily phosphorylated, a new type of IOH-NPs was developed by Claus Feldmann and colleagues at the Karlsruhe Institute of Technology. In this work, those new IOH-NPs loaded with calcitriol or its biologically inactive precursor cholecalciferol were characterised by analysing their cell-type specificity and toxicity as well as their cellular uptake mechanism and intracellular fate *in vitro*.

3.2.1. Biological effect of free and nanoformulated calcitriol in macrophages *in vitro*

To evaluate the anti-inflammatory activity of free calcitriol (VDa) as well as calcitriol nanoparticles (VDa-NPs) in comparison to GCs *in vitro*, the macrophage cell line RAW 264.7 was analysed after LPS challenge. To this end, the cells were pre-treated either with Dex, VDa or VDa-NP followed by addition of LPS to stimulate the macrophages. After a total of 10 hrs, RNA was extracted and analysed by quantitative RT-PCR. Upon LPS challenge only, gene expression of *Il6*, *Il1b*, *Tnfa*, and *Cox2* was increased, while cell additionally treated with Dex, which served as a control, showed significantly lower *Il6* and *Il1b* (Figure 26A and 26B) as well as slightly lower *Tnfa* and *Cox2* levels (Figure 26C and 26D) compared to the previous group. Importantly, both VDa and VDa-NP significantly diminished *Il6*, *Il1b* and *Cox2* compared to cells treated only with LPS

(Figure 26A, B und D), whereas a slight tendency was observed for *Tnfa* (Figure 26C). VDa and VDa-NP treatment did not show significant differences in their capacity to reduce gene expression compared to each another. Calcitriol treatments were slightly less efficient than GC treatment with regard to *Il6* and *Il1b* levels but not for the other two genes.

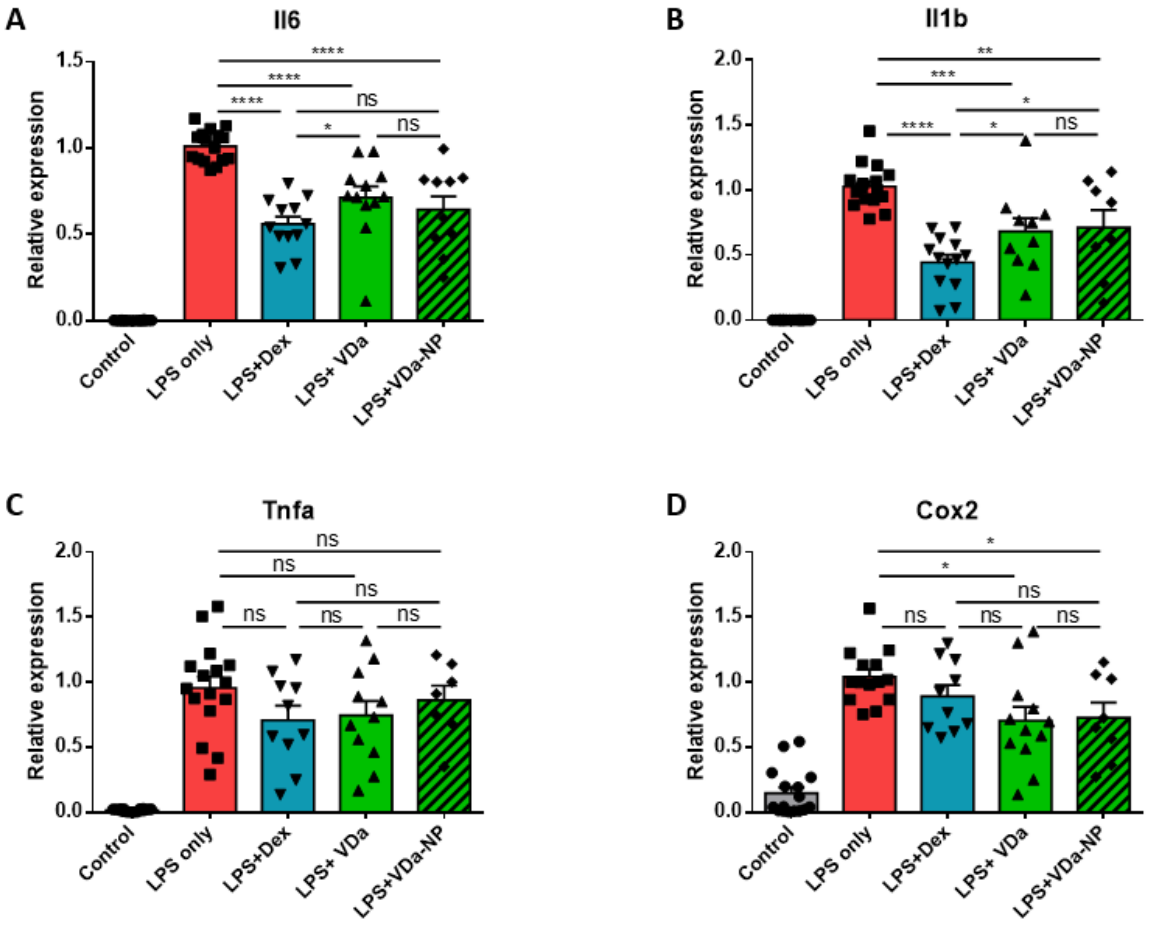

Figure 26: Effects of VDa and VDa-NPs in LPS-activated RAW 264.7 cells compared to GCs. *Cells were seeded in 24-well plates, pre-treated with dexamethasone, calcitriol or calcitriol nanoparticles for 8 hrs followed by 2 hrs of LPS challenge. Control cells were left untouched. Cells were then collected, RNA isolated and transcribed into cDNA. Subsequently, RT-qPCR was performed. The panels show Il6 (A), Il1b (B), Tnfa (C) and Cox2 (D) gene expressions. n=10-16; mean +/- SEM. Statistical analysis by 1-way ANOVA with Newman-Keuls multiple comparison test. *: p<0.05; **: p<0.01; ***: p<0.001; ****: p<0.0001; n.s.: p>0.05*

3.2.2. Cell type specific uptake of VDi-NP and cell viability upon VDi-NP treatment

Since it is well-known that different cell types show variations in their capacity to engulf small-sized material, cholecalciferol nanoparticles (VDi-NP) were characterised *in vitro* concerning this feature by using cell lines derived from immune cells and solid tissues. MH-S and RAW 264.7 cells are derived from macrophages, WEHI 7.15 and WEHI 231 are reminiscent of T and B cells, and the L929, LA-4 and C2C12 cell lines correspond to fibroblasts, epithelial cells and myoblasts, respectively (Figure 27A). First of all, the 7 cell lines were incubated with 25 μg/mL VDi-NP for up to 6 hrs and the fluorescent signal of the the dye luminogen red contained therein was measured by FACS (Figure 27B). The nanoparticles were efficiently engulfed by MH-S, L929 and RAW 264.7 cells and slightly by C2C12 cells. In contrast, neither WEHI 7.15, WEHI 231 nor LA-4 cells took up any nanoparticles. Based on these results, the three best cell lines were incubated with different VDi-NPs concentration, ranging from 0.25 μg/mL to 25 μg/mL, for 24 hrs and analysed by flow cytometry (Figure 27C). Important uptake of the nanoparticles in a time-dependent manner could again be observed but without any big differences between the three cell lines. These data suggest that cells are mainly taking up the nanoparticles within the first 6 hrs upon VDi-NP exposure and even quicker for RAW 264.7 cell line, for which around half of the nanoparticle engulfment happens already within the first 30 min (Figure 27B). Finally, the viability of the cell lines after exposure of 25 μg/mg VDi-NP for 24 hrs was analysed using an MTS assay (Figure 27D). No change in metabolic activity was observed after VDi-NP exposure compared to the control group, confirming that VDi-NP were a potentially harmless carrier system for targeting selective cell types.

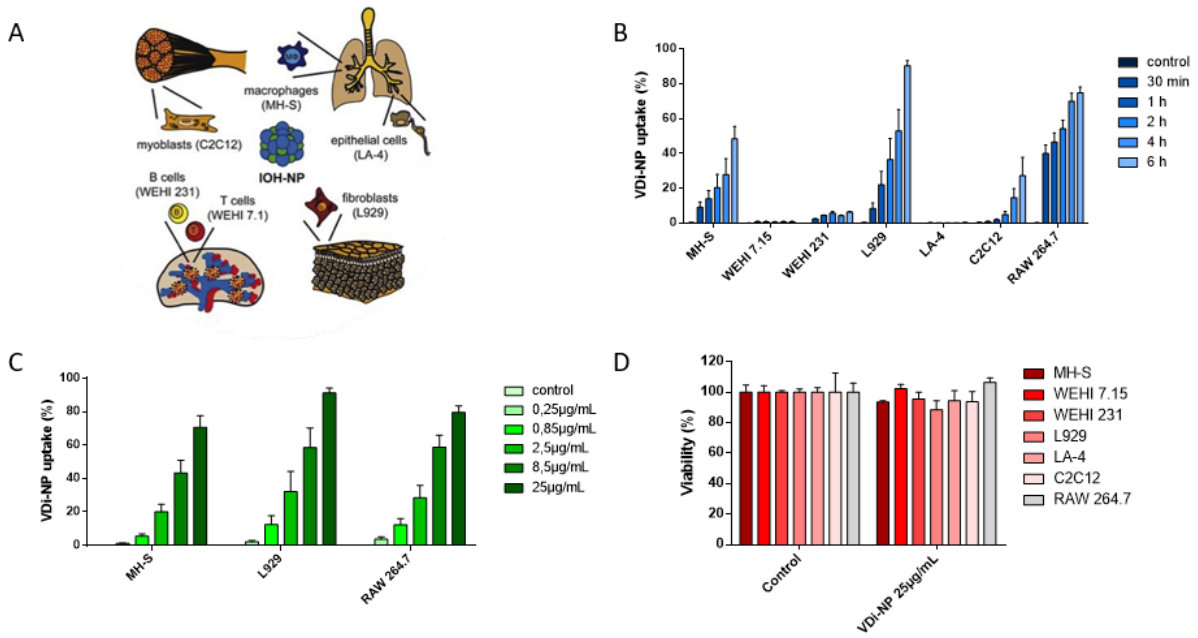

Figure 27: Cell type-selectivity of VDi-NP uptake in vitro. *The panels of this figure show a representation of the different cell lines used (A), the different cell lines VDi-NP uptake measured by FACS after cells treatment with 25µg/mL VDi-NP at different time points (B), all three MH-S, L929 and RAW 264.7 VDi-NP uptake after 24 hours incubation with different concentrations of VDi-NP (C) and the viability of the different cell lines upon 25µg/mL VDi-NP treatment for 24 hours measured by MTS assay (D). In all panels, controls were not treated with VDi-NP. n=3-8. Figure 27A is taken from Kaiser et al. (2020)* – [146]

3.2.3. Characterisation of the endocytic pathway used for VDi-NP uptake by RAW 264.7 cells

The endocytic pathway used for nanoparticle entry into cells can vary according to nanoparticle properties. Indeed, features such as the size, charge, shape and rigidity are known as important factors that determine the respective mechanism of uptake. [153]. To investigate the endocytic pathway of VDi-NP entry, the two inhibitors CytoD (cytochalasin D) and MDC (monodansyl-cadaverine) were used in RAW 264.7 cells (Figure 28A). CytoD blocks actin polymerisation thereby preventing the formation of macropinosomes and phagosomes, [154] whereas MDC inhibits clathrin-mediated endocytosis due to interferences with glutaminase, necessary for protein-crosslinking which mediates clustering and internalisation of clathrin. [155] CytoD and MDC were used at concentrations of 1 µg/mL and 150 µM, respectively.

First of all, RAW 264.7 cells were treated with 25 μg/mL VDi-NP in combination with either CytoD or MDC for up to 6 hours and analyzed by flow cytometry (Figure 28B). VDi-NP internalisation was strongly inhibited by MDC, but not by CytoD, therefore suggesting that VDi-NP uptake is mainly mediated via clathrin-dependant pinocytosis. VDi-NP uptake was also analysed 24 hrs after incubating RAW 264.7 cells with increasing concentration of VDi-NP, ranging from 2.5 μg/mL to 25 μg/mL, in the presence or absence of CytoD or MDC (Figure 28C). A reduce uptake could again be observed by flow cytometry in presence of MDC but not CytoD, thus providing further evidence for clathrin-dependant pinocytosis as the preferential VDi-NP uptake pathway. Finally, potentially toxic effects of both inhibitors in RAW 264.7 cells after 24 hrs incubation in the presence of different VDi-NP concentrations was evaluated using an MTS assay (Figure 28D). Generally, a good tolerance of both inhibitors could be observed at the chosen concentrations regardless of the presence of VDi-NP.

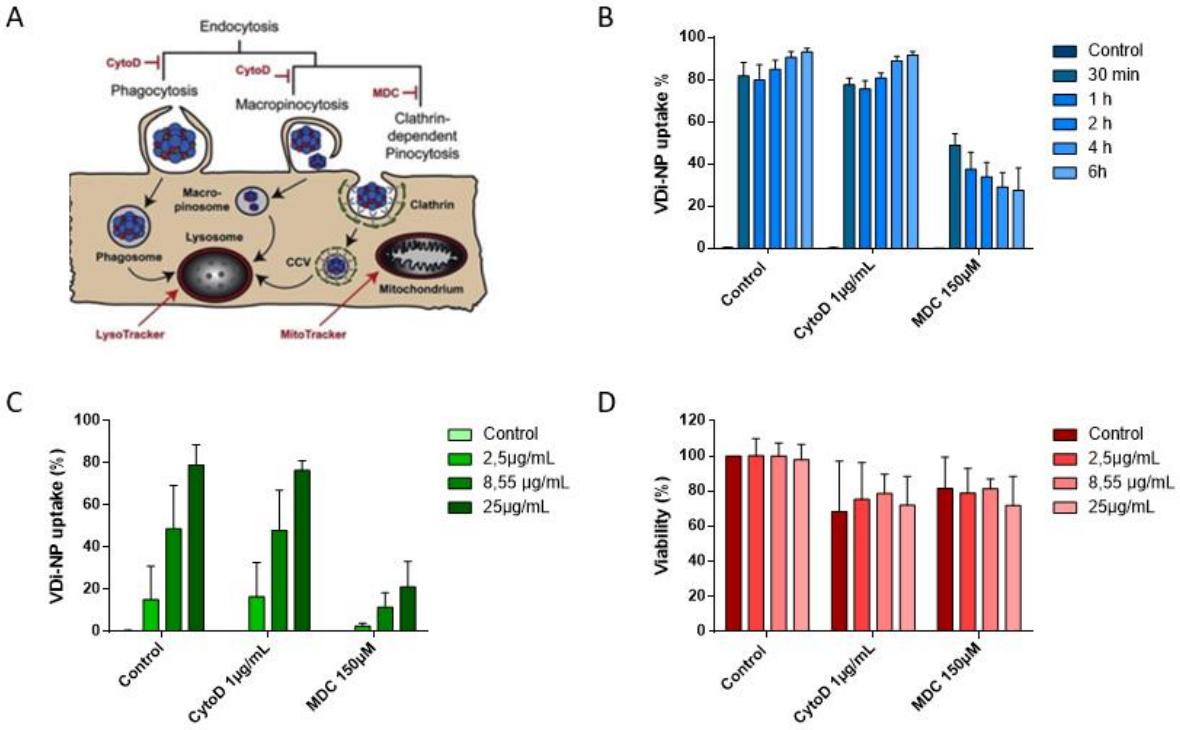

Figure 28: Analysis of the endocytic pathway of VDi-NP into RAW 264.7 cells in vitro. *The scheme illustrates the endocytic pathways, the activity of the different inhibitors as well as the intracellular organelles that can be visualised with fluorescent trackers (A). VDi-NP uptake by RAW 264.7 cells was measured by FACS after 30 min to 6 hrs after treatment with 25 μg/mL VDi-NP and 1 μg/mL CytoD or 150 μM MDC, respectively (B). VDi-NP uptake by RAW 264.7 cells was tested after 24 hrs incubation with different concentrations of VDi-NP together with the inhibitors CytoD or MDC. (C) RAW 264.7 cell viability was measured by MTS assay after 24 hrs of incubation with different concentrations of VDi-NP and the inhibitors CytoD or MDC. (D). In all panels, controls indicated in the X-axis legend were treated with VDi-NP but without any inhibitor, while the controls indicated in the upper right conner legend of each panel were not treated with VDi-NP at all. n=3-6. Figure 28A is taken from Kaiser et al. (2020) –* [146]

3.2.4. Intracellular fate of VDi-NP upon engulfment

Once taken up by cells, the fate of the nanoparticles is determined by intracellular sorting mechanisms mainly mediated by cellular endosomes in conjugation with the Golgi apparatus, the endoplasmic reticulum (ER) and the lysosomes. Since particle entry by clathrin-dependant endocytosis frequently end up in degradative lysosomes [156], we investigated whether this was also the case for VDi-NPs. To this end, RAW 264.7 cells were incubated with 8.55 μg/mL VDi-NP for 24 hrs and subsequently stained either with Mitotracker or Lysotracker. As both dyes were conjugated to a deep red (DR) dye, fluorescence could be visualised using imaging flow cytometry (Figure 29). The overlay of the Luminogen Red derived from the nanoparticles and the DR signals from the trackers resulted in isolated green and red dots when cells were stained with Mitotracker, while it resulted in a strong yellow signal due to the colocalization when the cell were stained with Lysotracker (Figure 29A). Furthermore, the degree of colocalization of the nanoparticles with lysosomes or mitochondria in the cells was determined based on the Bright Detail Similarity using the respective wizard tool of the IDEAS software (Figure 29B). Up to 40% of the cells showed a colocalization of VDi-NP with the lysosomal compartment, while less than 1.2% of the cells showed a colocalization of VDi-NP with the mitochondria (Figure 29C). Taken together, these data indicate that VDi-NP engulfed by RAW 264.7 via clathrin-dependant endocytosis traffic intracellularly to the lysosomes for degradation.

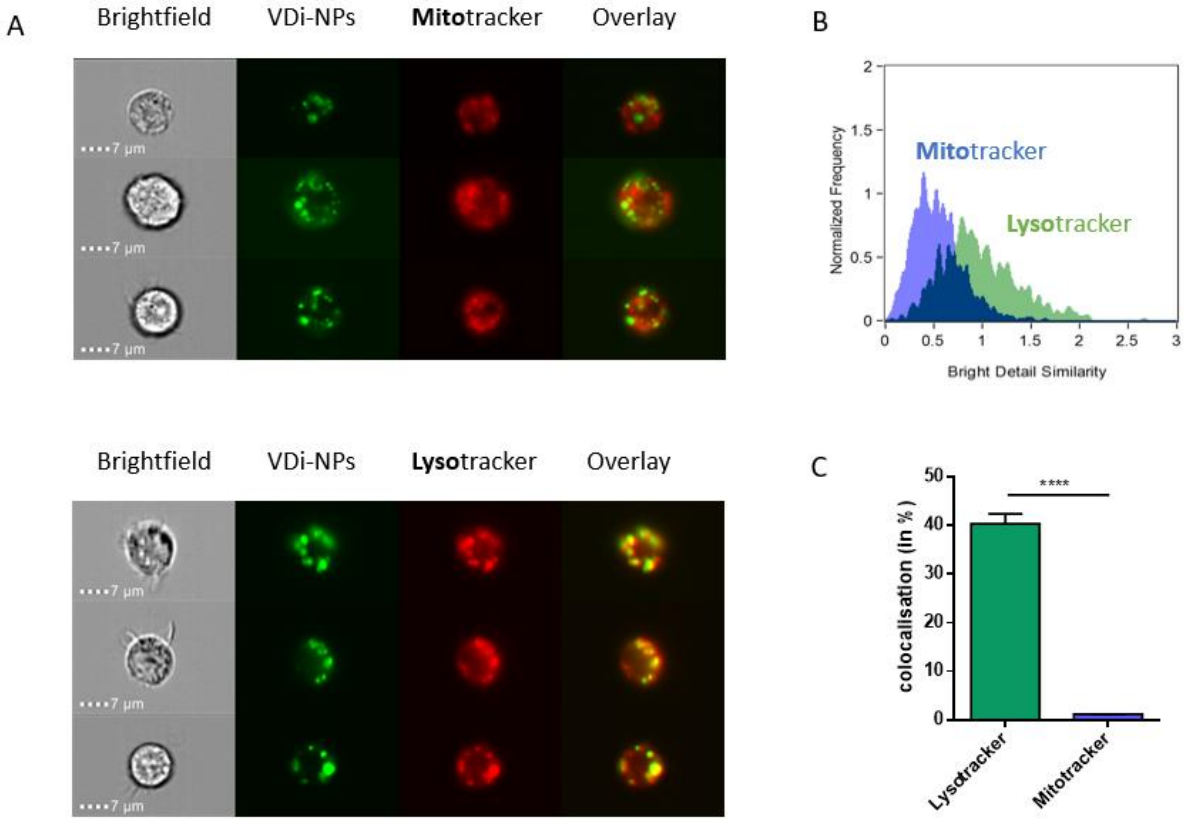

Figure 29: Detection of internalised VDi-NP in RAW 264.7 cells by imaging flow cytometry. *RAW 264.7 were incubated for 24 hrs with 8.55 μg/mL of VDi-NPs and stained with 50 nM MitoTracker Deep Red (upper panel) or 50 nM LysoTracker Deep Red (lower panel). The panels show exemplary brightfield and fluorescent images (each channel separately and as an overlay) (A). Double-positive cells for Lumogen Red and MitoTracker or LysoTracker were analysed for colocalization of both signals using the Bright Detail Similarity feature (B). Quantification of VDi-NP colocalization with lysosomes or mitochondria (C). Datas were determined in three separate experiments, each of them including >500 individual cells. n=3; mean +/- SEM. Statistical analysis was performed by unpaired t test. ***: p<0.001;*

4. Discussion

4.1. IOH-NPs as a new approach for GC therapy of sepsis

Previous results obtained by Kaiser and colleagues [146] suggested that the use of IOH-NPs is a promising strategy to achieve a targeted delivery of GCs in inflammatory conditions. In diseases such ALI and sepsis, GCs are clinically used to treat the so called "cytokine storm", although this may also aggravate the lymphocytopenia caused by sepsis, therefore leading to a severe risk of secondary infections and poor outcome. Targeting specific cell types in GC treatment could allow to overcome this side effect since IOH-NPs were shown to be mainly taken up by macrophages. Thus, we compared BMZ and BMP treatment in two mouse models: sepsis and ALI.

4.1.1. GC treatment of sepsis

Sepsis induction in C57BL/6 wildtype mice led to a weight, temperature and glucose reduction, which are all typical manifestations of sepsis in mice. [2] Additionally, a change in blood cell populations could be observed with a significant decrease in the frequency of T cells, B cells and NK cells, whereas the relative numbers of $CD11b^+$ and $CD11b^+/Ly6G^+$ myeloid cells increased and the percentage of monocytes remained unaltered. Those results are consistent with the previously described sepsis-induced lymphocytopenia. [23]–[25] Moreover, multiple organ damage, one of the most critical hallmarks of sepsis, [2] could be detected by histological analyses of spleen, liver and lung. Indeed, several physiological changes were provoked by sepsis with important cellular infiltrates and vascular congestion as well as morphologic changes in all three organs. Fluidigm® gene chip assay analysis of several genes, categorised in five groups, in spleen, liver and lung showed drastic changes after sepsis induction. As expected, cytokine and chemokine gene expression were increased during sepsis. In particular the latter category has pronounced chemoattractant properties, which results in the recruitment of additional leukocytes that will then in turn produce further pro-inflammatory mediators. Genes categorised as enzymes involved in the inflammation process (*Cox2*, *Nox2*, *Dusp1*) or endothelial barrier integrity (*Sphk1*) showed an increased expression during sepsis, and thus, along with the two first categories,

provide evidence of a strong pro-inflammatory profile in all three organs. Interestingly, *Il10* gene expression was increased in sepsis. IL-10 is indeed known to supress the production of IL-6 and IFNγ and antagonize TNFα and IL-1 signalling, [5] therefore fulfilling a mainly anti-inflammatory function. All four metabolic genes were also increased during sepsis. This is a characteristic effect of pro-inflammatory M1 macrophages predominance as these cells mainly rely on glycolysis. [157] A diverse response in the gene expression of myeloid cell molecules was noticed amongst the different organs. While some genes characteristic of an M2 macrophage phenotype (*Arg1*, *Cd163*, *Cd206*) were downregulated in spleen and liver, they seemed to be increased in the lung. This could be explained by the different micro-environments in these organs or could be related to a different macrophage population in the lung. Finally, cytokine and NO levels in the serum were significantly increased after sepsis induction, which is in line with the gene expression results supporting a strong pro-inflammatory profile in mice.

GCs are clinically used to treat the acute inflammatory phase of sepsis and septic shock due to their potent anti-inflammatory properties. [77],[78] Indeed, their use improves the patients' hemodynamic and decreases pro-inflammatory mediators as well as oxidative stress. [78] In our study, the synthetic GC betamethasone allowed us to rescue the decrease of temperature in septic mice while it did not prevent the loss of weight and the reduction of blood glucose. As the mice were severely sick, their food intake was altered, possibly due to the stress caused by sepsis, which could explain the incapacity of BMZ to rescue the weight loss in such a short time. Concerning the hypoglycaemia caused by sepsis, it has been linked to altered liver metabolism and the balance between glycolysis and gluconeogenesis but also, as for the weight loss, to reduced glucose intake. [158] The blood composition of septic mice receiving BMZ treatment showed a further reduction in the proportion of T cells, B cells and NK cells compared to septic mice not treated with BMZ while the frequency of $CD11b^+$ and $CD11b^+/Ly6G^+$ myeloid cells further increased together with the proportion of monocytes. This suggests that BMZ treatment, even though it is not significant, has the

tendency to further aggravate lymphocytopenia while myeloid cells rather get mobilized into the circulation. Histologically, BMZ could counteract physiological changes in the liver and the lung with less cell infiltration and vascular congestion. The incapacity of BMZ to change physiological damage caused by sepsis in the spleen can be explained by the strong lymphocytopenia after BMZ treatment, as the spleen immune microenvironment is composed of a mixture of T, B, and NK cells as well as macrophages while both the liver and lung contain a lower proportion of T, B, and NK cells and are rather populated by many resident macrophages. After BMZ treatment, the Fluidigm® gene chip assay analysis showed a general decrease of genes belonging to the following groups: cytokine, chemokines, enzymes, metabolism in all three analysed organs, thus showing the capacity of BMZ to exert its expected anti-inflammatory properties, with less leukocyte recruitment due to lower cytokine and chemokine levels as well as lower cellular infiltration and better organ barrier integrity as observed in histological staining due to reduced Cox2, Nox2, *Dusp1* and *Sphk1* expression. The reduced metabolic gene expression is in line with a reduction of the pro-inflammatory profile upon BMZ treatment therefore counteracting the glycolytic shift caused by sepsis. Variation could be again noticed among the different organs concerning the gene expression of myeloid cell molecules. Indeed, while some genes characteristic of an M2 macrophage phenotype (*Arg1*, *Cd163*, *Cd206*) were slightly increased in spleen, they were decreased in the lung. In the liver, complex variations were observed even between different M2 markers, e.g. *Cd206* expression was reduced upon BMZ therapy while *Cd163* and *Arg1* expression were increased. While the immune micro-environment could represent an explanation for the gene expression variations upon BMZ treatment between the different organ, the complex immune response mechanism still needs a better understanding. Finally, cytokine and NO levels in the serum were significantly decreased in septic mice receiving BMZ treatment, supporting previous results of the anti-inflammatory capacity of BMZ.

GC treatment using IOH-NPs (BMP) in septic mice showed largely similar results as BMZ treatment, although with a few variations in the blood cell populations. While application of BMZ slightly aggravated the sepsis-induced lymphocytopenia, BMP treatment did not seem to further reduce T, B, and NK cells proportions compared to non-treated septic mice although it did not reduce the lymphocytopenia caused by sepsis neither. On the other side, myeloid cell populations were similarly affected by both BMZ and BMP treatment. This could indicate a tendency of BMP-NPs to better target myeloid cells than lymphocytes therefore not aggravating sepsis-induced lymphocytopenia. However, histologically, similar effects of BMZ and BMP could be observed. BMP treatment also failed to counteract physiological changes in the spleen occurring after sepsis induction, which can be explained by a still marked lymphocytopenia upon BMP treatment. These findings enable us to conclude that BMZ and BMP treatment have similar effects with a tendency that BMP treatment does not aggravate the sepsis-caused lymphocytopenia compared to BMZ.

4.1.2. GC treatment of ALI

ALI induction in C57BL/6 wildtype mice led to high levels of cytokines in the serum as well as an increased neutrophil infiltration into the lung. Being a hallmark of ALI, [58] neutrophil infiltration into the lung confirmed a successful induction of ALI. High levels of cytokines are also consistent with the increased neutrophil infiltration as those ones, together with activated alveolar macrophages, produce important levels of pro-inflammatory mediators during the acute phase of ALI. [54], [56], [57] Moreover, increased levels of IL-1β are also linked to a reduction in VE-cadherin transcription, [159] thus leading to a disruption of the endothelial integrity. [58] This endothelial disruption also triggers the production of NO by endothelial cells [58] possibly contributing to the high NO levels in the serum of these mice. This indicates that ALI pathological features could be mimicked in the mouse model used in this study.

In the early phase of acute ARDS/ALI, GC treatment has proven to be beneficial for patients and allows to reduce mortality rates. Indeed, the use of low-dose GCs is recommended to prevent the progression of severe disease if previous treatments were insufficient, based on the GCs ability to inhibit neutrophil activation, fibroblast proliferation and collagen deposition [44] but also restore macrophage subset balance, lung function and ameliorate tissue injury. [87] In our study, treatment with the synthetic GC betamethasone drastically reduced neutrophil infiltration as well as the production of pro-inflammatory cytokines and NO. This shows that BMZ has the capacity to reduce major pathological features caused by ALI induction.

GC nanoparticle treatment (BMP) appeared to have similar effects as BMZ with a reduced neutrophil infiltration and lower levels of pro-inflammatory cytokines and NO in the serum. However, no significant differences in efficiency were seen between both GC treatments. Thus, we are unable to conclude anything about the efficacy of the targeting of myeloid cells in this model.

4.1.3. Metabolic switch in myeloid cells induced by GC therapy

The importance of glucose metabolism for immune cell function has gained much interest in recent years. [152] Since we had observed changes in metabolic gene expression in several organs both after sepsis induction in mice as well as after GC treatment, we aimed to further analyse this phenomenon *in vitro*. More specifically, we reached out to determine whether GCs exert some of their immunomodulatory effects in the context of sepsis by influencing glucose transport and glycolysis in myeloid cells. For several reasons, this phenomenon was studied in human peripheral blood monocytes. Here, we observed that LPS stimulation was responsible for a shift toward the M1 phenotype as *CD25*, a marker of monocyte/macrophage activation, *NOS2*, which is tightly link to NO production, and *IL6* expression were upregulated. On the contrary when treated with Dex, activated monocytes showed, in a dose-dependent manner, a reduction of the previously cited M1 markers and an increase of *CD163*, an M2 marker, thus confirming a shift towards an M2 phenotype. When focusing on six genes directly implicated in glycolysis and nutrient transport, an

increase of all genes could be observed upon LPS activation. This is characteristic of pro-inflammatory M1 monocytes/macrophages as they mainly rely on glycolysis. [157] When treated with Dex, monocytes showed a reduced expression of *GLUT1, GLUT3, HK2, SLC7A5* and *PFKFB3*, thus proving that GCs considerably affect the metabolism of monocytes.

4.2. *In vitro* characterization of calcitriol nanoparticles

As calcitriol has been shown to exert potent anti-inflammatory effects, it appears to be an interesting drug candidate and an alternative to GCs to treat inflammatory conditions such as sepsis or ALI. [121] However, due to possible side-effects of high doses of calcitriol, [103], [105] and its lipophilic nature, [148] which makes it difficult to administer it due to insufficient solubility and limited membrane permeability, the use of nanoparticles as a delivery vehicle are a possible strategy to overcome or minimize those problems. Since previous studies using IOH-NP loaded with GCs indicated that *in vitro* IOH-NPs were preferentially taken up by macrophages while T and B cells didn't engulf them, [146] we here analysed a new formulation of IOH-NPs adapted to calcitriol. For this, bioactivity, cell-type specificity and toxicity as well as the cellular uptake mechanism and intracellular fate *in vitro* were evaluated.

Calcitriol is known to inhibit pro-inflammatory mediators in monocytes such as *Il1*, *Il6* or *Tnfα.* [108] This notion is in line with our own results, which demonstrated a downregulation of *Il1b*, *Il6,* and *Cox2* pro-inflammatory mediators upon calcitriol treatment of the RAW 264.7 macrophage cell line. Similar anti-inflammatory effects could be observed by using our calcitriol nanoparticles VDa-NPs. Another recent study using targeted lipid calcitriol nanoparticles similarly revealed a downregulation of pro-inflammatory mediators but additionally an upregulation of *Cd163* and *Il10* expression, representative of an anti-inflammatory response, after treatment with calcitriol nanoparticles. [150] Compared to GCs used as a control, calcitriol exerted at first view comparable anti-inflammatory properties, however with a few differences for some genes.

As many cell types express the VDR, the engulfment capacity of several cell types such as macrophages, T and B cells but also fibroblast, myoblast and epithelial cells was characterised. Longer incubation times increased the uptake in all cell lines, therefore indicating an increasing accumulation of VDi-NPs within the cells. The nanoparticles were efficiently engulfed by MH-S, L929 and RAW 264.7 cells and slightly by C2C12 cells. In contrast, neither WEHI 7.15, WEHI 231 nor LA-4 cells took up the nanoparticles. Given that not only macrophages but also fibroblasts efficiently engulfed VDi-NPs, we assume that VDi-NPs are not fully cell type specific for macrophages even though they seem not to target all immune cell types as T or B cells did not show a good engulfment capacity for those nanoparticles. Those data need to be later considered when analysing the efficiency of VD-NPs in both sepsis and ALI moue models to reduce calcitriol side effects such as T and B cell apoptosis but also hypercalcemia even though the engulfment capacity of osteoblast for VDi-NPs was not tested yet.

As toxicity and side effects of nanoparticles are widely debated, [133] it is important to characterise these features. Here, a tetrazolium-based MTT assay was used in all previously mentioned cell types. Our results indicated that VDi-NPs were well tolerated by all cell lines.

When reaching the exterior membrane of the cells, nanoparticles interact with components of the plasma membrane and extracellular matrix to finally enter the cell by an endocytic pathway. [156] The endocytic pathway can however vary according to nanoparticle properties. Indeed, features such as the size, charge, shape and rigidity are known as important factors that determine the respective mechanism of uptake. [153]. To investigate the endocytic pathway of VDi-NP entry, the two commonly used inhibitors CytoD (cytochalasin D) and MDC (monodansyl-cadaverine) were administered to the RAW 264.7 macrophage cell line. CytoD blocks actin polymerisation thereby preventing the formation of macropinosomes and phagosomes, [154] whereas MDC inhibits clathrin-mediated endocytosis due to interferences with glutaminase, necessary for protein-crosslinking which mediates clustering and internalisation of clathrin. [155] The results showed a good tolerance of

both inhibitors at the chosen concentrations regardless of the presence of VDi-NP. As CytoD did not influence VDi-NP uptake in RAW 264.7, we concluded that neither phagocytosis nor macropinocytosis were involved in nanoparticle uptake. On the contrary, MDC importantly reduced the uptake, thus providing evidence for a clathrin-dependant endocytosis as the preferential VDi-NP uptake pathway. Taking place in the plasma membrane, clathrin-dependant endocytosis is the main mechanism by which cells obtain nutrient and plasma membrane component. [156] When triggered by the interaction of an agonist with its receptor, clathrin assembles to form a polygonal coating vesicle for internalisation. As most liposomes enter the cell by clathrin-dependant pinocytosis, lipidic nanoparticles uptake seems to follow the same pathway, [153] which is consistent with our findings for VDi-NP.

Moreover, in clathrin-dependant endocytosis, after internalisation the vesicle loses its clathrin before fusing with endosomes and finally lysosomes. [153] Our imaging flow cytometry results indicate indeed that VDi-NPs are travelling through lysosomes where the pharmacological agent is presumably released to become functional. The similar anti-inflammatory effects of VDa-NPs and VDa therefore confirm that once released from the nanoparticle, calcitriol still fulfils its function within the cells.

4.3. Conclusions

Our results revealed that free synthetic GCs and GC-containing nanoparticles efficiently reduce physiological, histological and molecular hallmarks of sepsis and ALI. The encapsulation of GCs in IOH-NPs slightly increases the cell type specificity without altering the therapeutic potential of GCs in sepsis and ALI. Moreover, GCs affect the metabolism of myeloid cells which are important for sepsis and ALI and could therefore represent a new target for therapeutic intervention. Finally, Calcitriol IOH-NPs have favourable features in vitro and thus the potential to serve an alternative anti-inflammatory therapy of sepsis and ALI.

References

[1] A. M. Taeb, M. H. Hooper, and P. E. Marik, “Sepsis: Current definition, pathophysiology, diagnosis, and management,” *Nutr. Clin. Pract.*, vol. 32, no. 3, pp. 296–308, 2017.

[2] J. Cavaillon, M. Singer, and T. Skirecki, “Sepsis therapies: learning from 30 years of failure of translational research to propose new leads,” *EMBO Mol. Med.*, vol. 12, no. 4, pp. 1–24, 2020.

[3] K. E. Rudd *et al.*, “Global, regional, and national sepsis incidence and mortality, 1990–2017: analysis for the Global Burden of Disease Study,” *The Lancet*, vol. 395, no. 10219. pp. 200–211, 2020.

[4] P. Arina and M. Singer, “Pathophysiology of sepsis,” *Curr. Opin. Anaesthesiol.*, vol. 34, no. 2, pp. 77–84, 2021.

[5] J. E. Gotts and M. A. Matthay, “Sepsis: Pathophysiology and clinical management,” *BMJ*, vol. 353, pp. 1–20, 2016.

[6] J. E. Lawn *et al.*, “Group B Streptococcal Disease Worldwide for Pregnant Women, Stillbirths, and Children: Why, What, and How to Undertake Estimates?,” *Clin. Infect. Dis.*, vol. 65, no. Suppl 2, pp. S89–S99, 2017.

[7] B. J. Stoll *et al.*, “Early onset neonatal sepsis: The burden of group B streptococcal and E. coli disease continues,” *Pediatrics*, vol. 127, no. 5, pp. 817–826, 2011.

[8] W. H. Organization, “Report on the Burden of Endemic Health Care-Associated Infection Worldwide Clean Care is Safer Care,” *World Heal. Organ.*, vol. 3, pp. 1–21, 2011.

[9] A. T. E. A, “DISEASES ORIGINAL,” pp. 146–149, 2018.

[10] S. Dugar, C. Choudhary, and A. Duggal, “Sepsis and septic shock: Guideline-based management,” *Cleve. Clin. J. Med.*, vol. 87, no. 1, pp. 53–64, 2020.

[11] M. Huang, S. Cai, and J. Su, “The pathogenesis of sepsis and potential therapeutic targets,” *Int. J. Mol. Sci.*, vol. 20, no. 21, 2019.

[12] A. Purcarea and S. Sovaila, “Sepsis, a 2020 review for the internist,” *Rom. J. Intern. Med.*, vol. 58, no. 3, pp. 129–137, 2020.

[13] J. Rello, F. Valenzuela-Sánchez, M. Ruiz-Rodriguez, and S. Moyano, “Sepsis: A Review of Advances in Management,” *Adv. Ther.*, vol. 34, no. 11, pp. 2393–2411, 2017.

[14] F. Gavelli, L. M. Castello, and G. C. Avanzi, “Management of sepsis and septic shock in the emergency department,” *Intern. Emerg. Med.*, vol. 16, no. 6, pp. 1649–1661, 2021.

[15] S. Esposito, G. De Simone, G. Boccia, F. De Caro, and P. Pagliano, “Sepsis and septic shock: New definitions, new diagnostic and therapeutic approaches,” *J. Glob. Antimicrob. Resist.*, vol. 10, pp. 204–212, 2017.

[16] M. D. Font, B. Thyagarajan, and A. K. Khanna, “Sepsis and Septic Shock – Basics of diagnosis, pathophysiology and clinical decision making,” *Med. Clin. North Am.*, vol. 104, no. 4, pp. 573–585, 2020.

[17] T. Sawada, “Prognosis and treatment,” *Behçet’s Dis. Prog. Recent Years Unmet Needs Futur.*, vol. 10, no. 10, pp. 171–184, 2015.

[18] A. Hunt, “Sepsis: An overview of the signs, symptoms, diagnosis, treatment and pathophysiology,” *Emerg. Nurse*, vol. 27, no. 5, pp. 32–41, 2019.

[19] J. Lee and M. M. Levy, “Treatment of Patients with Severe Sepsis and Septic Shock: Current Evidence-Based Practices.,” *R. I. Med. J. (2013)*, vol. 102, no. 10, pp. 18–21, 2019.

[20] F. Venet and G. Monneret, “Advances in the understanding and treatment of sepsis-induced immunosuppression,” *Nat. Rev. Nephrol.*, vol. 14, no. 2, pp. 121–137, 2018.

[21] C. de Roquetaillade, G. Monneret, M. Gossez, and F. Venet, “IL-7 and its beneficial role in sepsis-induced T lymphocyte dysfunction,” *Crit. Rev. Immunol.*, vol. 38, no. 6, pp. 433–451, 2018.

[22] C. Cao, M. Yu, and Y. Chai, “Pathological alteration and therapeutic implications of sepsis-induced immune cell apoptosis,” *Cell Death Dis.*, vol. 10, no. 10, pp. 1–14, 2019.

[23] J. Brady, S. Horie, and J. G. Laffey, “Role of the adaptive immune response in sepsis,” *Intensive Care Med. Exp.*, vol. 8, no. S1, pp. 1–19, 2020.

[24] I. Rubio *et al.*, “Current gaps in sepsis immunology: new opportunities for translational research,” *Lancet Infect. Dis.*, vol. 19, no. 12, pp. e422–e436, 2019.

[25] J. Chen and H. Wei, “Immune Intervention in Sepsis,” *Front. Pharmacol.*, vol. 12, no. July, pp. 1–19, 2021.

[26] C. Arens *et al.*, “Sepsis-induced long-term immune paralysis - results of a descriptive, explorative study,” *Crit. Care*, vol. 20, no. 1, pp. 10–13, 2016.

[27] T. Rimmelé *et al.*, “Immune cell phenotype and function in sepsis On behalf of the ADQI XIV Workgroup HHS Public Access,” *Shock*, vol. 45, no. 3, pp. 282–291, 2016.

[28] J. M. Cavaillon and M. Adib-Conquy, “Monocytes/macrophages and sepsis,” *Crit. Care Med.*, vol. 33, no. 12 SUPPL., pp. 10–13, 2005.

[29] D. R. Dyck and C. J. Zylak, “Acute respiratory distress in adults.,” *Radiology*, vol. 106, no. 3, pp. 497–501, 1973.

[30] G. R. Bernard *et al.*, “Gordon R. Bernard, Antonio Artigas, Kenneth L. Brigham, Jean Cat-let, Konrad Falke, Leonard Hudson, Maurice Lamy, Jean Roger LeGall, Alan Morris, Roger Spragg, and the Consensus Committee*,” *Intensive Care Med.*, vol. 9, no. 1, pp. 72–81, 1994.

[31] R. Blank and L. M. Napolitano, “Epidemiology of ARDS and ALI,” *Crit. Care Clin.*,

vol. 27, no. 3, pp. 439–458, 2011.

[32] V. Fanelli, A. Vlachou, S. Ghannadian, U. Simonetti, A. S. Slutsky, and H. Zhang, “Acute respiratory distress syndrome: New definition, current and future therapeutic options,” *J. Thorac. Dis.*, vol. 5, no. 3, pp. 326–334, 2013.

[33] J. Wind *et al.*, “Epidemiology of acute lung injury and acute respiratory distress syndrome in The Netherlands: A survey,” *Respir. Med.*, vol. 101, no. 10, pp. 2091–2098, 2007.

[34] F. Frutos-Vivar, N. D. Ferguson, and A. Esteban, “Epidemiology of acute lung injury and acute respiratory distress syndrome,” *Semin. Respir. Crit. Care Med.*, vol. 27, no. 4, pp. 327–336, 2006.

[35] T. Pham and G. D. Rubenfeld, “Fifty years of research in ards the epidemiology of acute respiratory distress syndrome a 50th birthday review,” *Am. J. Respir. Crit. Care Med.*, vol. 195, no. 7, pp. 860–870, 2017.

[36] G. D. Rubenfeld, “Epidemiology of acute lung injury,” *Crit. Care Med.*, vol. 31, no. 4 SUPPL., 2003.

[37] J. J. Zimmerman, S. R. Akhtar, E. Caldwell, and G. D. Rubenfeld, “Incidence and outcomes of pediatric acute lung injury,” *Pediatrics*, vol. 124, no. 1, pp. 87–95, 2009.

[38] N. S. MacCallum and T. W. Evans, “Epidemiology of acute lung injury,” *Curr. Opin. Crit. Care*, vol. 11, no. 1, pp. 43–49, 2005.

[39] R. Gotzev and P. Kenarov, “Acute Respiratory Distress Syndrome (ARDS),” *Anaesthesiol. Intensive Care*, vol. 42, no. 1, pp. 43–49, 2013.

[40] D. Mokra, “Acute Lung Injury – From Pathophysiology to Treatment Department of Physiology , Jessenius Faculty of Medicine in Martin , Comenius University in,” vol. 69, 2020.

[41] E. Fan, D. Brodie, and A. S. Slutsky, “Acute respiratory distress syndrome

advances in diagnosis and treatment," *JAMA - J. Am. Med. Assoc.*, vol. 319, no. 7, pp. 698–710, 2018.

[42] T. S. De Guia, "Acute respiratory distress syndrome: Diagnosis and management," *Respirology*, vol. 1, no. 1, pp. 23–30, 1996.

[43] C. Pan, L. Liu, J. F. Xie, and H. B. Qiu, "Acute respiratory distress syndrome: Challenge for diagnosis and therapy," *Chin. Med. J. (Engl).*, vol. 131, no. 10, pp. 1220–1224, 2018.

[44] J. V. Diaz, R. Brower, C. S. Calfee, and M. A. Matthay, "Therapeutic strategies for severe acute lung injury," *Crit. Care Med.*, vol. 38, no. 8, pp. 1644–1650, 2010.

[45] E. Mahone, Mark and B. Denckla, Martha, "untitled _ Enhanced Reader.pdf," *Clinical Infectious Diseases*. 2017.

[46] M. Umbrello, P. Formenti, L. Bolgiaghi, and D. Chiumello, "Current concepts of ARDS: A narrative review," *Int. J. Mol. Sci.*, vol. 18, no. 1, pp. 1–20, 2017.

[47] K. Raghavendran, D. Willson, and R. H. Notter, "Surfactant Therapy for Acute Lung Injury and Acute Respiratory Distress Syndrome," *Crit. Care Clin.*, vol. 27, no. 3, pp. 525–559, 2011.

[48] F. Gebistorf, O. Karam, J. Wetterslev, and A. Afshari, "Inhaled nitric oxide for acute respiratory distress syndrome (ARDS) in children and adults," *Cochrane Database Syst. Rev.*, vol. 2016, no. 6, 2016.

[49] J. E. Levitt and M. A. Matthay, "Treatment of acute lung injury: Historical perspective and potential future therapies," *Semin. Respir. Crit. Care Med.*, vol. 27, no. 4, pp. 426–438, 2006.

[50] J. M. Camamo, R. H. McCoy, and B. L. Erstad, "Retrospective evaluation of inhaled prostaglandins in patients with acute respiratory distress syndrome," *Pharmacotherapy*, vol. 25, no. 2, pp. 184–190, 2005.

[51] C. R. Bassford, D. R. Thickett, and G. D. Perkins, "The rise and fall of β-agonists in

the treatment of ARDS," *Crit. Care*, vol. 16, no. 2, 2012.

[52] R. P. Iii *et al.*, "NIH Public Access," vol. 40, no. 1, pp. 90–97, 2013.

[53] F. M. Lang, K. M. Lee, and J. A. Hamilton, "GM-CSF-based treatments in COVID-19 : reconciling opposing therapeutic approaches," *Nat. Rev. Immunol.*

[54] S. Han and R. K. Mallampalli, "The Acute Respiratory Distress Syndrome: From Mechanism to Translation," *J. Immunol.*, vol. 194, no. 3, pp. 855–860, 2015.

[55] V. Kumar, "Pulmonary Innate Immune Response Determines the Outcome of Inflammation During Pneumonia and Sepsis-Associated Acute Lung Injury," *Front. Immunol.*, vol. 11, no. August, p. 1722, 2020.

[56] Y. Butt, A. Kurdowska, and T. C. Allen, "Acute lung injury: A clinical and molecular review," *Arch. Pathol. Lab. Med.*, vol. 140, no. 4, pp. 345–350, 2016.

[57] J. Grommes and O. Soehnlein, "Contribution of neutrophils to acute lung injury," *Mol. Med.*, vol. 17, no. 3–4, pp. 293–307, 2011.

[58] R. B. Andrew J. Fritz1, Nitasha Sehgal2, Artem Pliss3, Jinhui Xu4, "乳鼠心肌提取 HHS Public Access," *Physiol. Behav.*, vol. 176, no. 3, pp. 139–148, 2020.

[59] K. D. Liu and M. A. Matthay, "Advances in critical care for the nephrologist: Acute lung injury/ARDS," *Clin. J. Am. Soc. Nephrol.*, vol. 3, no. 2, pp. 578–586, 2008.

[60] D. Mokra and P. Kosutova, "Biomarkers in acute lung injury," *Respir. Physiol. Neurobiol.*, vol. 209, pp. 52–58, 2015.

[61] P. Cheng, S. Li, and H. Chen, "Macrophages in lung injury, repair and fibrosis," *Cells*, vol. 10, no. 2, pp. 1–17, 2021.

[62] S. Timmermans, J. Souffriau, and C. Libert, "A general introduction to glucocorticoid biology," *Front. Immunol.*, vol. 10, no. JULY, 2019.

[63] D. W. Cain and J. A. Cidlowski, "Immune regulation by glucocorticoids," *Nat. Rev. Immunol.*, vol. 17, no. 4, pp. 233–247, 2017.

[64] N. C. Nicolaides, E. Kyratzi, A. Lamprokostopoulou, G. P. Chrousos, and E. Charmandari, “Stress, the stress system and the role of glucocorticoids,” *Neuroimmunomodulation*, vol. 22, pp. 6–19, 2014.

[65] J. P. Herman *et al.*, “Response,” vol. 6, no. 2, pp. 603–621, 2016.

[66] G.-Z. Rosenstein, “Dysfunction,” *Income Choice Biol. Control Syst.*, pp. 107–136, 2020.

[67] A. E. Coutinho and K. E. Chapman, “The anti-inflammatory and immunosuppressive effects of glucocorticoids, recent developments and mechanistic insights,” *Mol. Cell. Endocrinol.*, vol. 335, no. 1, pp. 2–13, 2011.

[68] L. Escoter-Torres, G. Caratti, A. Mechtidou, J. Tuckermann, N. H. Uhlenhaut, and S. Vettorazzi, “Fighting the fire: Mechanisms of inflammatory gene regulation by the glucocorticoid receptor,” *Front. Immunol.*, vol. 10, no. AUG, pp. 1–17, 2019.

[69] M. E. Bauer, “Stress, glucocorticoids and ageing of the immune system,” *Stress*, vol. 8, no. 1, pp. 69–83, 2005.

[70] A. Shimba and K. Ikuta, “Glucocorticoids Regulate Circadian Rhythm of Innate and Adaptive Immunity,” *Front. Immunol.*, vol. 11, no. September, pp. 1–8, 2020.

[71] U. Baschant and J. Tuckermann, “The role of the glucocorticoid receptor in inflammation and immunity,” *J. Steroid Biochem. Mol. Biol.*, vol. 120, no. 2–3, pp. 69–75, 2010.

[72] M. A. Bassi, M. A. Lopez, L. Confalone, R. M. Gaudio, L. Lombardo, and D. Lauritano, “Enhanced Reader.pdf,” *Nature*, vol. 388. pp. 539–547, 2020.

[73] S. Ronchetti, E. Ricci, G. Migliorati, M. Gentili, and C. Riccardi, “How glucocorticoids affect the neutrophil life,” *Int. J. Mol. Sci.*, vol. 19, no. 12, 2018.

[74] A. Shimba and K. Ikuta, “Control of immunity by glucocorticoids in health and disease,” *Semin. Immunopathol.*, vol. 42, no. 6, pp. 669–680, 2020.

[75] D. Diaz-Jimenez, J. P. Kolb, and J. A. Cidlowski, “Glucocorticoids as Regulators of

Macrophage-Mediated Tissue Homeostasis," *Front. Immunol.*, vol. 12, no. May, pp. 1–14, 2021.

[76] P. E. Marik, "Glucocorticoids in sepsis: Dissecting facts from fiction," *Crit. Care*, vol. 15, no. 3, pp. 2010–2012, 2011.

[77] S. R. Moss and H. C. Prescott, "Current Controversies in Sepsis Management," *Semin. Respir. Crit. Care Med.*, vol. 40, no. 5, pp. 594–603, 2019.

[78] M. Aziz and P. Wang, "Glucocorticoid resistance and hyperlactatemia: A tag team to worsen sepsis," *Cell Metab.*, vol. 33, no. 9, pp. 1717–1718, 2021.

[79] K. Dendoncker and C. Libert, "Glucocorticoid resistance as a major drive in sepsis pathology," *Cytokine Growth Factor Rev.*, vol. 35, pp. 85–96, 2017.

[80] J. Vandewalle *et al.*, "Combined glucocorticoid resistance and hyperlactatemia contributes to lethal shock in sepsis," *Cell Metab.*, vol. 33, no. 9, p. 1763–1776.e5, 2021.

[81] E. Antonucci, E. Fiaccadori, F. S. Taccone, and J. L. Vincent, "Glucocorticoid administration in sepsis and septic shock: Time for a paradigm change?," *Minerva Anestesiol.*, vol. 80, no. 9, pp. 1058–1062, 2014.

[82] J. Vandewalle and C. Libert, "Glucocorticoids in Sepsis: To Be or Not to Be," *Front. Immunol.*, vol. 11, no. July, pp. 1–14, 2020.

[83] R. B. Moraes, "Corticosteroid Therapy for Severe Sepsis and Septic Shock," *Jama*, vol. 302, no. 15, p. 1643, 2009.

[84] F. Fang *et al.*, "Association of Corticosteroid Treatment with Outcomes in Adult Patients with Sepsis: A Systematic Review and Meta-analysis," *JAMA Internal Medicine*, vol. 179, no. 2. pp. 213–223, 2019.

[85] B. M. Batzofin, C. L. Sprung, and Y. G. Weiss, "The use of steroids in the treatment of severe sepsis and septic shock," *Best Pract. Res. Clin. Endocrinol. Metab.*, vol. 25, no. 5, pp. 735–743, 2011.

[86] G. C. Khilnani and V. Hadda, “Corticosteroids and ARDS: A review of treatment and prevention evidence,” *Lung India*, vol. 28, no. 2, pp. 114–119, 2011.

[87] G. wei Tu *et al.*, “Glucocorticoid attenuates acute lung injury through induction of type 2 macrophage,” *J. Transl. Med.*, vol. 15, no. 1, pp. 1–11, 2017.

[88] S. Vettorazzi *et al.*, “Glucocorticoids limit acute lung inflammation in concert with inflammatory stimuli by induction of SphK1,” *Nat. Commun.*, vol. 6, pp. 1–12, 2015.

[89] V. I. Alexaki and H. Henneicke, “The Role of Glucocorticoids in the Management of COVID-19,” *Horm. Metab. Res.*, vol. 53, no. 1, pp. 9–15, 2021.

[90] Mattos-Silva P, Felix NS, Silva PL, Robba C, Battaglini D, Pelosi P, Rocco PRM, Cruz FF. Pros and cons of corticosteroid therapy for COVID-19 patients. Respir Physiol Neurobiol. 2020 Sep;280:103492.

[91] Xiang Z, Liu J, Shi D, Chen W, Li J, Yan R, Bi Y, Hu W, Zhu Z, Yu Y, Yang Z. Glucocorticoids improve severe or critical COVID-19 by activating ACE2 and reducing IL-6 levels. Int J Biol Sci. 2020 Jun 27;16(13):2382-2391.

[92] Ye ZW, Yuan S, Chan JF, Zhang AJ, Yu CY, Ong CP, Yang D, Chan CC, Tang K, Cao J, Poon VK, Chan CC, Cai JP, Chu H, Yuen KY, Jin DY. Beneficial effect of combinational methylprednisolone and remdesivir in hamster model of SARS-CoV-2 infection. Emerg Microbes Infect. 2021 Dec;10(1):291-304.

[93] Edalatifard M, Akhtari M, Salehi M, Naderi Z, Jamshidi A, Mostafaei S, Najafizadeh SR, Farhadi E, Jalili N, Esfahani M, Rahimi B, Kazemzadeh H, Mahmoodi Aliabadi M, Ghazanfari T, Sattarian M, Ebrahimi Louyeh H, Raeeskarami SR, Jamalimoghadamsiahkali S, Khajavirad N, Mahmoudi M, Rostamian A. Intravenous methylprednisolone pulse as a treatment for hospitalised severe COVID-19 patients: results from a randomised controlled clinical trial. Eur Respir J. 2020 Dec 24;56(6):2002808.

[94] RECOVERY Collaborative Group, Horby P, Lim WS, Emberson JR, Mafham M, Bell

JL, Linsell L, Staplin N, Brightling C, Ustianowski A, Elmahi E, Prudon B, Green C, Felton T, Chadwick D, Rege K, Fegan C, Chappell LC, Faust SN, Jaki T, Jeffery K, Montgomery A, Rowan K, Juszczak E, Baillie JK, Haynes R, Landray MJ. Dexamethasone in Hospitalized Patients with Covid-19. N Engl J Med. 2021 Feb 25;384(8):693-704.

[95] Ramiro S, Mostard RLM, Magro-Checa C, van Dongen CMP, Dormans T, Buijs J, Gronenschild M, de Kruif MD, van Haren EHJ, van Kraaij T, Leers MPG, Peeters R, Wong DR, Landewé RBM. Historically controlled comparison of glucocorticoids with or without tocilizumab versus supportive care only in patients with COVID-19-associated cytokine storm syndrome: results of the CHIC study. Ann Rheum Dis. 2020 Sep;79(9):1143-1151.

[96] WHO Rapid Evidence Appraisal for COVID-19 Therapies (REACT) Working Group, Sterne JAC, Murthy S, Diaz JV, Slutsky AS, Villar J, Angus DC, Annane D, Azevedo LCP, Berwanger O, Cavalcanti AB, Dequin PF, Du B, Emberson J, Fisher D, Giraudeau B, Gordon AC, Granholm A, Green C, Haynes R, Heming N, Higgins JPT, Horby P, Jüni P, Landray MJ, Le Gouge A, Leclerc M, Lim WS, Machado FR, McArthur C, Meziani F, Møller MH, Perner A, Petersen MW, Savovic J, Tomazini B, Veiga VC, Webb S, Marshall JC. Association Between Administration of Systemic Corticosteroids and Mortality Among Critically Ill Patients With COVID-19: A Meta-analysis. JAMA. 2020 Oct 6;324(13):1330-1341.

[97] Agarwal A, Rochwerg B, Lamontagne F, Siemieniuk RA, Agoritsas T, Askie L, Lytvyn L, Leo YS, Macdonald H, Zeng L, Amin W, Barragan FAJ, Bausch FJ, Burhan E, Calfee CS, Cecconi M, Chanda D, Dat VQ, De Sutter A, Du B, Freedman S, Geduld H, Gee P, Gotte M, Harley N, Hashimi M, Hunt B, Jehan F, Kabra SK, Kanda S, Kim YJ, Kissoon N, Krishna S, Kuppalli K, Kwizera A, Lado Castro-Rial M, Lisboa T, Lodha R, Mahaka I, Manai H, Mino G, Nsutebu E, Preller J, Pshenichnaya N, Qadir N, Relan P, Sabzwari S, Sarin R, Shankar-Hari M, Sharland M, Shen Y, Ranganathan SS, Souza JP, Stegemann M, Swanstrom R, Ugarte S, Uyeki T,

Venkatapuram S, Vuyiseka D, Wijewickrama A, Tran L, Zeraatkar D, Bartoszko JJ, Ge L, Brignardello-Petersen R, Owen A, Guyatt G, Diaz J, Kawano-Dourado L, Jacobs M, Vandvik PO. A living WHO guideline on drugs for covid-19. BMJ. 2020 Sep 4;370:m3379. doi: 10.1136/bmj.m3379.

[98] Borel P, Caillaud D, Cano NJ. Vitamin D bioavailability: state of the art. Crit Rev Food Sci Nutr. 2015;55(9):1193-205.

[99] Holick MF, Binkley NC, Bischoff-Ferrari HA, Gordon CM, Hanley DA, Heaney RP, Murad MH, Weaver CM; Endocrine Society. Evaluation, treatment, and prevention of vitamin D deficiency: an Endocrine Society clinical practice guideline. J Clin Endocrinol Metab. 2011 Jul;96(7):1911-30.

[100] Holick MF. Sunlight and vitamin D for bone health and prevention of autoimmune diseases, cancers, and cardiovascular disease. Am J Clin Nutr. 2004 Dec;80(6 Suppl):1678S-88S.

[101] Holick MF. The vitamin D deficiency pandemic: Approaches for diagnosis, treatment and prevention. Rev Endocr Metab Disord. 2017 Jun;18(2):153-165.

[102] Casseb GAS, Kaster MP, Rodrigues ALS. Potential Role of Vitamin D for the Management of Depression and Anxiety. CNS Drugs. 2019 Jul;33(7):619-637.

[103] Holick MF, Chen TC. Vitamin D deficiency: a worldwide problem with health consequences. Am J Clin Nutr. 2008 Apr;87(4):1080S-6S.

[104] Giustina A, Adler RA, Binkley N, Bollerslev J, Bouillon R, Dawson-Hughes B, Ebeling PR, Feldman D, Formenti AM, Lazaretti-Castro M, Marcocci C, Rizzoli R, Sempos CT, Bilezikian JP. Consensus statement from 2nd International Conference on Controversies in Vitamin D. Rev Endocr Metab Disord. 2020 Mar;21(1):89-116.

[105] Jones G. Pharmacokinetics of vitamin D toxicity. Am J Clin Nutr. 2008 Aug;88(2):582S-586S.

[106] Bartley J. Vitamin D: emerging roles in infection and immunity. Expert Rev Anti Infect Ther. 2010 Dec;8(12):1359-69.

[107] Lagishetty V, Liu NQ, Hewison M. Vitamin D metabolism and innate immunity. Mol Cell Endocrinol. 2011 Dec 5;347(1-2):97-105.

[108] Maruotti N, Cantatore FP. Vitamin D and the immune system. J Rheumatol. 2010 Mar;37(3):491-5.

[109] Szodoray P, Nakken B, Gaal J, Jonsson R, Szegedi A, Zold E, Szegedi G, Brun JG, Gesztelyi R, Zeher M, Bodolay E. The complex role of vitamin D in autoimmune diseases. Scand J Immunol. 2008 Sep;68(3):261-9.

[110] Zughaier SM, Lubberts E, Bener A. Editorial: Immune-Modulatory Effects of Vitamin D. Front Immunol. 2020 Sep 29;11:596611.

[111] Prietl B, Treiber G, Pieber TR, Amrein K. Vitamin D and immune function. Nutrients. 2013 Jul 5;5(7):2502-21.

[112] Sassi F, Tamone C, D'Amelio P. Vitamin D: Nutrient, Hormone, and Immunomodulator. Nutrients. 2018 Nov 3;10(11):1656.

[113] Alharbi A. A Potential Role of Vitamin D on Platelet Leukocyte Aggregation and Pathological Events in Sepsis: An Updated Review. J Inflamm Res. 2021 Jul 30;14:3651-3664.

[114] Xiao D, Zhang X, Ying J, Zhou Y, Li X, Mu D, Qu Y. Association between vitamin D status and sepsis in children: A meta-analysis of observational studies. Clin Nutr. 2020 Jun;39(6):1735-1741.

[115] Kempker JA, Tangpricha V, Ziegler TR, Martin GS. Vitamin D in sepsis: from basic science to clinical impact. Crit Care. 2012 Jul 19;16(4):316.

[116] Rech MA, Hunsaker T, Rodriguez J. Deficiency in 25-hydroxyvitamin D and 30-day mortality in patients with severe sepsis and septic shock. Am J Crit Care. 2014 Sep;23(5):e72-9.

[117] Kempker JA, Han JE, Tangpricha V, Ziegler TR, Martin GS. Vitamin D and sepsis: An emerging relationship. Dermatoendocrinol. 2012 Apr 1;4(2):101-8.

[118] Chapman K, Alhajhusain A. A few follow-up questions to a recent calcitriol and sepsis study. Am J Respir Crit Care Med. 2014 Nov 15;190(10):1194.

[119] Leaf DE, Raed A, Donnino MW, Ginde AA, Waikar SS. Randomized controlled trial of calcitriol in severe sepsis. Am J Respir Crit Care Med. 2014 Sep 1;190(5):533-41.

[120] Han JE, Ziegler TR. Vitamin D supplementation in sepsis and critical illness: where are we now? Am J Respir Crit Care Med. 2014 Sep 1;190(5):483-5.

[121] Takeuti FAC, Guimaraes FSF, Guimaraes PSF. Applications of vitamin D in sepsis prevention. Discov Med. 2018 Jun;25(140):291-297.

[122] Watkins RR, Yamshchikov AV, Lemonovich TL, Salata RA. The role of vitamin D deficiency in sepsis and potential therapeutic implications. J Infect. 2011 Nov;63(5):321-6.

[123] Ahmad S, Arora S, Khan S, Mohsin M, Mohan A, Manda K, Syed MA. Vitamin D and its therapeutic relevance in pulmonary diseases. J Nutr Biochem. 2021 Apr;90:108571.

[124] Herr C, Greulich T, Koczulla RA, Meyer S, Zakharkina T, Branscheidt M, Eschmann R, Bals R. The role of vitamin D in pulmonary disease: COPD, asthma, infection, and cancer. Respir Res. 2011 Mar 18;12(1):31.

[125] Bartley J. Vitamin D, innate immunity and upper respiratory tract infection. J Laryngol Otol. 2010 May;124(5):465-9.

[126] Jachvadze M, Cholokava N, Gogberashvili K. INFLUENCE OF VITAMIN D ON HUMAN HEALTH (REVIEW). Georgian Med News. 2021 Dec;(321):36-41.

[127] Kloc M, Ghobrial RM, Lipińska-Opałka A, Wawrzyniak A, Zdanowski R, Kalicki B, Kubiak JZ. Effects of vitamin D on macrophages and myeloid-derived suppressor

cells (MDSCs) hyperinflammatory response in the lungs of COVID-19 patients. Cell Immunol. 2021 Feb;360:104259.

[128] Ohaegbulam KC, Swalih M, Patel P, Smith MA, Perrin R. Vitamin D Supplementation in COVID-19 Patients: A Clinical Case Series. Am J Ther. 2020 Sep/Oct;27(5):e485-e490.

[129] Zelzer S, Prüller F, Curcic P, Sloup Z, Holter M, Herrmann M, Mangge H. Vitamin D Metabolites and Clinical Outcome in Hospitalized COVID-19 Patients. Nutrients. 2021 Jun 22;13(7):2129.

[130] Quesada-Gomez JM, Entrenas-Castillo M, Bouillon R. Vitamin D receptor stimulation to reduce acute respiratory distress syndrome (ARDS) in patients with coronavirus SARS-CoV-2 infections: Revised Ms SBMB 2020_166. J Steroid Biochem Mol Biol. 2020 Sep;202:105719.

[131] Xu J, Yang J, Chen J, Luo Q, Zhang Q, Zhang H. Vitamin D alleviates lipopolysaccharide-induced acute lung injury via regulation of the renin-angiotensin system. Mol Med Rep. 2017 Nov;16(5):7432-7438.

[132] Gorman S, Buckley AG, Ling KM, Berry LJ, Fear VS, Stick SM, Larcombe AN, Kicic A, Hart PH. Vitamin D supplementation of initially vitamin D-deficient mice diminishes lung inflammation with limited effects on pulmonary epithelial integrity. Physiol Rep. 2017 Aug;5(15):e13371.

[133] Yetisgin AA, Cetinel S, Zuvin M, Kosar A, Kutlu O. Therapeutic Nanoparticles and Their Targeted Delivery Applications. Molecules. 2020 May 8;25(9):2193.

[134] Cardoso AM, Guedes JR, Cardoso AL, Morais C, Cunha P, Viegas AT, Costa R, Jurado A, Pedroso de Lima MC. Recent Trends in Nanotechnology Toward CNS Diseases: Lipid-Based Nanoparticles and Exosomes for Targeted Therapeutic Delivery. Int Rev Neurobiol. 2016;130:1-40.

[135] De Jong WH, Borm PJ. Drug delivery and nanoparticles:applications and hazards. Int J Nanomedicine. 2008;3(2):133-49.

[136] Mitchell MJ, Billingsley MM, Haley RM, Wechsler ME, Peppas NA, Langer R. Engineering precision nanoparticles for drug delivery. Nat Rev Drug Discov. 2021 Feb;20(2):101-124.

[137] Poupot R, Goursat C, Fruchon S. Multivalent nanosystems: targeting monocytes/macrophages. Int J Nanomedicine. 2018 Sep 19;13:5511-5521.

[138] Mukherjee B. Nanosize drug delivery system. Curr Pharm Biotechnol. 2013;14(15):1221.

[139] Hosseini SH, Maleki A, Eshraghi HR, Hamidi M. Preparation and in vitro/pharmacokinetic/pharmacodynamic evaluation of a slow-release nano-liposomal form of prednisolone. Drug Deliv. 2016 Oct;23(8):3008-3016.

[140] Montes-Cobos E, Ring S, Fischer HJ, Heck J, Strauß J, Schwaninger M, Reichardt SD, Feldmann C, Lühder F, Reichardt HM. Targeted delivery of glucocorticoids to macrophages in a mouse model of multiple sclerosis using inorganic-organic hybrid nanoparticles. J Control Release. 2017 Jan 10;245:157-169.

[141] Jhaveri AM, Torchilin VP. Multifunctional polymeric micelles for delivery of drugs and siRNA. Front Pharmacol. 2014 Apr 25;5:77.

[142] Ren K, Dusad A, Yuan F, Yuan H, Purdue PE, Fehringer EV, Garvin KL, Goldring SR, Wang D. Macromolecular prodrug of dexamethasone prevents particle-induced peri-implant osteolysis with reduced systemic side effects. J Control Release. 2014 Feb 10;175:1-9.

[143] Larson N, Ghandehari H. Polymeric conjugates for drug delivery. Chem Mater. 2012 Mar 13;24(5):840-853.

[144] Lühder F, Reichardt HM. Novel Drug Delivery Systems Tailored for Improved Administration of Glucocorticoids. Int J Mol Sci. 2017 Aug 24;18(9):1836.

[145] Heck JG, Napp J, Simonato S, Möllmer J, Lange M, Reichardt HM, Staudt R, Alves F, Feldmann C. Multifunctional phosphate-based inorganic-organic hybrid

nanoparticles. J Am Chem Soc. 2015 Jun 17;137(23):7329-36.

[146] Kaiser TK, Khorenko M, Moussavi A, Engelke M, Boretius S, Feldmann C, Reichardt HM. Highly selective organ distribution and cellular uptake of inorganic-organic hybrid nanoparticles customized for the targeted delivery of glucocorticoids. J Control Release. 2020 Mar 10;319:360-370.

[147] Kaiser TK, Li H, Roßmann L, Reichardt SD, Bohnenberger H, Feldmann C, Reichardt HM. Glucocorticoids delivered by inorganic-organic hybrid nanoparticles mitigate acute graft-versus-host disease and sustain graft-versus-leukemia activity. Eur J Immunol. 2020 Aug;50(8):1220-1233.

[148] Glowka E, Stasiak J, Lulek J. Drug Delivery Systems for Vitamin D Supplementation and Therapy. Pharmaceutics. 2019 Jul 18;11(7):347.

[149] Rudd KE, Johnson SC, Agesa KM, Shackelford KA, Tsoi D, Kievlan DR, Colombara DV, Ikuta KS, Kissoon N, Finfer S, Fleischmann-Struzek C, Machado FR, Reinhart KK, Rowan K, Seymour CW, Watson RS, West TE, Marinho F, Hay SI, Lozano R, Lopez AD, Angus DC, Murray CJL, Naghavi M. Global, regional, and national sepsis incidence and mortality, 1990-2017: analysis for the Global Burden of Disease Study. Lancet. 2020 Jan 18;395(10219):200-211.

[150] Rafique A, Etzerodt A, Graversen JH, Moestrup SK, Dagnæs-Hansen F, Møller HJ. Targeted lipid nanoparticle delivery of calcitriol to human monocyte-derived macrophages in vitro and in vivo: investigation of the anti-inflammatory effects of calcitriol. Int J Nanomedicine. 2019 Apr 23;14:2829-2846.

[151] Ramalho MJ, Loureiro JA, Gomes B, Frasco MF, Coelho MA, Pereira MC. PLGA nanoparticles as a platform for vitamin D-based cancer therapy. Beilstein J Nanotechnol. 2015 Jun 12;6:1306-18.

[152] Domínguez-Andrés J, Joosten LA, Netea MG. Induction of innate immune memory: the role of cellular metabolism. Curr Opin Immunol. 2019 Feb;56:10-16.

[153] Manzanares D, Ceña V. Endocytosis: The Nanoparticle and Submicron Nanocompounds Gateway into the Cell. Pharmaceutics. 2020 Apr 17;12(4):371.

[154] Shoji K, Ohashi K, Sampei K, Oikawa M, Mizuno K. Cytochalasin D acts as an inhibitor of the actin-cofilin interaction. Biochem Biophys Res Commun. 2012 Jul 20;424(1):52-7.

[155] Guo S, Zhang X, Zheng M, Zhang X, Min C, Wang Z, Cheon SH, Oak MH, Nah SY, Kim KM. Selectivity of commonly used inhibitors of clathrin-mediated and caveolae-dependent endocytosis of G protein-coupled receptors. Biochim Biophys Acta. 2015 Oct;1848(10 Pt A):2101-10.

[156] Behzadi S, Serpooshan V, Tao W, Hamaly MA, Alkawareek MY, Dreaden EC, Brown D, Alkilany AM, Farokhzad OC, Mahmoudi M. Cellular uptake of nanoparticles: journey inside the cell. Chem Soc Rev. 2017 Jul 17;46(14):4218-4244.

[157] Viola A, Munari F, Sánchez-Rodríguez R, Scolaro T, Castegna A. The Metabolic Signature of Macrophage Responses. Front Immunol. 2019 Jul 3;10:1462.

[158] Weis S, Carlos AR, Moita MR, Singh S, Blankenhaus B, Cardoso S, Larsen R, Rebelo S, Schäuble S, Del Barrio L, Mithieux G, Rajas F, Lindig S, Bauer M, Soares MP. Metabolic Adaptation Establishes Disease Tolerance to Sepsis. Cell. 2017 Jun 15;169(7):1263-1275.e14.

[159] Xiong S, Hong Z, Huang LS, Tsukasaki Y, Nepal S, Di A, Zhong M, Wu W, Ye Z, Gao X, Rao GN, Mehta D, Rehman J, Malik AB. IL-1β suppression of VE-cadherin transcription underlies sepsis-induced inflammatory lung injury. J Clin Invest. 2020 Jul 1;130(7):3684-3698.

Acknowledgements

First, I would like to thank my supervisor Prof. Dr. Holger Reichardt for giving me the opportunity to realise my thesis in his laboratory. I would also like to thank him for his availability, guidance, patience and support. I appreciated learning from his analytical scientific skills and suggestions throughout the time of my PhD.

I also would like to express my thanks to my thesis committee members: Prof. Dr. Lutz Walter and Prof. Dr. Francesca Odoardi for their scientific suggestions and advice proposed at the thesis academy meetings and their interest in my project.

Many thanks go to Prof. Dr. Lutz Walter for providing methods and a platform for me to carry out the gene CHIP analysis and Dr. Bohnenberger for histological analysis as well. Also thank Nico, Leslie, and Jennifer for their excellent technical support.

I would like to thank Sybille for her help and support, as well as Amina for supporting me not only in my scientific but also in my daily life. Many thanks go to my lovely colleagues, Chiara, Hu, Fabian and Tina. Working and sharing with you make scientific life so wonderful and enjoyable. I would also like to thank the rest of the Department of Cellular and Molecular Immunology for their kind help.

In the end, I want to specially thank my family and all my friends for their support and for always being there even in the hard times.